Imprints of Massive Scalars on Primordial Non-Gaussianities

Thesis by
Alexander Karas Ridgway

In Partial Fulfillment of the Requirements for the
Degree of
Doctor of Philosophy

CALIFORNIA INSTITUTE OF TECHNOLOGY
Pasadena, California

2019
Defended May 24, 2019

© 2019

Alexander Karas Ridgway
ORCID: 0000-0002-2592-1848

All rights reserved

ACKNOWLEDGEMENTS

I thank my friends, my family, my academic brother Michael McAneny, my advisor Mark Wise, my fiancé Erin Uhlfelder, and my dog Eddie. This work was supported by the DOE Grant DE-SC0011632

ABSTRACT

In this thesis, we modify the standard single-field inflation scenario by adding additional massive scalars to the inflationary field content. Due to the breaking of time translational invariance by the inflaton background, the inflaton can interact with these extra scalars through a kinetic mixing term. If these scalars have self-interactions, then their kinetic mixings with the inflaton induce potentially large primordial non-gaussianities in the scalar curvature fluctuations, which could be observed in the cosmic microwave background (CMB) and large-scale structure (LSS). We derive expressions for these non-Gaussianities in the limits the scalar masses are much larger than or much smaller than the Hubble constant during inflation and compute their contributions to dark matter halo correlation functions.

PUBLISHED CONTENT AND CONTRIBUTIONS

These references make up chapters two through five of this thesis. I was a primary author for these papers, meaning I helped calculate the results in these papers and prepare the manuscripts.

[1] M. McAneny, and A. K. Ridgway, "New Shapes of Primordial Non-Gaussianity from Quasi-Single Field Inflation with Multiple Isocurvatons", (2019), arXiv:1903.11607 [astro-ph.CO].

[2] H. An, M. McAneny, A. K. Ridgway, and M. B. Wise, "Non-Gaussian Enhancements of Galactic Halo Correlations in Quasi-Single Field Inflation", Physical Review **D97**, 123528 (2018), arXiv:1711.02667 [hep-ph].

[3] H. An, M. McAneny, A. K. Ridgway, and M. B. Wise, "Quasi Single Field Inflation in the non-perturbative regime", Journal of High Energy Physics **06**, 105 (2018), arXiv:1706.09971 [hep-ph].

[4] M. McAneny, A. K. Ridgway, M. P. Solon, and M. B. Wise, "Stochastic bias from loops of massive particles during inflation", Physics Letters **B785**, 332–337 (2018), arXiv:1712.07657 [astro-ph.CO].

TABLE OF CONTENTS

LIST OF ILLUSTRATIONS

Chapter 1

INTRODUCTION

The Big Bang cosmology has been a remarkably successful theory. It has provided theoretical explanations for the light element abundances, the Hubble expansion of distant galaxies and the cosmic microwave background (CMB) which have been confirmed experimentally to good accuracy and precision (see, for example, [1]). Despite this success, several puzzles still reminain. In particular, the facts that the CMB is nearly isotropic and that the universe is nearly flat can only be explained by fine tunings of initial conditions in this paradigm. While it is indeed possible that the initial conditions are fine tuned, the degree of the fine tuning needed to explain the homogeneity and flatness of the observable universe would have to be very high. It is well known that one can avoid these fine tunings by postulating a period of inflation, i.e. exponential growth of the scale factor in the FRW metric that occurs shortly after the big bang [2–7]. Such an era would imply that patches of the universe that are causally disconnected today were in causal contact earlier on in the history of the universe, thereby expalining why the universe looks almost the same in every direction. Inflation would also drive the curvature of the universe to a very low value. Inflation then provides dynamical explanations for what appear to be fine tunings in a standard Big Bang cosmology.

To achieve a period of exponential growth, the universe has to be dominated by vacuum energy density which has an equation of state $w = -1$. Single field slow roll inflation provides a simple mechanism to generate such a vacuum energy density (see [8] for a good review). In this model, a scalar field, known as the inflation, is displaced from the minima of its potential (known as the slow roll potential). The potential is assumed to be flat enough early on in the inflatons trajectory such that it's kinetic energy is much smaller than its potential energy. This potential energy fills all space and sources the vacuum energy that drives the universes exponential growth. As time progresses, the inflaton background gains speed as it rolls down its potential. After around 60 efolds, the inflaton's kinetic energy will become comparable to its potential energy and the pressure will no longer be negative. Inflation will then end and be followed by a period of reheating, after which the radiation dominated era of the standard Big Bang cosmology begins.

Aside from providing an elegant solution to the Big Bang puzzles, inflation gives a quantum mechanical origin to the inhomogeneities we observe in the CMB and large-scale structure (LSS) [9–13]. The inflaton is a quantum mechanical field which fluctuates around its background trajectory at every point in space. Depending on which way the inflaton fluctuates at each location, different patches of the universe expand different amounts, thereby generating inhomogeneities in the scalar perturbations of the metric which propagate into the CMB and LSS. In the simplest single field inflation theories, the inflaton and the scalar perturbations it sources are nearly Gaussian.

All cosmological observations to date are consistent with the inflaton being a Gaussian field that generates a nearly scale invariant Harrison-Zeldovich power spectrum for the initial scalar curvature perturbations [14]. This power spectrum is characterized by two numbers, its magnitude and tilt. There are many inflationary models, each with different degrees of freedom and interactions, that can explain these two numbers. Of course, only one model can be correct, so it is necessary to test other features of these models. To this end, there has been a lot of interest in primordial non-Gaussianities. If they were observed, in say the CMB or LSS, they could be used to constrain the inflationary field content and interactions.

A simple way to generate potentially observable non-Gaussianities is to add extra fields, such as self-interacting massive scalars, to the inflationary field content. A well-studied class of such models is quasi-single field inflation (qsfi), which includes a massive scalar called the isocurvaton [15]. In these models, the isocurvaton never fulfills the role of the inflaton, i.e. the isocurvaton's vacuum expectation value (vev) never drives the exponential growth of the universe. Rather, its purpose is to interact directly with the inflaton fluctuations to generate primordial non-Gaussianities. The non-Gaussianities in quasi-single field inflation leave distinctive imprints on the primordial non-Gaussianities, which could be tested against experiment and used to constrain the parameters of the theory.

In this thesis, I study the primordial non-Gaussianities in quasi-single field inflation in a few different regions of parameter space. First, I study the theory in the regime where the isocurvaton mass is much larger than the Hubble constant during inflation. In this case, the scalar curvature 3-point function in the squeezed limit displays logarithmic oscillations in the ratio of the squeezed wavevector magnitude k_s and the long wave vector magnitude k_l, and grows as $k_s^{-3/2}$ as $k_s \to 0$ in this limit. Next, I study quasi-single field inflation in the limit where the isocurvaton

mass is much lighter than the Hubble constant during inflation. In this regime, the squeezed bispectrum does not display logarithmic oscillations, however it grows almost as k_s^{-3} as $k_s \to 0$ in the squeezed limit, which is much stronger growth than in the large mass regime. Due to this strong power law growth of the squeezed three point, we will find that the Fourier transforms of the galaxy two point function $P_h(q)$ and three point function $B(k_1, k_2)$ can exhibit potentially observable deviations from what they would have been if there were no primordial non-Gaussianities.

In the following chapter, we will study the four point function of curvature perturbations induced by a quantum mechanical loop. We will see that in the "collapsed" limit, this loop will behave almost as $1/k_s^3$, where k_s is the collapsed momentum. Due to the strong power law growth of this contribution as $k_s \to 0$, $P_{hh}(q)$ can develop a large stochastic contribution which could be observed. Finally, we will generalize the quasi-single field paradigm to include an additional isocurvaton field. With the addition of an extra isocurvaton field, one can have additional kinetic mixings among the isocurvatons. These mixings generate late time oscillations in the inflaton and isocurvaton mode functions, which impact the primordial three point function of scalar curvature perturbations. For certain choices of parameters, the three point function will behave as $k_s^{-3}\cos \mathrm{Log} k_s/k_l$ in the squeezed limit, i.e. the squeezed three point in a multi-isocurvaton theory can display oscillatory features and strong power law growth as $k_s \to 0$. This is very different from quasi-single field inflation models which only contain one isocurvaton. In these models one can only have nearly cubic power law growth and oscillatory behavior in different limits of parameter space.

Chapter 2

QUASI-SINGLE FIELD INFLATION IN THE NON-PERTURBATIVE REGIME

In quasi-single field inflation there are massive fields that interact with the inflaton field. If these other fields are not much heavier than the Hubble constant during inflation (H) these interactions can lead to important consequences for the cosmological energy density perturbations. The simplest model of this type has a real scalar inflaton field that interacts with another real scalar S (with mass m). In this model there is a mixing term of the form $\mu\dot{\pi}S$, where π is the Goldstone fluctuation that is associated with the breaking of time translation invariance by the time evolution of the inflaton field during the inflationary era. In this chapter we study this model in the region $(\mu/H)^2 + (m/H)^2 > 9/4$ and $m/H \sim O(1)$ or less. For a large part of the parameter space in this region standard perturbative methods are not applicable. Using numerical and analytic methods we study how large μ/H has to be for the large μ/H effective field theory approach to be applicable.

2.1 Introduction

There is very strong evidence that the universe was once in a radiation dominated era followed by a matter dominated era. Today the universe is dominated by vacuum energy density and we are entering an inflationary era where the scale factor $a(t) \propto e^{H_0 t}$, with H_0 near the Hubble constant today. It is widely believed that at very early times there was another inflationary era where the energy density was dominated by false vacuum energy giving rise to a Robertson Walker scale factor with time dependence $a(t) \propto e^{Ht}$, where H is the Hubble constant during that inflationary era [2–7]. After more than about 60 e-folds, this inflationary era ends and the universe reheats to a radiation dominated (Robertson Walker) Universe. If this is the case then the horizon and flatness problems can be solved and in addition there is an attractive mechanism based on quantum fluctuations for generating density perturbations with wavelengths that were once outside the horizon [9–13] (see Ref. [8] for a review of inflation). It has been argued that it requires tuning to enter the inflationary era [16, 17] (see however [18]) and furthermore that there are issues with its predictability [19–21] (see also [22] for a recent discussion of these issues). Nevertheless, because of the simplicity of the dynamics of the inflationary universe

paradigm and the ability within it to do explicit calculations of the properties of the cosmological energy density perturbations [9–13] and primordial gravitational waves [2, 23–26], it seems worth studying particular inflationary models in some detail.

The simplest inflationary model is standard slow roll inflation with only a single real scalar field, the inflaton $\phi(x)$. It is conventional to work in a gauge where fluctuations in the inflaton field about the classical slow roll solution $\phi_0(t)$ vanish. Then using the Stückelberg trick the curvature fluctuations that are constant outside the horizon and become the density perturbations when they reenter the horizon (in the radiation and matter dominated eras) arise from quantum correlations in the Goldstone mode $\pi(x)$ calculated during the de-Sitter inflationary era[1]. In this model non gaussianities in cosmological density correlations arise because of connected higher point correlations of π, but they are very small [28].

Larger non-gaussianities can be achieved if there are other fields with masses around or less than the inflationary Hubble constant[2], that couple to π (see Ref. [31] for a review). In quasi-single field inflation these extra fields do not directly influence the classical evolution of the inflaton field but impact the cosmological density perturbations since they couple to the inflaton as "virtual particles" and hence affect the the correlations of π [15]. To simplify matters we will assume an approximate shift symmetry on the inflaton field, $\phi(x) \to \phi(x) + c$ (where c is a constant) that is only broken by the potential, V_ϕ, for ϕ. Furthermore, we assume an unbroken discrete symmetry, $\phi(x) \to -\phi(x)$. The simplest quasi-single field model introduced by Chen and Wang [31] has a single additional (beyond the inflaton) real scalar field S. The Lagrange density in this model contains an unusual kinetic mixing of the form $\mu\dot{\pi}S$.

This model has been extensively studied in the perturbative region[3] where $\mu/H \ll 1$ [15, 32–40]. In the non-perturbative region where $\mu/H \gg 1$, an elegant effective field theory formulation has been derived by Baumann and Green [37], and by Gwyn, Palma, Sakellariadou, and Sypsas [41]. The curvature perturbation power spectrum and a contribution to its bispectrum have been calculated using this formulation. It has been studied numericaly in [42] for other regions of the parameter space.

[1] The effective field theory formulation for inflation [27] provides an elegant method to compute correlations of π in a model independent fashion.

[2] There are other ways to have large non-gaussianities. For example, DBI inflation [29]. For an early example of another type, see [30].

[3] By perturbation theory we mean a series expansion in μ/H.

Throughout this chapter we treat μ as a constant independent of time. There has been a study of the case where μ changes suddenly with time, becoming large momentarily [43].

In this chapter we focus on the region of parameter space where $(\mu/H)^2 + (m/H)^2 > 9/4$ and $m/H \sim O(1)$ or less (recall m is the mass term for S). In this region, non-gaussianities have an interesting oscillatory behavior [35]. We use numerical non-perturbative methods similar to those developed in [42] and the effective field theory for large μ/H to study the model in this region of parameter space. We study how large μ/H must be for the effective field theory method to be quantitatively correct. In addition we derive the n_S, r plot for the model with inflaton potential $V_\phi = m_\phi^2\phi^2/2$ and derive the limit on μ/H and the S potential parameter V_S''' from Planck limits on non-gaussianity.

In section 2.2 we discuss the Lagrange density of the model we use in detail. Section 2.3 reviews quantization of the free part of the Lagrange density in flat space-time. Even this theory is non-trivial because of the unusual Lorentz non-invariant kinetic mixing between the Goldstone field π and the excitations of the massive scalar S. The massless mode has an unusual energy momentum relation that, for momentum in the range $m \ll q \ll \mu$, has a non-relativistic flavor, $E_q = q^2/\mu$ [37]. The other mode is heavy with a mass $\sqrt{\mu^2 + m^2}$. The fact that this mode's mass does not go to zero as $m \to 0$ is what regularizes the divergences that occur at $m = 0$ when one treats μ perturbatively.

Quantization of the free field theory in de-Sitter space-time is discussed in section 2.4. In de-Sitter space-time a mode's physical momentum q evolves with time. At early times modes have wavelengths much less than the horizon $1/H$ but at later times the wavelengths get red-shifted outside the horizon. The mode functions are calculated non-perturbatively by numerically solving the differential equations they satisfy in the region of parameter space, $(\mu/H)^2 + (m/H)^2 > 9/4$ and $m/H \sim O(1)$ or less. Quantum fluctuations in the field S fall off rapidly for wavelengths outside the horizon and it is the quantum fluctuations in the field π that determine the curvature and density fluctuations just as in standard slow roll single field inflation. Nevertheless, these quantum fluctuations are influenced by π's couplings to S.

In section 2.4 we analyze (in the non-perturbative regime) the curvature perturbation power spectrum in this model focusing on the transition between the perturbative regime and the regime where the effective theory applies.

Section 2.5 derives the n_S, r plot in this theory for the simple inflaton potential $V_\phi = m_\phi^2\phi^2/2$.

Non-gaussianities are discussed in Sec 2.6. We calculate the bispectrum in the the equilateral and squeezed configurations in the non-perturbative region numerically. In the large μ/H region we show that the numerical results agree with the results from the effective theory. We derive the constraints on μ/H and the S potential parameter V_S''' from Planck limits on non-gaussianity.

In section 2.7 we review the derivation of the effective field theory for large μ/H and the derivation of the power spectrum using it. We then compute the bispectrum in this effective field theory including a contribution from the potential for S that was not previously presented in the literature.

Our conclusions are summarized in Sec. 2.8.

2.2 The Model

The simplest quasi-single field inflation model has a real scalar inflaton field ϕ that interacts with another real scalar field S. We impose a $\phi \to -\phi$ symmetry and an approximate shift symmetry $\phi \to \phi + c$, where c is a constant. The shift symmetry is only broken by the inflaton potential $V_\phi(\phi)$. The Lagrangian we use has the form

$$\mathcal{L} = \mathcal{L}_\phi + \mathcal{L}_S + \mathcal{L}_{int} \tag{2.1}$$

where

$$\mathcal{L}_\phi = \frac{1}{2}g^{\mu\nu}\partial_\mu\phi\partial_\nu\phi - V_\phi(\phi), \quad \mathcal{L}_S = \frac{1}{2}g^{\mu\nu}\partial_\mu S\partial_\nu S - V_S(S) \tag{2.2}$$

Interactions between the inflaton ϕ and the massive field S first occur at dimension 5 and if we neglect operators with dimension higher than this the interaction Lagrangian is

$$\mathcal{L}_{int} = \frac{1}{\Lambda}g^{\mu\nu}\partial_\mu\phi\partial_\nu\phi S. \tag{2.3}$$

One natural choice for the mass scale Λ is the Planck mass. This higher dimensional operator would then arise from the transition from the theory of quantum gravity to a quantum field theory. In this case the non-gaussianities are very small. However, another possibility is that there is physics at a scale Λ that is large compared to the Hubble constant during inflation but well below the Planck scale. Integrating out this physics can give rise to such an operator.

We work in a gauge where the inflaton field is only a function of time, $\phi(x) = \phi_0(t)$ and take the background metric to have the form, $ds^2 = dt^2 - a(t)^2 d\mathbf{x}^2$, with the

scale factor $a(t) = e^{Ht}$. The Goldstone boson associated with the time translation invariance breaking by the classical evolution $\phi_0(t)$ is denoted by $\pi(x)$. The curvature perturbation is proportional to this field, $\zeta = -H\pi$. We expand S about a background classical value $S(x) = S_0 + s(x)$ and assume that the background solution S_0 is independent of time. This assumption is consistent with the dynamical equations of evolution for the fields provided we neglect second time derivatives of $\phi_0(t)$. With those assumptions $\phi_0(t)$ and S_0 satisfy,

$$\left(1 + \frac{2S_0}{\Lambda}\right) 3H\dot{\phi}_0 + \frac{dV_\phi(\phi_0)}{d\phi_0} = 0, \tag{2.4}$$

and

$$\frac{\dot{\phi}_0^2}{\Lambda} - \frac{dV_S(S_0)}{dS_0} = 0. \tag{2.5}$$

The dynamics for the fluctuations $\pi(x)$ and $s(x)$ are controlled by the Lagrange density,

$$\mathcal{L} = \mathcal{L}_0 + \mathcal{L}_{int} \tag{2.6}$$

where the free part of the Lagrange density for the fields π and s is,

$$\mathcal{L}_0 = \frac{1}{2}\dot{\phi}_0^2\left(1 + \frac{2S_0}{\Lambda}\right)\left(\dot{\pi}^2 - \frac{1}{a^2}\nabla\pi\cdot\nabla\pi\right) + \frac{1}{2}\left(\dot{s}^2 - \frac{1}{a^2}\nabla s\cdot\nabla s - m^2 s^2\right) + \frac{2}{\Lambda}\dot{\phi}_0^2\dot{\pi}s \tag{2.7}$$

where $m^2 = V''(S_0)$. Throughout this chapter we assume that the mass parameter m for the additional scalar s is of order the Hubble constant during inflation or smaller.

The interaction part of the Lagrange density is

$$\mathcal{L}_{int} = \frac{\dot{\phi}_0^2}{\Lambda}\left(\dot{\pi}^2 - \frac{1}{a^2}\nabla\pi\cdot\nabla\pi\right)s + \left(\dot{\pi} + \frac{\dot{\pi}^2}{2}\right)\dot{s}^2 - \frac{1}{3!}V_S'''(S_0)s^3 - \frac{1}{4!}V_S''''(S_0)s^4 + \ldots \tag{2.8}$$

It is convenient to introduce a rescaled π that has a properly normalized kinetic term,

$$\tilde{\pi} = \sqrt{\dot{\phi}_0^2(1 + 2S_0/\Lambda)}\pi = |\dot{\tilde{\phi}}_0|\pi \tag{2.9}$$

where,

$$\tilde{\phi}_0 = \sqrt{(1 + 2S_0/\Lambda)}\phi_0. \tag{2.10}$$

In terms of these rescaled fields the gravitational curvature perturbation becomes,

$$\zeta = -(H/|\dot{\tilde{\phi}}_0|)\tilde{\pi}. \tag{2.11}$$

The free and interacting Lagrange densities, after introducing a redefined scale $\tilde{\Lambda} = (1 + 2S_0/\Lambda)\Lambda$, are

$$\mathcal{L}_0 = \frac{1}{2}\left(\dot{\tilde{\pi}}^2 - \frac{1}{a^2}\nabla\tilde{\pi}\cdot\nabla\tilde{\pi}\right) + \frac{1}{2}\left(\dot{s}^2 - \frac{1}{a^2}\nabla s\cdot\nabla s - m^2 s^2\right) + \mu\dot{\tilde{\pi}}s \tag{2.12}$$

and

$$\mathcal{L}_{int} = \frac{1}{\tilde{\Lambda}}\left(\dot{\tilde{\pi}}^2 - \frac{1}{a^2}\nabla\tilde{\pi}\cdot\nabla\tilde{\pi}\right)s - \frac{1}{3!}V_S'''(S_0)s^3 + \ldots. \tag{2.13}$$

In eq. (2.12) we have introduced

$$\mu = 2\dot{\tilde{\phi}}_0/\tilde{\Lambda}. \tag{2.14}$$

and in eq. (2.13) only explicitly kept those terms that play a role in the calculations performed in this chapter. In the following sections we will drop the tilde on the Goldstone field $\tilde{\pi}$ to simplify the notation. Moreover, we adopt sign conventions for ϕ and S so that $\dot{\phi}_0$ and μ are positive.

As mentioned in the introduction the purpose of this chapter is to study this model in the region of parameter space where $(\mu^2 + m^2)^{1/2}/H > 3/2$ and $m \sim O(H)$ or smaller. Some of this region, *i*.e. where μ/H is small or very large have been previously studied. We will compare with those results to find out how small and how large μ/H has to be for the approximate methods used in those regions to be accurate.

First let's imagine that $S_0 = 0$. This can always be arranged by tuning the linear term in the potential $V_S(S)$ to cancel the linear term in S from the $1/\Lambda$ interaction term. Then $\mu/H = (2\dot{\phi}_0/H^2)(H/\Lambda)$. The measured power spectrum for the curvature perturbations implies that $\dot{\phi}_0/H^2$ is very large so even for small H/Λ one can achieve large values for μ/H.

Next we allow a non zero S_0 but simplify the potential so it contains no terms with more than two powers of S, explicitly $V_S = V_S'S + m^2S^2/2$. In this case μ/H can be written as,

$$\frac{\mu}{H} = \frac{2\dot{\phi}_0/\Lambda H}{\left[1 + 2\frac{(\dot{\phi}_0/\Lambda H)^2 - V_S'/H^2\Lambda}{m^2/H^2}\right]^{1/2}}\,. \tag{2.15}$$

Therefore, without tuning the tadpole in V_S to cancel $\dot{\phi}_0^2 S/\Lambda$, it is not possible to have the mass parameter m of order the Hubble constant (or smaller) and μ/H large. Nonetheless it seems worth studying this region of parameter space since there are some novel features that arise there.

Naive dimensional analysis suggests that higher dimension operators that couple derivatives of ϕ to a single S are smaller than the dimension 5 operator we kept provided $\dot{\phi}_0/\Lambda^2 = (\mu/H)^2(H^2/\dot{\phi}_0) < 1$. The higher powers of S will be small if in addition $S_0/\Lambda < 1$. Since the measured amplitude of the density perturbations implies that $H^2/\dot{\phi}_0$ is quite small the ratio μ/H can be large in the region of parameter space where the operator expansion in powers of $1/\Lambda$ is justified. Indeed, comparing the calculated power spectrum at large μ/H given in (2.37) with it's measured value, the upper limit for μ/H for power counting in the $1/\Lambda$ expansion to be valid is $\mu/H \lesssim 300$. Of course, this is just a naturalness constraint and can be violated without the model being inconsistent.

2.3 Free Field Theory in Flat Space-time

In this section we review, for pedagogical reasons, quantization in flat space-time of the free field theory with Lagrange density in eq. (2.12). The results presented here have, by in large, been noted previously in [37, 41].

Dropping the tildes and setting $a(t) = 1$ the Lagrange density in eq. (2.12) becomes,

$$\mathcal{L}_0 = \frac{1}{2}\left(\dot{\pi}^2 - \nabla\pi\cdot\nabla\pi\right) + \frac{1}{2}\left(\dot{s}^2 - \nabla s\cdot\nabla s - m^2 s^2\right) + \mu\dot{\pi}s. \tag{2.16}$$

This corresponds to normal kinetic terms for two real scalar fields but with an unusual Lorentz non-invariant kinetic mixing. The Lagrange density has the shift symmetry $\pi \longrightarrow \pi + c$ for the Goldstone field π.

The classical equations of motion for the fields π and s are,

$$\ddot{\pi} - \nabla^2\pi + \mu\dot{s} = 0 \tag{2.17}$$

and

$$\ddot{s} - \nabla^2 s + m^2 s - \mu\dot{\pi} = 0 \tag{2.18}$$

Quantization proceeds by expanding the fields in modes,

$$\pi(\mathbf{x},t) = \int \frac{d^3q}{(2\pi)^3}\left(a^{(1)}(\mathbf{q})\pi_q^{(1)}(t)e^{i\mathbf{q}\cdot\mathbf{x}} + a^{(2)}(\mathbf{q})\pi_q^{(2)}(t)e^{i\mathbf{q}\cdot\mathbf{x}} + \text{h.}c.\right) \tag{2.19}$$

and

$$s(\mathbf{x},t) = \int \frac{d^3q}{(2\pi)^3}\left(a^{(1)}(\mathbf{q})s_q^{(1)}(t)e^{i\mathbf{q}\cdot\mathbf{x}} + a^{(2)}(\mathbf{q})s_q^{(2)}(t)e^{i\mathbf{q}\cdot\mathbf{x}} + \text{h.}c.\right) \tag{2.20}$$

The annihilation operators $a^{(1,2)}(\mathbf{q})$ and creation operators $a^{(1,2)}(\mathbf{q})^\dagger$ satisfy the usual commutation relations[4]. The time dependence of the mode functions $\pi_q^{(1,2)}(t)$ and

[4]More explicitly the non-zero commutators are: $[a^{(1)}(\mathbf{q}), a^{(1)}(\mathbf{q}')^\dagger] = (2\pi)^3\delta^3(\mathbf{q}-\mathbf{q}')$ and $[a^{(2)}(\mathbf{q}), a^{(2)}(\mathbf{q}')^\dagger] = (2\pi)^3\delta^3(\mathbf{q}-\mathbf{q}')$

$s_q^{(1,2)}(t)$ are determined by solving the classical equations of motion and their normalization is fixed by the canonical commutation relations of the fields with their canonical momenta. A difference from the usual case where there is no Lorentz non-invariant mixing is that the canonical momentum for the field π is not $\dot{\pi}$ but rather $\dot{\pi} + \mu s$. So $\dot{\pi}$ and $\dot{s}$ don't commute at equal time but rather satisfy $[\dot{\pi}(\mathbf{x}, t), \dot{s}(\mathbf{x}', t)] = -i\mu\delta^3(\mathbf{x} - \mathbf{x}')$.

The time dependence of the modes has the usual exponential form $\pi_q^{(1,2)}(t) \propto \exp(-iE_q^{(1,2)}t)$, $s_q^{(1,2)}(t) \propto \exp(-iE_q^{(1,2)}t)$. The dispersion relations for the energies is determined by solving the classical equations of motion. This yields,

$$E_q^{(1,2)} = \left[q^2 + \frac{m^2 + \mu^2}{2} \pm \frac{1}{2}\left((m^2 + \mu^2)^2 + 4q^2\mu^2\right)^{1/2}\right]^{1/2}, \tag{2.21}$$

which is a massless mode that we label by (1) corresponding to the minus sign and a massive mode that we label by (2) corresponding to the plus sign. The mass of mode (2) is $\sqrt{m^2 + \mu^2}$. Because this mode remains massive even when $m = 0$ there will be no divergences in our calculations in de-Sitter space.

We now focus on the large mixing region of parameter space, $\mu \gg q, m$. As discussed in the literature [37] the dispersion relations of the two modes can be written as

$$E_q^{(1)} \simeq \frac{q\sqrt{q^2 + m^2}}{\mu}, \quad E_q^{(2)} \simeq \mu. \tag{2.22}$$

The (1) mode is massless but for q much larger than m the energy grows not linearly with q but rather quadratically (like a non relativistic particle). The other mode is massive with mass μ. For very small momentum, $q \ll m$, the massive scalar s only contains the massive (2) mode, *i*.e., $|s_q^{(1)}(t)/s_q^{(2)}(t)| \to 0$ as $q \to 0$. On the other hand the Goldstone field π contains equal amounts of the (1) and (2) modes.

The infrared, $q \to 0$, behavior of the mode function $s_q^{(1,2)}$ changes in the special case that $m = 0$. Then integrating-by-parts, the kinetic mixing term in Eq. (2.16) can be recast as $-\mu\pi\dot{s}$, and so it is clear that there is also a shift symmetry in s. For $m = 0$ the scalar field s also contains equal amounts of the two modes.

Since for large μ the second mode is heavy it is appropriate for the physics at low momentum $q \ll \mu$ to integrate it out from the theory and write an effective Lagrange density in terms of a single massless field. For the light mode a time derivative gives factors of $1/\mu$ and (for $m \neq 0$) at very large μ the s field contains only a small amount of that massless mode. Hence (2.18) implies that,

$$s \simeq \left(\frac{\mu}{m^2 - \nabla^2}\right)\dot{\pi} \tag{2.23}$$

Putting this into the Lagrange density in eq. (2.16) and dropping terms suppressed by powers of $1/\mu$ (recall a time derivative on π is suppressed by $1/\mu$) yields the effective Lagrange density for the massless mode,

$$\mathcal{L}_{eff} = \frac{1}{2}\left(\frac{\mu^2}{m^2 - \nabla^2}\right)\dot{\pi}^2 - \frac{1}{2}\nabla\pi\cdot\nabla\pi \tag{2.24}$$

which yields the dispersion relation for the massless mode given in eq. (2.22).

In the next section we perform the quantization in curved de-Sitter space-time (with Hubble constant H). Then the physics of the massless (1) mode should be similar to that in flat space-time when the momentum and energy for that mode are large compared to H *i*.e., $q > H$ and $E_q^{(1)} > H$. In the flat space-time large μ discussion we assumed $q < \mu$. The energy condition $E_q^{(1)} > H$ implies q must also satisfy $q > \sqrt{\mu H}$ in order for our de-Sitter space-time computations to resemble the flat space-time large μ case discussed in this subsection.

2.4 Free Field Theory in de-Sitter Space time

Introducing conformal time, $\tau = -e^{-Ht}/H$, and including the measure factor $\sqrt{-g}$ in the Lagrange density so that the action is equal to $\int d^3x d\tau \mathcal{L}$ we have

$$\mathcal{L}_0 = \frac{1}{2H^2\tau^2}\left((\partial_\tau\pi)^2 - \nabla\pi\cdot\nabla\pi + (\partial_\tau s)^2 - \frac{m^2}{H^2\tau^2}s^2 - \nabla s\cdot\nabla s - \frac{2\mu}{H\tau}s\partial_\tau\pi\right). \tag{2.25}$$

As in flat space we expand the quantum fields in terms of creation and annihilation operators. Introducing $\eta = k\tau$ we write,

$$\pi(\mathbf{x},\tau) = \int \frac{d^3k}{(2\pi)^3}\left(a^{(1)}(\mathbf{k})\pi_k^{(1)}(\eta)e^{i\mathbf{k}\cdot\mathbf{x}} + a^{(2)}(\mathbf{k})\pi_k^{(2)}(\eta)e^{i\mathbf{k}\cdot\mathbf{x}} + \text{h.}c.\right) \tag{2.26}$$

and

$$s(\mathbf{x},\tau) = \int \frac{d^3k}{(2\pi)^3}\left(a^{(1)}(\mathbf{k})s_k^{(1)}(\eta)e^{i\mathbf{k}\cdot\mathbf{x}} + a^{(2)}(\mathbf{k})s_k^{(2)}(\eta)e^{i\mathbf{k}\cdot\mathbf{x}} + \text{h.}c.\right) \tag{2.27}$$

The mode functions obey the classical equations of motion,

$$\pi_k'' - \frac{2\pi_k'}{\eta} + \pi_k - \frac{\mu}{H}\left(\frac{s_k'}{\eta} - \frac{3s_k}{\eta^2}\right) = 0 \tag{2.28}$$

and

$$s_k'' - \frac{2s_k'}{\eta} + \left(1 + \frac{m^2}{H^2\eta^2}\right)s_k + \frac{\mu}{H}\frac{\pi_k'}{\eta} = 0\,, \tag{2.29}$$

where a " $'$ " represents an η derivative.

Numerical results

In the mode expansion for for the fields s and π, k is the magnitude of the comoving wavevector. The physical wavevector has magnitude $q = k/a = -H\eta$. Hence the condition that a mode have wavelength well within the de-Sitter horizon $1/H$ is $q/H \gg 1$ which is equivalent to $-\eta \ll 1$. At fixed k as time evolves a mode goes from physical wavelength well within the horizon to outside the horizon.

In the region well within the horizon, $-\eta \gg \mu/H$ and $-\eta \gg 1$, the differential equations (2.28) and (2.29) simplify to

$$\begin{aligned} \pi_k'' + \pi_k &= 0\,, \\ s_k'' + s_k &= 0\,. \end{aligned} \tag{2.30}$$

Here we suppressed the superscripts $(1, 2)$ that label mode type. The leading behavior of the mode functions is

$$\pi_k \sim s_k \sim e^{-i\eta} \tag{2.31}$$

and so it is convenient to represent the general solution in the region deeply inside the horizon as

$$\pi_k = A_k e^{-i\eta}\,, \quad s_k = B_k e^{-i\eta}\,. \tag{2.32}$$

A and B are functions of η with $|A'/A|, |B'/B| \ll 1$. Substituting π_k and s_k back into (2.28) and (2.29) and keeping only the leading order terms in η^{-1} we find

$$\begin{aligned} 2A_k' - \frac{2A}{\eta} - \frac{\mu}{H\eta} B_k &= 0 \\ 2B_k' - \frac{2B}{\eta} + \frac{\mu}{H\eta} A_k &= 0 \end{aligned} \tag{2.33}$$

which gives

$$A_k \propto (-\eta)^{1 \pm \frac{i\mu}{2H}}\,, \quad B_k = \pm i A_k\,. \tag{2.34}$$

Therefore, in this region the canonically normalized form of π_k and s_k can be written as

$$\pi_k^{(1,2)} = \frac{H}{\sqrt{4k^3}} e^{-i\eta} (-\eta)^{1 \pm \frac{i\mu}{2H}}\,, \quad s_k^{(1,2)} = \pm i \pi_k^{(1,2)}\,, \tag{2.35}$$

where the factor $H/\sqrt{4k^3}$ is determined by the canonical commutation relations.

Eq. (2.35) is used to determine the initial conditions $\pi_k^{(1,2)}(\eta_0)$, $s_k^{(1,2)}(\eta_0)$ and $\pi_k'^{(1,2)}(\eta_0)$, $s_k'^{(1,2)}(\eta_0)$ at a value of η_0 that is large in magnitude. The differential

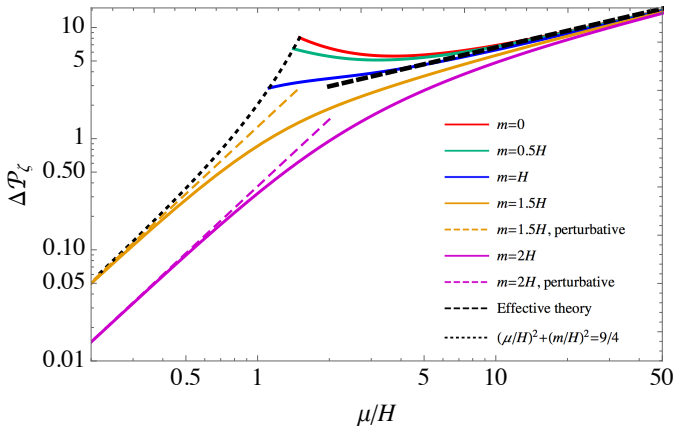

Figure 2.1: The correction of the power spectrum of curvature perturbation $\Delta\mathcal{P}_\zeta$ in units of $(H^4/\dot{\phi}_0^2)(1/2k^3)$ due to the mixing with the new field s. The red, blue, green, orange and magenta curves are for $m = 0, 0.5H, H, 1.5H$ and $2H$. The black dashed curve shows the result from the effective theory and the colored dashed lines are perturbation theory.

equations in (2.28) and (2.29) can then be solved numerically and used to determine the power spectrum for the curvature perturbation in this model.

The correction to the power spectrum $\Delta\mathcal{P}_\zeta$ is defined by, $\Delta\mathcal{P}_\zeta = \mathcal{P}_\zeta - \mathcal{P}_\zeta^{(0)}$, where

$$\mathcal{P}_\zeta^{(0)}(k) = \frac{H^4}{\dot{\phi}_0^2}\frac{1}{2k^3}\,, \tag{2.36}$$

is the power spectrum of the curvature perturbation in usual slow roll single field inflation. $\Delta\mathcal{P}_\zeta$ is shown in Fig. 2.1. In the region of $\mu \ll H$ $\Delta\mathcal{P}_\zeta$ goes like μ^2 which agrees with the perturbative calculation [15]. In the region where μ is larger than about $10H$ the power spectrum $\mathcal{P}_\zeta$ grows as $\mu^{1/2}$ and can be approximated by,

$$\mathcal{P}_\zeta(k) = C\left(\frac{\mu}{H}\right)^{1/2}\mathcal{P}_\zeta^{(0)}(k)\,, \tag{2.37}$$

where

$$C = \frac{16\pi}{\Gamma^2(-1/4)} \simeq 2.09. \tag{2.38}$$

Corrections to eqs. (2.37) and (2.38) become negligible as $\mu \to \infty$. The power spectrum in the large μ/H limit was calculated using the large μ/H effective field theory in [41]. For completeness we briefly review that calculation in Sec. 2.7.

As shown in Ref. [15], the perturbative result diverges in the limit of $m \to 0$. From the red curve shown in Fig. 2.1 we can see that the curvature perturbation is well defined at $m = 0$. Perturbation theory can be very misleading at modest values of

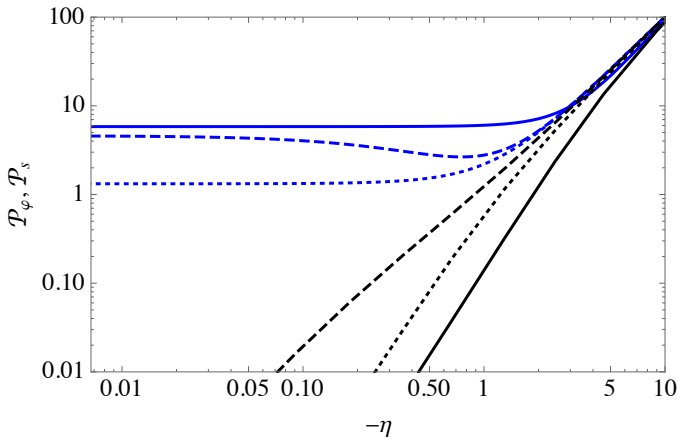

Figure 2.2: Power spectrum of the π and s fields in the unit of $H^2/2k^3$. The solid, dotted, and dashed curves are for $(\mu/H, m/H) = (10, 2), (1, 2)$ and $(1.2, 0.9)$, respectively.

m/H and values of μ/H not very much larger than unity. For example for $m = 0.5H$ and $\mu = 1.5H$ it gives a value for $\Delta\mathcal{P}_\zeta$ (in the units used for Fig. 2.1) equal to 310 while our numerical result is 6.2.

For the curvature perturbations one calculates the power spectrum of the π field as $-\eta \to 0$. However the power spectra for the fields can be calculated at any η. For $\mu/H > 1$ the power spectrum for the s field $\mathcal{P}_s(k)$ falls off rapidly as $-\eta$ falls below unity. The numerical results of the power spectrum of the s field $\mathcal{P}_s(k)$ in units of $H^2/2k^3$ as a function of η for a few values of μ and m are shown in Fig. 2.2. One can see that all the curves decrease with $-\eta$ and become small as $-\eta$ falls below unity.

In the usual single field inflation model $\mathcal{P}_\pi$ goes to unity in units of $H^2/2k^3$ as $-\eta \to 0$. In this model of quasi-single field inflation, as shown in Fig. 2.2 for the $\mu = 10H$, $m = 2H$ case the asymptotic value of $\mathcal{P}_\pi$ is much larger than unity. This is due to the change in the dispersion relation of the π field and can be understood using the large μ/H effective theory. From Fig. 2.2 we see that the asymptotic value of $\mathcal{P}_\pi$ for the case $\mu = 1.2H, m = 0.9H$ is also much larger than 1.

Qualitative analysis

We can understand qualitatively the shape of the mode functions analytically. In the region well outside the horizon, $-\eta \ll 1$, eqs. (2.28) and (2.29) can be simplified to

$$\begin{aligned} -\pi_k'' + \frac{2\pi_k'}{\eta} - \frac{\mu}{H}\left(\frac{3s_k}{\eta^2} - \frac{s_k'}{\eta}\right) = 0 \\ -s_k'' + \frac{2s_k'}{\eta} - \frac{m^2 s_k}{H^2\eta^2} - \frac{\mu}{H}\frac{\pi_k'}{\eta} = 0 \end{aligned} \tag{2.39}$$

which is invariant under the transformation

$$\pi_k \to \lambda^2 \pi_k\,, \quad s_k \to \lambda^2 s_k\,, \quad \eta \to \lambda\eta\,. \tag{2.40}$$

Therefore, the general form of the solution can be written as

$$\pi_k = Q_k(-\eta)^\alpha\,, \quad s_k = R_k(-\eta)^\alpha\,. \tag{2.41}$$

Putting this back into the differential equations gives equations for the power α and the coefficients Q_k and R_k

$$\begin{aligned} (\alpha^2 - 3\alpha)Q_k + \frac{\mu}{H}(3-\alpha)R_k &= 0\,, \\ \frac{\mu}{H}\alpha Q_k + \left(\alpha^2 - 3\alpha + \frac{m^2}{H^2}\right)R_k &= 0\,. \end{aligned} \tag{2.42}$$

To have nontrivial solutions for Q_k and R_k requires

$$\alpha(\alpha-3)\left[\alpha^2 - 3\alpha + \frac{m^2+\mu^2}{H^2}\right] = 0\,. \tag{2.43}$$

There are four solutions to this equation

$$\alpha_1 = 0\,, \quad \alpha_2 = 3\,, \quad \alpha_\pm = \frac{3}{2} \pm \left(\frac{9}{4} - \frac{m^2+\mu^2}{H^2}\right)^{1/2}\,. \tag{2.44}$$

For the region of parameter space we focus on, $\alpha_\pm$ are complex, which can have observational consequences for the non-gaussianities [35].

For large values of μ/H the infrared behavior of the mode functions $\pi_k^{(1,2)}$ and $s_k^{(1,2)}$ match directly onto the solutions in eq. (2.44). This is shown in Fig. 2.3 using $m = 2H$ and $\mu = 10H$. The $\alpha_1 = 0$ mode is constant outside the horizon. The $\alpha_2 = 3$ behavior vanishes outside the horizon and can be thought of as a subdominant contribution to the massless mode. The $\alpha_\pm$ solutions correspond to the mode functions for a free scalar field with mass equal to $(m^2+\mu^2)^{1/2}$. They play

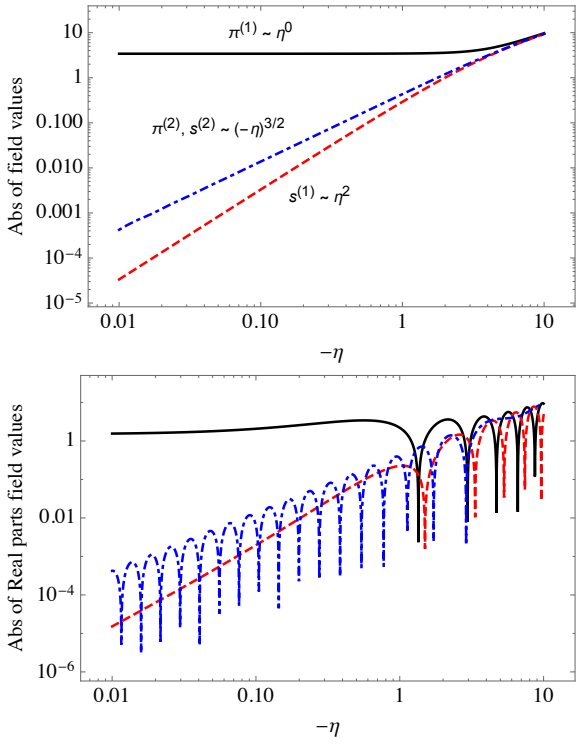

Figure 2.3: Left: Absolute values of the field values with $m = 2H$ and $\mu = 10H$. The solid black and the dashed red curves are for the π and s mode with the index $\alpha = 0$. The dot-dashed blue curve illustrates the π and s modes whose dominant small $-\eta$ behavior comes from the index $\alpha = 3/2 \pm (9/4 - (m^2 + \mu^2)/H^2)^{1/2}$. Right: Showing the absolute value of the real parts of each mode corresponding to the ones in the left panel.

an important role in the calculation of non-gaussianities. For $m = 2H$ and $\mu = 10H$ the behavior of this mode is shown by the blue dot-dashed curves in Fig. 2.3. One can see that it oscillates logarithmically with frequency $(m^2 + \mu^2)^{1/2}$, and decreases with a power of $3/2$ for small $-\eta$. To get the curves shown in Fig. 2.3 we solve the differential equations (2.28) and (2.29) with the initial conditions (2.35). The $\pi^{(2)}$ mode shown in the left panel of Fig. 2.3 eventually goes to a constant as $-\eta$ gets smaller. Similarly, the absolute value of the $s^{(1)}$ mode eventually goes like $(-\eta)^{3/2}$ for very small $-\eta$.

In this paragraph we focus on the $\alpha_1 = 0$ solution. Putting $\alpha_1 = 0$ back Eq. (2.42) we find that $R_k = 0$. Since there is no shift symmetry in the s field it should not contain the massless mode in the far infrared. We can get the leading behavior of the s_k mode function outside the horizon by putting $\pi_k = Q_k$ back into the exact differential equation (2.28). This gives the first order inhomogeneous differential

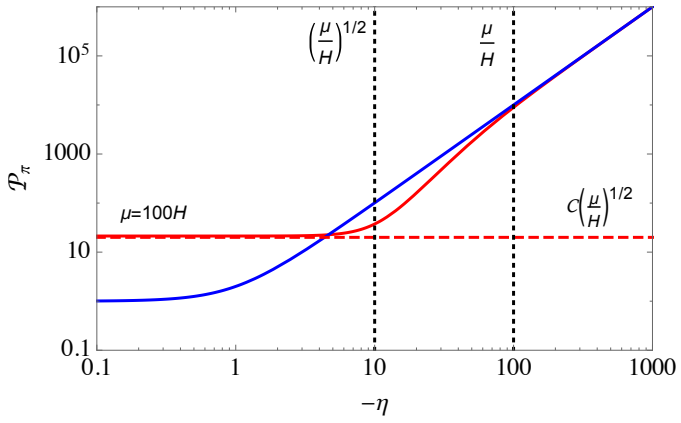

Figure 2.4: Numerical result of $\mathcal{P}_\pi(k)$ as a function of η in the unit of $H^2/(2k^3)$ for $m = 0$ and $\mu = 100H$. For comparison in blue we show the result for standard single field inflation.

equation

$$-Q_k = \frac{\mu}{H}\left(\frac{3s_k}{\eta^2} - \frac{s_k'}{\eta}\right) \tag{2.45}$$

with general solution

$$s_k = -\frac{Q_k H \eta^2}{\mu} \,. \tag{2.46}$$

This behavior is shown by the red dashed curves in Fig. 2.3.

The large μ/H region

In this subsection we focus on some properties of the solutions for the mode functions that only apply for very large μ/H. We find that the curvature perturbation goes to a constant when $-\eta < (\mu/H)^{1/2}$ instead of the usual condition that it be outside the horizon, *i*.e., $-\eta < 1$. This is illustrated in Fig. 2.4 which shows the numerical results for the power spectrum of $\mathcal{P}_\pi$ as a function of η.

Examining eq. (2.29), in the region $-\eta < (\mu/H)^{1/2}$ it is clear that the last term on the left hand side is the largest. Neglecting the other terms the solution in this region satisfies

$$\pi' = 0 \,, \tag{2.47}$$

which implies that π_k is constant and s_k is proportional to η^2, as in eq. (2.46).

In the region $(\mu/H)^{1/2} < -\eta < \mu/H$ one can show that the differential equations for the mode functions are solved approximately by

$$\pi_k \propto (-\eta)^{3/2} \exp\left[\frac{iH\eta^2}{2\mu}\right] \,, \quad s_k \propto (-\eta)^{3/2} \exp\left[\frac{iH\eta^2}{2\mu}\right] \,. \tag{2.48}$$

The physical wavevector of a mode with comoving wavevector k is

$$q = ka^{-1} = -kH\tau \ . \tag{2.49}$$

Therefore the change of the phase of these solutions within a small time period $\Delta\eta$ can be written as

$$\Delta \mathrm{p}hase = \frac{\eta_0 \Delta\eta H}{\mu} = -\frac{q^2}{\mu}\Delta t \ , \tag{2.50}$$

where $\Delta t = a\Delta\tau$ has been used. This agrees with the dispersion relation in flat space given in eq. (2.22) for the massless mode. From Fig. 2.4, one can see that it is in this region the solution for $\mu \gg H$ starts to deviate from the standard slow roll solution, which corresponds to $\mu = 0$ in the model we are studying. This is because in this region the solutions in de-Sitter space should resemble those in flat space and the light mode has a flat space dispersion relation $E_q = q^2/\mu$ which is quite different from a single massless field with dispersion relation $E_q = q$.

Putting the solution we have found back into the differential equations (2.28) and (2.29), one can see that the terms

$$-\pi_k'' + \frac{2\pi_k'}{\eta} \ \ \mathrm{a}nd \ \ -s_k'' + \frac{2s_k'}{\eta} \tag{2.51}$$

are suppressed, which means that the terms

$$(\partial_\tau \pi)^2 \ \ \mathrm{a}nd \ \ (\partial_\tau s)^2 \tag{2.52}$$

in the Lagrange density (2.25) can be neglected. After neglecting these two terms, there are no terms in (2.25) that contain time derivatives of s. This indicates that s has become a Lagrange multiplier and can be replaced in the Lagrange density using its classical equation of motion to express it in terms of π. This amounts to summing the tree graphs that contain virtual s propogators and is the origin of the effective theory approach developed in Refs. [37] and [41] for the behavior of π in this region. We will briefly review the basic setup for this effective field theory and use it to calculate the two- and three-point functions of the curvature perturbation in the large μ/H limit in Sec. 2.7.

2.5 Impact on observables

The dimensionless power spectrum is defined as [44]

$$\Delta^2_\zeta(k) = \frac{k^3}{2\pi^2}\mathcal{P}_\zeta(k) = \frac{H^4}{(2\pi)^2\dot{\phi}_0^2} f(\mu/H, m/H) = 2.12 \times 10^{-9} \ , \tag{2.53}$$

where f is a function of the μ and m. $f-1$ is shown in Fig. 2.1 as a function of μ/H for fixed values of m. The above power spectrum relies on the assumption that the tadpole cancellation in (2.5) is possible at all times. However, S will develop a time-dependent vaccuum expectation value due to the evolution of ϕ_0. We will show later in this section that this remains negligible in $m_\phi^2\phi^2$ inflation, which we consider here.

In terms of the slow roll parameter

$$\epsilon_0 = \frac{\dot{\phi}_0^2}{2H^2 M_{\rm p}^2} \tag{2.54}$$

$\Delta_\zeta^2(k)$ can be written as

$$\Delta_\zeta^2(k) = \frac{H^2}{8\pi^2\epsilon_0 M_{\rm p}^2} f\left(\frac{\sqrt{8\epsilon_0}M_{\rm p}}{\Lambda}, \frac{m}{H}\right) . \tag{2.55}$$

The tilt of the power spectrum is defined as

$$n_S - 1 \equiv \frac{d\log\Delta_\zeta^2}{d\log k} , \tag{2.56}$$

and can be written as

$$n_S - 1 = \frac{d\log\Delta_\zeta^2}{d\log k} = \frac{d\log\Delta_\zeta^2}{dN} \times \frac{dN}{d\log k} , \tag{2.57}$$

where N is the number of e-folds between when the modes of interest exit the horizon and inflation ends. From Eq. (2.53) we have

$$\begin{aligned} \frac{d\log\Delta_\zeta^2}{dN} &= 2\frac{d\log H}{dN} - \frac{d\log\epsilon_0}{dN} \\ &+ \left(\frac{\partial\log f}{\partial\log\hat{\mu}}\frac{d\log\hat{\mu}}{d\log\epsilon_0}\frac{d\log\epsilon_0}{dN} + \frac{\partial\log f}{\partial\log\hat{m}}\frac{d\log\hat{m}}{d\log H}\frac{d\log H}{dN}\right) \\ &= -4\epsilon_0 + 2\eta_0 + (\epsilon_0 - \eta_0)\frac{\partial\log f}{\partial\log\hat{\mu}} + \epsilon_0\frac{\partial\log f}{\partial\log\hat{m}} \end{aligned} \tag{2.58}$$

where the standard results of slow roll inflation have been used [8], and η_0 is the other slow roll parameter defined as $-\ddot{\phi}_0/(H\dot{\phi}_0)$. $\hat{\mu}$ and $\hat{m}$ are defined as

$$\hat{\mu} \equiv \frac{\mu}{H} , \quad \hat{m} \equiv \frac{m}{H} . \tag{2.59}$$

Up to leading order in the slow roll parameters we have that,

$$\frac{d\log k}{dN} = 1 \tag{2.60}$$

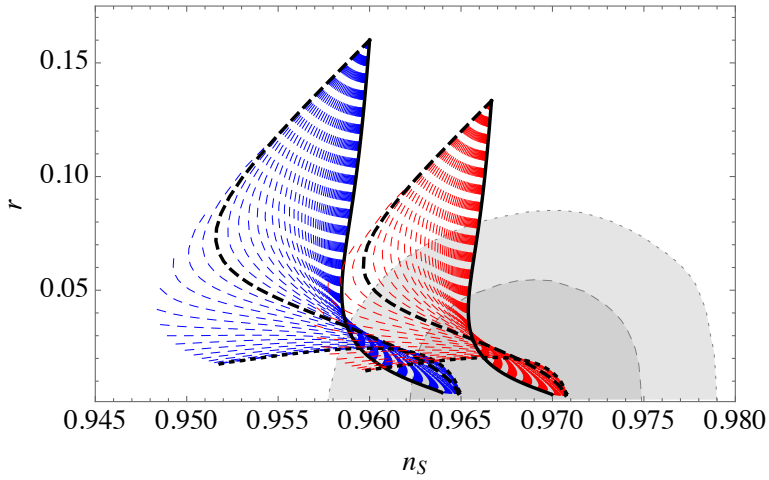

Figure 2.5: Impact on the scalar spectrum index n_S and the tensor-to-scalar ratio r for the ϕ^2 inflation model with μ from 0 to $100H$ and m from 0 to $6H$, and $(\mu^2+m^2)^{1/2} > 3H/2$. The blue and red regions are for $N_{cmb} = 50$ and 60 respectively. The dotted, dashed and solid curves are for m fixed to be 0, $3H/2$ and $6H$ respectively. The gray regions are the one-sigma and two-sigma constraints from the combination of the Planck data and the BICEP2/Keck data [45].

Therefore at leading order in slow roll parameters

$$n_S - 1 = -4\epsilon_0 + 2\eta_0 + (\epsilon_0 - \eta_0)\frac{\partial \log f}{\partial \log \hat{\mu}} + \epsilon_0 \frac{\partial \log f}{\partial \log \hat{m}} \,. \tag{2.61}$$

Another important observable is the tensor-scalar ratio. Since the gravitational wave production is only related to the structure of the de-Sitter metric, the dimensionless tensor spectrum can still be written as

$$\Delta_t^2 = \frac{2}{\pi^2}\frac{H^2}{M_{\rm pl}^2} \,. \tag{2.62}$$

Then the tensor-scalar ratio can be written

$$r = \frac{\Delta_t^2(k)}{\Delta_\zeta^2(k)} = 16\epsilon_0 \times f^{-1}(\hat{\mu}, \hat{m}) \,. \tag{2.63}$$

$m_\phi^2\phi^2$ inflation

Here we use the model where the inflaton potential $V_\phi = m_\phi^2\phi^2/2$ as an example to discuss the effect of large μ/H on the observables. In this simple model, we have

$$\phi_{cmb} = 2\sqrt{N_{cmb}} M_{\rm pl} \simeq 15 M_{\rm pl} \,. \tag{2.64}$$

and

$$\epsilon_0 \simeq 2\left(\frac{M_{\rm pl}}{\phi_{cmb}}\right)^2 \simeq \frac{1}{2N_{cmb}} \,, \quad \eta_0 \simeq O\left(N_{cmb}^{-2}\right) \,, \tag{2.65}$$

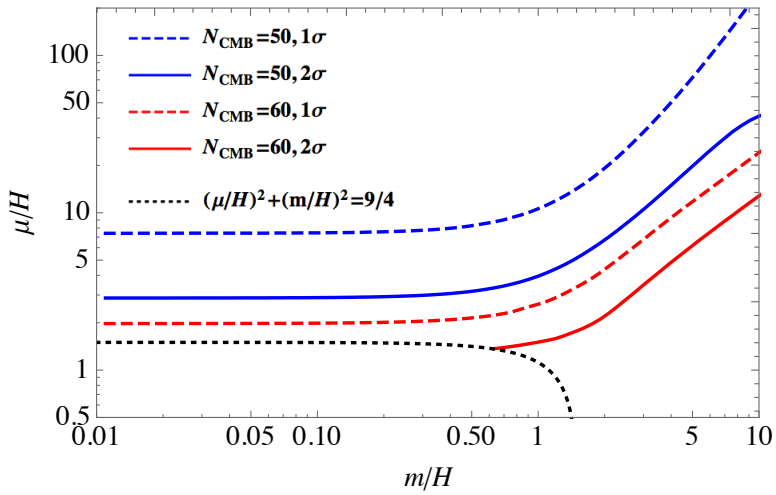

Figure 2.6: Constraints on the $m - \mu$ parameter space from the combination of the Planck data and the BICEP/Keck data [45], where the blue curves are for $N_{CMB} = 50$ and the red curves $N_{CMB} = 60$. The regions above the curves are allowed.

where N_{cmb} is the number of e-folds between when CMB scale leaves the horizon and when slow roll inflation ends.

The n_S, r plot for this model is shown in Fig. 2.5. The dotted regions are for μ from 0 to $100H$ and m from 0 to $6H$ with $(\mu/H)^2 + (m/H)^2 > 9/4$. On these curves as μ increases r decreases, so the uppermost point of the curves corresponds to standard slow roll inflation. The constraints on the $m - \mu$ parameter space for $N_{CMB} = 50$ and 60 are also shown in Fig. 2.6 where the regions below the curves are excluded. Clearly larger values of μ improve the agreement of the model's predictions with the measured value of n_S and the bound on r.

Time-Dependent S Background

We now justify that the time-dependent vaccuum expectation value of S/Λ remains small and evolves slowly enough in $m_\phi^2\phi^2$ inflation that it can be ignored in the above computation of the tilt and tensor-scalar ratio.

Denote the background vevs of the inflaton and isocurvaton fields as $\phi = \phi_0(t)$ and $S = S_0(t)$. The Lagrangian describing the vevs is

$$\mathcal{L} = \frac{1}{2}\dot{\phi}_0^2\left(1 + \frac{2S_0}{\Lambda}\right) + \frac{1}{2}\dot{S}_0^2 + \frac{1}{2}m_\phi^2\phi_0^2 + \frac{1}{2}m^2S_0^2 + V_S'S_0 \tag{2.66}$$

From this Lagrangian, it is straightforward to compute the coupled equations of motion for ϕ_0 and S_0, as well as the Friedmann equation. From these equations, one

can determine the slow roll parameters:

$$\epsilon \equiv -\frac{\dot{H}}{H^2} = \frac{1}{2H^2 M_{\rm pl}^2}\left(\dot{\phi}_0^2\left(1+\frac{2S_0}{\Lambda}\right)+\dot{S}_0^2\right) \tag{2.67}$$

$$\eta \equiv \epsilon - \frac{1}{2}\frac{d\log\epsilon}{dN} = -\frac{\ddot{\phi}_0}{H\dot{\phi}_0} - \frac{1}{2}\partial_N\left(1+\frac{2S_0}{\Lambda}+\frac{\dot{S}_0^2}{\dot{\phi}_0^2}\right) \tag{2.68}$$

Moreover, from the equation of motion for S_0, we find up to slow roll suppressed corrections

$$\frac{\dot{S}_0}{\Lambda H} \simeq -\frac{1}{2}\left(\frac{2\dot{\phi}_0}{\Lambda m}\right)^2\left(-\frac{\ddot{\phi}_0}{H\dot{\phi}_0}\right) \tag{2.69}$$

Note that the first term in parentheses is essentially $(\mu/m)^2$, and the second term is η_0. Then to estimate the size of $\dot{S}_0/\Lambda H$, it will be necessary to determine the size of η_0 in this theory. From (2.68) and (2.69), we can express:

$$\eta \simeq \eta_0\left(1+\frac{1}{2}\left(\frac{\mu}{m}\right)^2\right) \tag{2.70}$$

In terms of the slow roll parameters, the Friedmann equation can be written:

$$(3-\epsilon)H^2 M_{\rm pl}^2 = \frac{1}{2}m_\phi^2\phi_0^2 \tag{2.71}$$

where we have assumed that ϕ drives inflation, *i.e.* the potential for ϕ_0 dominates over the potential for S_0. Taking derivatives of the above equation, we find the following two expressions:

$$-\frac{\dot{\phi}_0}{H\phi_0} = \epsilon\left(\frac{1-\eta/3}{1-\epsilon/3}\right) \tag{2.72}$$

$$2\eta-\eta_0 = \frac{\epsilon}{3}\left(\frac{\epsilon-\eta}{1-\epsilon/3}\right)+\frac{d\log(1-\eta/3)}{dN} \tag{2.73}$$

This second equation can be written using (2.70):

$$\eta\left(\frac{1+\left(\frac{\mu}{m}\right)^2}{\frac{1}{2}+\left(\frac{\mu}{m}\right)^2}\right) \simeq \frac{\epsilon}{3}\left(\frac{\epsilon-\eta}{1-\epsilon/3}\right)+\frac{d\log(1-\eta/3)}{dN} \tag{2.74}$$

From (2.72), one can show that to leading order, we still have $\epsilon \simeq (2N_{cmb})^{-1}$. On the other hand, by solving (2.74) perturbatively in ϵ and η, one can show that the leading contribution to η goes like N_{cmb}^{-2} [46]:

$$\eta \simeq \frac{1}{12N_{cmb}^2}\left(\frac{\frac{1}{2}+\left(\frac{\mu}{m}\right)^2}{1+\left(\frac{\mu}{m}\right)^2}\right) \tag{2.75}$$

We can determine η_0 using (2.70) and (2.75). Then (2.69) becomes

$$\frac{\dot{S}_0}{\Lambda H} \simeq -\frac{1}{24N_{cmb}^2}\frac{\mu^2}{m^2+\mu^2} \tag{2.76}$$

Since $\dot{S}_0/\Lambda H \ll \epsilon$, the evolution of S_0 will not significantly affect the tilt. Moreover, as long as $S_0 = 0$ at some point early on in inflation, S_0/Λ will still be very small during CMB mode crossings. Accordingly, S_0/Λ will not significantly affect the tensor-scalar ratio.

It is worth noting that $\eta = O(N_{cmb}^{-2})$ is specific to $m_\phi^2\phi^2$ inflation, and not general. In general, η goes like N_{cmb}^{-1}, and the time-dependence of S_0 becomes equally important as the ϵ terms in computing the tilt. In computing these effects, it is important to recognize that for nonzero S_0, the power spectrum gets normalized slightly differently:

$$P_\zeta(k) = \frac{H^4}{2\dot{\phi}_0^2(1+2S_0/\Lambda)k^3} f(\mu/H, m/H) \tag{2.77}$$

and μ is defined as

$$\mu = \frac{2\dot{\phi}_0}{\Lambda\,(1+2S_0/\Lambda)^{1/2}} \tag{2.78}$$

Using these facts, it is straightforward to compute the tilt once $\dot{S}_0/\Lambda H$ is computed from the equations of motion.

2.6 Non-Gaussianities

In this section we calculate the dependence of the inflaton three-point function as a function of μ and m. The small μ/H behavior of the bispectrum was first studied in [15]. The effective field theory for large μ/H was used to compute the contribution from the $\partial\pi\partial\pi s$ interaction to the bispectrum [37, 41]. Here we use the numerical mode functions to extend the analysis to other values of μ.

The curvature perturbation bispectrum $B_\zeta(\mathbf{k}_1, \mathbf{k}_2, \mathbf{k}_3)$ is defined by

$$\begin{aligned}\langle\zeta(\mathbf{x}_1,0)\zeta(\mathbf{x}_2,0)\zeta(\mathbf{x}_3,0)\rangle = \int \frac{d^3k_1}{(2\pi)^3}\frac{d^3k_2}{(2\pi)^3}\frac{d^3k_3}{(2\pi)^3} e^{i(\mathbf{k}_1\cdot\mathbf{x}_1+\mathbf{k}_2\cdot\mathbf{x}_2+\mathbf{k}_3\cdot\mathbf{x}_3)} B_\zeta(\mathbf{k}_1,\mathbf{k}_2,\mathbf{k}_3) \\ \times (2\pi)^3\delta^3(\mathbf{k}_1+\mathbf{k}_2+\mathbf{k}_3)\end{aligned} \tag{2.79}$$

and we can define $B_\pi(\mathbf{k}_1, \mathbf{k}_2, \mathbf{k}_3)$ analogously. They can be computed using the in-in formalism [47] using the interaction Lagrangian in eq. (2.13).

In this section we focus mostly on the $O(V_S''')$ term (where $V_S''' \equiv V_S'''(S_0)$) which, for $V_S''' \sim O(H)$, typically dominates over the contribution from the $\partial\pi\partial\pi s$ term. We express the $O(V_S''')$ contribution to the bispectrum in terms of the mode functions discussed earlier. Evaluating the correlator in the far future $\tau = 0$, we find

$$B_\pi(\mathbf{k}_1, \mathbf{k}_2, \mathbf{k}_3) = -2V_S''' H^{-4} \mathrm{Im}\left[\int_{-\infty}^{0} \frac{d\tau}{\tau^4} \prod_{i=1}^{3} \left(\pi_{k_i}^{(1)*}(0) s_{k_i}^{(1)}(k_i\tau) + \pi_{k_i}^{(2)*}(0) s_{k_i}^{(2)}(k_i\tau)\right)\right]. \tag{2.80}$$

Equation (2.80) is true for all values of k_i, however we are mostly interested in its behavior in the so-called equilateral and squeezed limits. In the equilateral limit, the external momenta all have equal magnitude $k_i \equiv k$. In this case, the integral's dependence on k can be factored out of the integral by rescaling the integration variable from τ to $\eta = k\tau$:[5]

$$B_\pi^{\mathrm{equil}}(k) = -2V_S''' H^{-4} k^3 \mathrm{Im}\left[\int_{-\infty}^{0} \frac{d\eta}{\eta^4} \left(\pi_k^{(1)*}(0) s_k^{(1)}(\eta) + \pi_k^{(2)*}(0) s_k^{(2)}(\eta)\right)^3\right] \tag{2.81}$$

We can compute this integral numerically using the numeric mode functions, but there are a couple of subtleties in its evaluation that need to be addressed. The integrand in (2.81) is highly oscillatory at large τ. For m/H and μ/H values of order one or larger, the magnitude of these oscillations does not decay quickly and it becomes difficult to perform the numerical integrations by brute force. We can alleviate this problem by Wick rotating the integral, thereby transforming the rapid oscillations into exponential decay.

Before Wick rotating it is convenient to factor out the oscillatory behavior from the mode functions. The large τ limit given in eq. (2.32) suggests that we should extract the oscillatory behavior by factorizing the mode functions as $\pi_k^{(i)}(\eta) = A_k^{(i)}(\eta) e^{-i\eta}$ and $s_k^{(i)}(\eta) = B_k^{(i)}(\eta) e^{-i\eta}$. Plugging this factorization into $B_\pi^{\mathrm{equil}}(k)$ gives

$$\begin{aligned} B_\pi^{\mathrm{equil}}(k) &= -2V_S''' H^{-4} k^3 \mathrm{Im}\left[\int_{-\infty}^{0} \frac{d\eta}{\eta^4} e^{-3i\eta} \left(\pi_k^{(1)*}(0) B_k^{(1)}(\eta) + \pi_k^{(2)*}(0) B_k^{(2)}(\eta)\right)^3\right] \\ &= -2V_S''' H^{-4} k^3 \mathrm{Re}\left[\int_{-\infty}^{0} \frac{dx}{x^4} e^{3x} \left(\pi_k^{(1)*}(0) B_k^{(1)}(ix) + \pi_k^{(2)*}(0) B_k^{(2)}(ix)\right)^3\right]. \end{aligned} \tag{2.82}$$

In the second line we used Cauchy's theorem to rotate the region of integration from the real to the imaginary axis and changed the integration variable from η to $x = -i\eta$.

[5] By, $B_\pi^{equil}(k)$, we mean B_π evaluated in the equilateral configuration where the three wavevectors have the same magnitude k.

The numerical solutions found previously for $A_k^{(i)}(\eta)$ and $B_k^{(i)}(\eta)$ are functions of the real variable η and cannot be integrated along the imaginary axis. However, we can analytically continue them to the imaginary axis by Wick rotating the original mode equations (2.28) and (2.29) (see [42]). After factoring out the oscillatory behavior and changing variables to $x = -i\eta$, we find that the analytically continued functions $A_k^{(i)}$ and $B_k^{(i)}$ obey

$$x^2 A_k''(ix) + (2x^2 - 2x)A_k'(ix) - 2xA_k(ix) - \frac{\mu}{H}xB_k'(ix) + (3-x)\frac{\mu}{H}B_k(ix) = 0 \tag{2.83}$$

$$x^2 B_k''(ix) + (2x^2 - 2x)B_k'(ix) + \left(\frac{m^2}{H^2} - 2x\right)B_k(ix) + \frac{\mu}{H}xA_k'(ix) + \frac{\mu}{H}xA_k(ix) = 0 \tag{2.84}$$

where a prime denotes a derivative with respect to x and we have dropped the superscripts for simplicity. The solutions should asymptote at large $-x$ to[6]

$$\begin{aligned} A_k^{(1)}(ix) &= \frac{H}{2k^{3/2}}(-ix)^{1+i\mu/2H} \quad A_k^{(2)}(ix) = \frac{H}{2k^{3/2}}(-ix)^{1-i\mu/2H} \\ B_k^{(1)}(ix) &= \frac{iH}{2k^{3/2}}(-ix)^{1+i\mu/2H} \quad B_k^{(2)}(ix) = \frac{-iH}{2k^{3/2}}(-ix)^{1-i\mu/2H}. \end{aligned} \tag{2.85}$$

These solutions and their derivatives with respect to x give the initial conditions for numerical integration of the differential equations for A_k and B_k. Note that $A_k^{(i)}$ and $B_k^{(i)}$ contain an overall factor of $k^{-3/2}$. Moreover, $\pi_k^{(i)}$ and $s_k^{(i)}$ have the same k-dependent normalization. This implies that $B_\zeta^{\text{equil}}(k)/\mathcal{P}_\zeta^{\text{equil}}(k)^2$ is k-independent.

In figures 2.7 and 2.8, we plot the contributions to the scaled equilateral three-point functions $B_\zeta^{equil}(k)/(\mathcal{P}_\zeta(k))^2$ due to the $\partial\pi\partial\pi s$ and s^3 interaction terms respectively[7]. Moreover, we have superimposed a dotted line which corresponds to the prediction of the effective field theory appropriate for large μ/H (which will be discussed in detail in section 2.7). Of course, the numerical results converge to the effective field theory results in the large μ/H limit. However, the effective field theory is only a good approximation of these non-gaussianities for $\mu \gtrsim 10H$. This further suggests that there is a substantial portion of the parameter space in μ that is described neither by the large μ/H effective theory description nor the small μ/H perturbative description.

[6] If we hadn't first extracted the oscillatory factor, an exponentially suppressed factor would have appeared in (2.85) that would have made the boundary conditions too small to solve (2.83) numerically.

[7] For brevity we have not described in any detail the calculation of the contribution due to the $s\partial\pi\partial\pi$ term in this section.

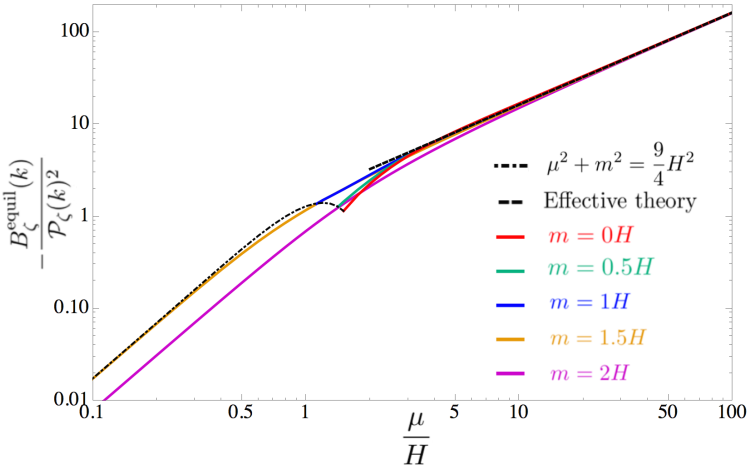

Figure 2.7: The scaled equilateral three-point function due to the $s\dot{\partial}\pi\partial\pi$ interaction, $B_\zeta^{\rm equil}(k)/\mathcal{P}_\zeta(k)^2$ as a function of μ/H. Several values of m are plotted: $m = 0$, $0.5H$, H, $1.5H$, and $2H$, and there is also a black dashed line representing the result computed in the large μ/H effective theory.

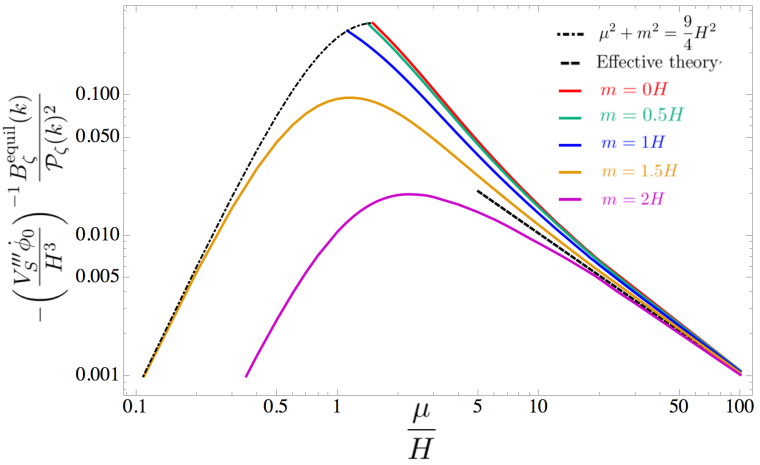

Figure 2.8: The scaled equilateral three-point function due to the s^3 interaction, $B_\zeta^{\rm equil}(k)/\mathcal{P}_\zeta(k)^2$ as a function of μ/H. Several values of m are plotted: $m = 0$, $0.5H$, H, $1.5H$, and $2H$, and there is also a black dashed line representing the result computed in the large μ/H effective theory.

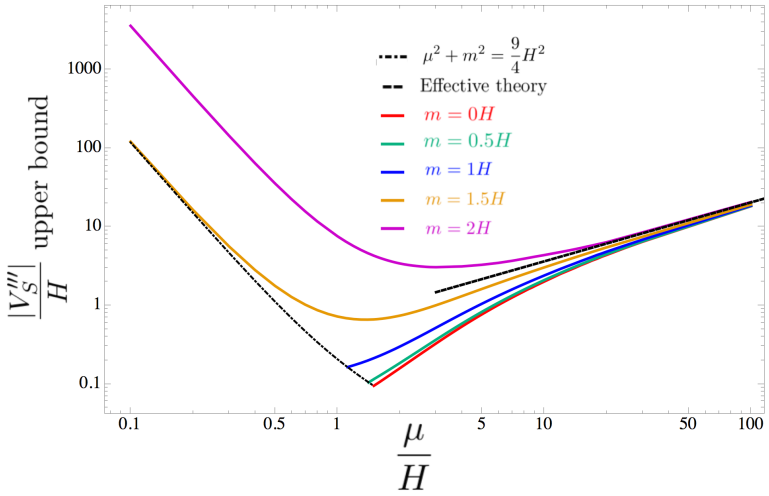

Figure 2.9: Upper bounds on $|V_S'''|$ as a function of μ/H. These bounds are imposed by experimental bounds on $f_{\rm NL}^{\rm equil}$. Bounds are plotted for $m = 0$, $0.5H$, H, $1.5H$, and $2H$. There is also a bound computed from the large μ/H effective theory, shown in the figure as a black dashed line.

The Planck collaboration has derived constraints on the magnitude of the bispectrum of the curvature perturbations using various models/templates for its dependence on the wavevectors [14]. These are usually expressed in terms of the quantity $f_{\rm NL}$. Although the model we are discussing is different from the equilateral model/template used to derive the constraint $f_{\rm NL}^{\rm equil} = 4 \pm 43$ by the Planck collaboration in Ref. [14], we use this constraint to estimate a bound on V_S'''. Furthermore we estimate f_{NL}^{equil} using just the equilateral configuration where the three wavevectors have the same magnitude taking,

$$f_{\rm NL}^{equil} \simeq \frac{5}{18} \times \frac{B_\zeta^{equil}(k)}{(\mathcal{P}_\zeta(k))^2}. \tag{2.86}$$

To determine upper bounds for V_S''' we assume that each interaction s^3 and $s\partial\pi\partial\pi$ is separately constrained by $f_{\rm NL}^{\rm equil}$ and thus ignore any possible tuning between the two terms that may make these bounds weaker. Figure 2.9 shows the 2σ upper bounds for a variety of s masses, as well as the upper bound predicted in the large μ/H effective theory.

The squeezed limit of (2.80) occurs when $k_1 \approx k_2 \equiv k \gg k_3$. In this limit, define the ratio $c \equiv k_3/k$, where $c \ll 1$, and introduce the notation $B_\pi^{sq}(k, c)$ for B_π. We

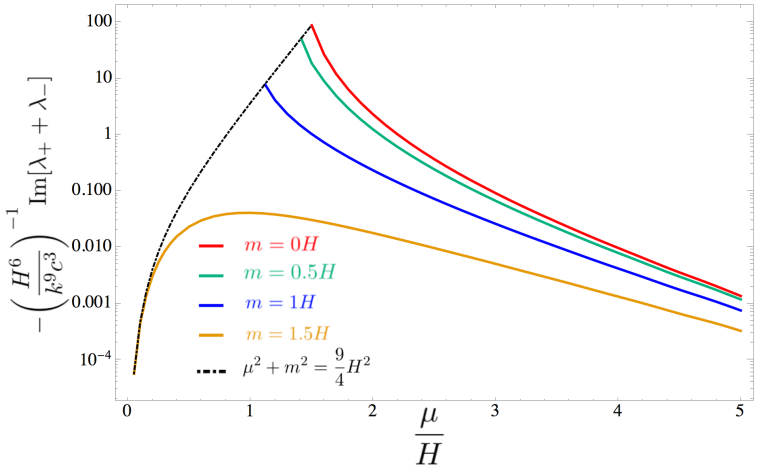

Figure 2.10: The coefficients of the cosine term in equation (2.90) for $m = 0$, $0.5H$, H, and $1.5H$.

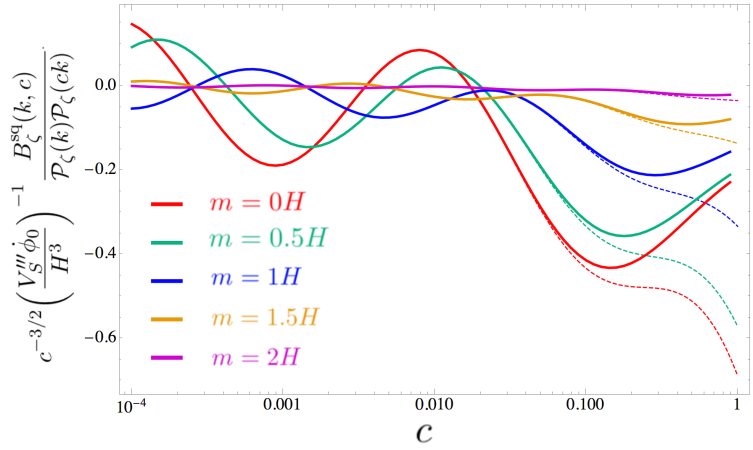

Figure 2.11: In the squeezed limit, the three-point function logarithmically oscillates as a function of c. This behavior is illustrated for $\mu = 2H$ and $m = 0$, $0.5H$, H, $1.5H$, and $2H$. The solid lines show the exact behavior as a function of c (*i*.e. using equation (2.87)) whereas the dotted lines show the approximate behavior to quadratic order in c (*i*.e. using equation (2.88)).

again rescale the integration variable to $\eta = k\tau$ to find

$$B_\pi^{sq}(k,c) = -2V_S'''' H^{-4} k^3 \mathrm{Im}\Bigg[\int_{-\infty}^{0} \frac{d\eta}{\eta^4} \left(\pi_k^{(1)*}(0) s_k^{(1)}(\eta) + \pi_k^{(2)*}(0) s_k^{(2)}(\eta)\right)^2 \times \left(\pi_{ck}^{(1)*}(0) s_{ck}^{(1)}(c\eta) + \pi_{ck}^{(2)*}(0) s_{ck}^{(2)}(c\eta)\right) \Bigg]$$

$$= -2V_S'''' H^{-4} k^3 c^{-3} \mathrm{Im}\Bigg[\int_{-\infty}^{0} \frac{d\eta}{\eta^4} \left(\pi_k^{(1)*}(0) s_k^{(1)}(\eta) + \pi_k^{(2)*}(0) s_k^{(2)}(\eta)\right)^2 \times \left(\pi_k^{(1)*}(0) s_k^{(1)}(c\eta) + \pi_k^{(2)*}(0) s_k^{(2)}(c\eta)\right) \Bigg] \tag{2.87}$$

We can analyze the leading behavior of (2.87) in c by replacing $s_k^{(i)}(c\eta)$ with the first few terms of its power series expansion (see section 2.4) $b_-^{(i)}(-c\eta)^{\alpha_-} + b_+^{(i)}(-c\eta)^{\alpha_+} + b_2^{(i)}(-c\eta)^2$:

$$\begin{aligned} B_\pi^{\mathrm{sq}}(k,c) &= -2V_S'''' H^{-4} k^3 c^{-3} \mathrm{Im}\Bigg[\int_{-\infty}^{0} \frac{d\eta}{\eta^4} \left(\pi_k^{(1)*}(0) s_k^{(1)}(\eta) + \pi_k^{(2)*}(0) s_k^{(2)}(\eta)\right)^2 \\ &\qquad \times \left(\beta_-(-c\eta)^{\alpha_-} + \beta_+(-c\eta)^{\alpha_+} + \beta_2(-c\eta)^2 + \dots\right) \Bigg] \\ &= V_S'''' H^{-4} k^3 c^{-3} \mathrm{Im}\left[c^{\alpha_-}\lambda_-(\mu,m) + c^{\alpha_+}\lambda_+(\mu,m) + c^2\lambda_2(\mu,m)\right] \end{aligned} \tag{2.88}$$

where $\beta_- = \pi_k^{(1)*}(0) b_-^{(1)} + \pi_k^{(2)*}(0) b_-^{(2)}$, $\beta_+ = \pi_k^{(1)*}(0) b_+^{(1)} + \pi_k^{(2)*}(0) b_+^{(2)}$, $\beta_2 = \pi_k^{(1)*}(0) b_2^{(1)} + \pi_k^{(2)*}(0) b_2^{(2)}$ and

$$\begin{aligned} \lambda_-(\mu,m) &= -2\beta_- \int_{-\infty}^{0} \frac{d\eta}{\eta^4} \left(\pi_k^{(1)*}(0) s_k^{(1)}(\eta) + \pi_k^{(2)*}(0) s_k^{(2)}(\eta)\right)^2 (-\eta)^{\alpha_-} \\ \lambda_+(\mu,m) &= -2\beta_+ \int_{-\infty}^{0} \frac{d\eta}{\eta^4} \left(\pi_k^{(1)*}(0) s_k^{(1)}(\eta) + \pi_k^{(2)*}(0) s_k^{(2)}(\eta)\right)^2 (-\eta)^{\alpha_+} \\ \lambda_2(\mu,m) &= -2\beta_2 \int_{-\infty}^{0} \frac{d\eta}{\eta^4} \left(\pi_k^{(1)*}(0) s_k^{(1)}(\eta) + \pi_k^{(2)*}(0) s_k^{(2)}(\eta)\right)^2 (-\eta)^2. \end{aligned} \tag{2.89}$$

We can compute β_-, β_+, and β_2 by fitting the numerical mode functions $s_k^{(i)}(\eta)$ to their power series expansions at small $-\eta$ and extracting $b_\pm^{(i)}$, $b_2^{(i)}$ from the fits. The integrals in (2.89) can be computed using the same Wick rotation technique used to

compute $B_\pi^{\rm equil}$. Then, rearranging (2.88) gives

$$\begin{aligned} B_\pi^{\rm sq} = V_S''' H^{-4} k^3 c^{-3/2} \\ \times \left(\mathrm{Im}\left[\lambda_+ + \lambda_-\right] \cos\left(\log(c) \mathrm{I}m\left[\alpha_+\right]\right)\right. \\ \left. + \mathrm{Re}\left[\lambda_+ - \lambda_-\right] \sin\left(\log(c) \mathrm{I}m\left[\alpha_+\right]\right) + c^{1/2} \mathrm{Im}\left[\lambda_2\right]\right) \end{aligned} \tag{2.90}$$

We plot $\mathrm{Im}\left[\lambda_+ + \lambda_-\right]$ in figure 2.10. The sine term is usually smaller and so we have not displayed it in a figure. Equation (2.90) shows that the squeezed limit of the three-point function oscillates logarithmically as a function of c. This behavior is illustrated in figure 2.11. Note that that the dependence of $\mathrm{I}m\left[\alpha_+\right] = \sqrt{m^2/H^2 + \mu^2/H^2 - 9/4}$ on μ has an important effect on the oscillations. This impacts the two point function of biased objects, see for example [48].

The oscillatory terms in eq. (2.90) are enhanced by a factor of $c^{-1/2}$, but are suppressed in the large μ/H limit.

2.7 Calculating non-gaussianity in the effective theory

Brief review of the effective theory for large μ/H

In this subsection we begin with a brief review the effective theory approach to the case when μ/H is large. In terms of π and s the Lagrange density is

$$\begin{aligned} \mathcal{L} &= \frac{1}{2H^2\tau^2}\left[(\partial_\tau\pi)^2 - (\nabla\pi)^2 + (\partial_\tau s)^2 - (\nabla s)^2 - \frac{m^2}{H^2}\frac{s^2}{\tau^2} - \frac{2\mu}{H\tau} s\partial_\tau\pi\right] \\ &\quad + \frac{1}{H^2\tau^2}\frac{s}{\Lambda}\left[(\partial_\tau\pi)^2 - (\nabla\pi)^2\right] - \frac{1}{H^4\tau^4}\frac{V_S'''' s^3}{3!} \end{aligned} \tag{2.91}$$

As discussed in Sec. 2.3, in flat space-time with large mixing μ there is a very massive mode and a massless mode. When $\mu \gg H$ and $k/a < \mu$, one may integrate out the heavy mode to get an effective theory just involving π which can be used to calculate curvature perturbations. As discussed in Sec. 2.4, for that purpose the $(\partial_\tau s)^2$ and $(\partial_\tau\pi)^2$ terms in eq. (2.91) can be neglected. Since we assume $m \sim O(H)$ or smaller m can also be neglected in eq. (2.91). With these approximations the equation of motion for s becomes

$$0 = \frac{\delta\mathcal{L}}{\delta s} = \frac{1}{H^2\tau^2}\left[\nabla^2 s - \frac{\mu\partial_\tau\pi}{H\tau} - \frac{1}{\Lambda}(\nabla\pi)^2 - \frac{V_S'''' s^2}{2H^2\tau^2}\right] . \tag{2.92}$$

Up the second order in π, the solution for s is

$$s = \frac{\mu}{H\tau}\frac{1}{\nabla^2}\partial_\tau\pi + \frac{1}{\Lambda}\frac{1}{\nabla^2}(\nabla\pi)^2 + \frac{V_S''''}{2H^2\tau^2}\frac{\mu^2}{H^2\tau^2}\frac{1}{\nabla^2}\left[\frac{1}{\nabla^2}\partial_\tau\pi\right]^2 \tag{2.93}$$

Putting this solution back into eq. (2.91), the quadratic and cubic terms of the effective Lagrangian of π can be written as

$$\mathcal{L}^{(2)}_{eff} = -\frac{1}{2H^2\tau^2}\left[(\nabla\pi)^2 + \frac{\mu^2}{H^2\tau^2}(\partial_\tau\pi)\nabla^{-2}\partial_\tau\pi\right] \tag{2.94}$$

and

$$\mathcal{L}^{(3)}_{eff} = -\frac{\mu}{\Lambda}\frac{1}{H^3\tau^3}\left[\nabla^{-2}\partial_\tau\pi\right]\left[(\nabla\pi)^2\right] - \frac{\mu^3}{H^7\tau^7}\frac{V_S'''}{3!}\left[\nabla^{-2}\partial_\tau\pi\right]^3 . \tag{2.95}$$

Quantizing the free field part of this effective theory we write for the field operator,

$$\pi(\mathbf{x},\tau) = \int \frac{d^3k}{(2\pi)^3}\left(a(\mathbf{k})\pi_k(\eta)e^{i\mathbf{k}\cdot\mathbf{x}} + a^\dagger(\mathbf{k})\pi_k(\eta)^* e^{-i\mathbf{k}\cdot\mathbf{x}}\right). \tag{2.96}$$

The mode function $\pi_k(\eta)$ satisfies the classical equation of motion,

$$\frac{\mu^2}{H^2}\frac{d}{d\eta}\left(\frac{1}{\eta^4}\frac{d\pi_k}{d\eta}\right) + \frac{\pi_k}{\eta^2} = 0 . \tag{2.97}$$

which can be solved analytically for the mode function $\pi_k(\eta)$. The normalization of $\pi_k(\eta)$ is determined by the canonical commutation relations. This yields,

$$\pi_k(\eta) = \left(\frac{2\pi^2\mu}{H}\right)^{1/4}\frac{H}{(2k^3)^{1/2}}\left(\frac{\eta^2 H}{2\mu}\right)^{5/4} H^{(1)}_{5/4}\left(\frac{\eta^2 H}{2\mu}\right) . \tag{2.98}$$

The power spectrum of the curvature perturbation is

$$\mathcal{P}_\zeta = \frac{H^2}{\dot\phi_0^2}|\pi_k(\eta)|^2_{|\eta|\ll\sqrt{\mu/H}} = \frac{H^4}{\dot\phi_0^2}\left(\frac{1}{2k^3}\right)\left[\frac{16\pi}{\Gamma^2(-1/4)}\left(\frac{\mu}{H}\right)^{1/2}\right] . \tag{2.99}$$

This result was originally derived in Ref. [37, 41].

The plot of $\mathcal{P}_\zeta$ as a function of μ/H was shown in Fig. 2.1. The result from the effective theory is shown by the black dashed line. One can see that for $\mu > 10H$ the result from the effective theory agrees with the numerical result.

Non-Gaussianity of equilateral configuration

The three-point function $B_\zeta(\mathbf{k}_1,\mathbf{k}_2,\mathbf{k}_3)$ of the curvature perturbation is defined in (2.79). Following standard steps and using the explicit expression of π_k in (2.98) for the equilateral configuration ($|\mathbf{k}_1| = |\mathbf{k}_2| = |\mathbf{k}_3| = k$), we have

$$B^{equil}_\zeta(k) = -\frac{6\mu}{\Lambda}\frac{H^6}{\dot\phi_0^3 k^6}\frac{2^{5/4}\pi^3}{\Gamma^3(-1/4)}\mathcal{B}_1 - \frac{V_S'''}{H}\frac{H^6}{\dot\phi_0^3 k^6}\frac{2^{9/4}\pi^3}{\Gamma^3(-1/4)}\mathcal{B}_2 , \tag{2.100}$$

where

$$\mathcal{B}_1 = \mathrm{R}e\int_0^\infty dx x^{5/4}\left[H^{(1)}_{5/4}(x)\right]^3 \simeq -0.94$$
$$\mathcal{B}_2 = \mathrm{R}e\int_0^\infty dx x^{-5/2}\left[\frac{d}{dx}\left(x^{5/4}H^{(1)}_{5/4}(x)\right)\right]^3 \simeq -0.09. \quad (2.101)$$

As previously discussed we take

$$f^{equil}_{\rm NL} \simeq \frac{5}{18}\times\frac{B^{equil}_\zeta(k)}{(\mathcal{P}_\zeta(k))^2} = -\frac{5}{3}\times 2^{-23/4}\pi\Gamma(-1/4)\left[\mathcal{B}_1\frac{\mu}{H}+\frac{2}{3}\mathcal{B}_2\frac{V'''_S}{\mu}\frac{\dot\phi_0}{H^2}\right]$$
$$\simeq -0.45\times\frac{\mu}{H}-0.03\times\frac{V'''_S}{\mu}\frac{\dot\phi_0}{H^2}\,. \quad (2.102)$$

The factor $\dot\phi_0/H$ can be calculated in terms of the density perturbation and μ/H using (2.53). Using the measured value of Δ_ζ we have that

$$f^{equil}_{\rm NL} \simeq -0.45\times\frac{\mu}{H}-140\times\frac{V'''_S}{H}\left(\frac{H}{\mu}\right)^{3/4}. \quad (2.103)$$

In addition, using the Planck data, the 2σ constraint on μ is estimated to be[8]

$$\mu/H < 200\,. \quad (2.104)$$

Non-gaussianity of squeezed configuration

For the squeezed configuration we consider $k = k_1 \simeq k_2 \gg k_3 = ck$. Taking the contribution from the $1/\Lambda$ term in the interaction Lagrange density we have

$$B^{sq}_\zeta(k,c) = -\frac{4H^6}{\dot\phi_0^3}\frac{\mu}{\Lambda}\frac{1}{c^3k^6}\frac{\pi^3 2^{9/4}}{\Gamma^3(-1/4)}(\mathcal{B}_3+\mathcal{B}_4)\,, \quad (2.105)$$

where

$$\mathcal{B}_3 = \mathrm{R}e\int_0^\infty dx\, x[H^{(1)}_{5/4}(x)]^2\,\frac{d}{dy}\left[y^{5/4}H^{(1)}_{5/4}(y)\right]\Big|_{y\to c^2x} \quad (2.106)$$
$$\mathcal{B}_4 = \mathrm{R}e\int_0^\infty dx\, xH^{(1)}_{1/4}(x)H^{(1)}_{5/4}(x)\left[c^2y^{5/4}H^{(1)}_{5/4}(y)\right]\Big|_{y\to c^2x}\,. \quad (2.107)$$

Note that $H^{(1)}_{5/4}(x)$ and $H^{(1)}_{1/4}(x)$ oscillate rapidly when $x > 1$. Therefore, the integral is mainly supported in the region $x < 1$, which means $c^2x \ll 1$. Around $y = 0$ we have

$$y^{5/4}H^{(1)}_{5/4}(y) = -\frac{2^{5/4}i}{\pi}\Gamma(5/4) - \frac{2^{5/4}i}{\pi}\Gamma(5/4)y^2 + \mathrm{h}igher\ orders\,, \quad (2.108)$$

[8]Here we have neglected the V'''_S term. It is of course possible that there are cancelations between the contribution proportional to μ and that proportional to V''' which would relax the bound on μ.

which implies that

$$\frac{d}{dy}\left[y^{5/4}H^{(1)}_{5/4}(y)\right]\Big|_{y\to c^2x} = -\frac{2^{9/4}ic^2}{\pi}\Gamma(5/4)x + \mathrm{h}igher\ orders\ . \tag{2.109}$$

For $c \ll 1$, $\mathcal{B}_3$ and $\mathcal{B}_4$ go like c^2 and we have that in the squeezed limit $B^{\rm sq}_\zeta \sim c^{-1}$. Even though this contribution is enhanced by a power of $1/c$, it is still suppressed compared to what local non-gaussianity would give which is proportional to $\mathcal{P}_\zeta(k_1)\mathcal{P}_\zeta(k_2) + \mathcal{P}_\zeta(k_2)\mathcal{P}_\zeta(k_3) + \mathcal{P}_\zeta(k_3)\mathcal{P}_\zeta(k_1) \sim c^{-3}$. This c^{-1} behavior in the squeezed limit is also seen in equilateral non-Gaussianity.

For the contribution proportional to V'''_S we find

$$B^{\rm sq}_\zeta(k,c) = -\frac{V'''_S}{H}\frac{H^6}{\dot\phi_0^3}\frac{1}{c^3k^6}\frac{\pi^3 2^{9/4}}{\Gamma^3(-1/4)}\mathcal{B}_5\ , \tag{2.110}$$

where in this case

$$\mathcal{B}_5 = \mathrm{R}e\int_0^\infty dx\ \left[H^{(1)}_{1/4}(x)\right]^2\left[\frac{d(y^{5/4}H^{(1)}_{5/4}(y))}{dy}\right]\Big|_{y\to c^2x} \tag{2.111}$$

Therefore, the V'''_S interaction also gives a c^{-1} contribution to $B^{\rm sq}_\zeta$.

2.8 Concluding Remarks

We studied a simple quasi-single field inflation model where the inflaton couples to another scalar field S. The model contains an unusual mixing term between the inflaton and the new scalar characterized by a dimensionful parameter μ. It has been extensively studied in the literature using perturbation theory in the region where the parameter μ/H is small and using an effective field theory approach in the region of large μ/H. It has also been studied using numerical methods in other regions of parameter space. When the mass parameter m of the additional scalar field is zero perturbation theory diverges.

We numerically calculated the power spectrum and the bispectrum of the curvature perturbations when μ and the mass m satisfy $(\mu/H)^2+(m/H)^2 > 9/4$ with $m \sim O(H)$ or smaller. In much of this region, perturbation theory and the effective field theory approach are not applicable. We found that typically the effective field theory approach is valid for $\mu/H > 10$. The numerical approach is non-perturbative in μ/H and there are no divergences at $m = 0$. This occurs because the heavy mode has mass $\sqrt{m^2+\mu^2}$ which does not vanish as $m \to 0$.

In the case where the inflaton potential is $m_\phi^2\phi^2/2$, we derived constraints on the parameters m and μ from n_S and r for $N_{cmb} = 50$ and $N_{cmb} = 60$. Larger values of μ make this inflaton potential more compatible with the data.

We computed the contributions from the $\partial\pi\partial\pi s$ and the s^3 interactions to the equilateral limit of the bispectrum of the curvature perturbations numerically and compared it with the results from the effective theory. Using these results and the Planck bounds on f_{NL} we derived upper bounds on V_S''' and μ.

We also analyzed the squeezed limit of the bispectrum, showing that in this model it is much smaller than for local non-gaussianity. The contribution to the squeezed bispectrum proportional to V_S''' exhibits interesting oscillatory behavior as a function of the ratio of the small momenta to the larger one.[9] We noted that the oscillation wavelength has μ dependence that is not evident in perturbation theory. This behavior could potentially be observed in future experiments.

For small μ and m, there are potentially interesting observational consequences of the behavior of the four point function on the wavevectors that characterize its shape. We will present results on this in a further publication.

[9] This oscillatory behavior was previously noted using perturbation theory for the contribution of the $\partial\pi\partial\pi s$ interaction to the bispectrum and trispectrum [35].

Chapter 3

NON-GAUSSIAN ENHANCEMENTS OF GALACTIC HALO CORRELATIONS IN QUASI-SINGLE FIELD INFLATION

We consider a quasi-single field inflation model in which the inflaton interacts with a massive scalar field called the isocurvaton. Due to the breaking of time translational invariance by the inflaton background, these interactions induce kinetic mixing between the inflaton and isocurvaton, which is parameterized by a constant μ. We derive analytic formulae for the curvature perturbation two-, three-, four-, five-, and six-point functions explicitly in terms of the external wave-vectors in the limit where μ and the mass of the isocurvaton m are both much smaller than H. In previous work, it has been noted that when m/H and μ/H are small, the non-Gaussianities predicted by quasi-single field inflation give rise to long wavelength enhancements of the power spectrum for biased objects (*e.g.*, galactic halos). We review this calculation, and calculate the analogous enhanced contribution to the bispectrum of biased objects. We determine the scale at which these enhanced terms are larger than the Gaussian piece. We also identify the scaling of these enhanced parts to the n-point function of biased objects.

3.1 Introduction

The inflationary paradigm [2, 4–7] proposes an era in the very early universe during which the energy density is dominated by vacuum energy. It explains why the universe is close to flat and the near isotropy of the cosmic microwave background radiation. In addition, it has a simple quantum mechanical mechanism for generating energy density perturbations with wavelengths that are well outside the horizon in the early universe. The energy density perturbations resulting from inflation have an almost scale invariant Harrison-Zeldovich power spectrum. The simplest inflation models consist of a single scalar field ϕ called the inflaton. The quantum fluctuations in the Goldstone mode π associated with the breaking of time translation invariance by the inflaton [27] source the energy density fluctuations. In the simplest of these single field inflationary models, the density perturbations are approximately Gaussian [28].

Quasi-single field inflation [15] is a simple generalization of single field inflation that consists of a massive scalar field, the isocurvaton field s, that couples to the inflaton.

This coupling can give rise to significant non-Gaussianities in the correlators of π. The Lagrange density in this model contains an unusual kinetic mixing of the form $\mu\dot{\pi}s$ that gives rise to a wealth of interesting phenomena.

In this chapter, we study the effects of primordial non-Gaussianities on large scale structure. One complication that is not present for the microwave background radiation is that galaxies are biased objects. They do not trace the mass distribution but rather arise at special points, for example where the fluctuations in the mass density exceed some threshold. It was realized in [30] and [49] that the power spectrum for biased objects can deviate significantly from Harrison-Zeldovich on large scales if the primordial mass density perturbations are non-Gaussian. These effects have become known as scale-dependent bias and stochastic bias. In [50] these enhancements for the power spectrum of biased objects were systematically explored within the context of quasi-single field inflation.[1] Quantitative predictions for the power spectrum of galactic halos in quasi-single field inflation (and other models for non-Gaussian primordial fluctuations) were recently made in [48]. Very recently the scale-dependent bias introduced by higher spin fields [35] coupled to the inflaton has been explored [51].

In this chapter we continue and extend the work of [50] and compute the galactic halo power spectrum and bispectrum in quasi-single field inflation. The bispectrum for galaxies was computed for local non-Gaussianity in [52] and for equilateral non-Gaussianity [53]. We make explicit numerical predictions by adopting the very simple model in which galaxies arise at points where the underlying energy density fluctuations (averaged over a volume) are above a threshold [54].[2] Also, we identify the scaling of the n-point function of the halo overdensity in quasi-single field inflation within this threshold model.

The impact of the non-Gaussianities in quasi-single field inflation is largest when the kinetic mixing μ and the isocurvaton mass m are small compared to the Hubble constant during inflation H. We derive new analytic methods to calculate the correlations of π in this region of parameter space. These are applied to derive analytic expressions for the two-, three-, four-, five-, and six-point functions of π. We apply these results to derive explicit expressions for the galactic halo power spectrum and bispectrum. The effects in the power spectrum and the bispectrum of

[1] We refer to these effects as enhancements even though for some range of wave-vectors and model parameters they can interfere destructively with the usual part arising from Gaussian primordial density fluctuations.

[2] Kaiser applied this model to explain the biasing of rich clusters of galaxies [55].

galaxies due to primordial non-Gaussianities can become pronounced at the scale $q \simeq 1/(200h^{-1}\mathrm{M}pc)$. In this work we neglect the time evolution of the galaxy distribution after galaxies form. Even though this is not a small effect, we do not expect that neglecting it will qualitatively impact our conclusions. Furthermore, the computations we perform of the higher correlations of π will be useful for a more complete computation of the galaxy bispectrum.

In section 3.2 we outline the quasi-single field inflation model. We discuss the power series expansion of the mode functions of the quantum fields π and s at small $|\tau|$, where τ is conformal time. For small μ/H and m/H, a method is developed to determine the power series coefficients needed to compute the two-, three-, four-, five- and six-point correlations of the curvature perturbation ζ.[3] In section 3.3 we compute the three-, four-, five- and six-point correlations of ζ. The three- and four-point functions are computed for general wave-vectors, but the five- and six-point functions are only computed for the configurations of wave-vectors that are relevant to the long wavelength enhancements to the galactic halo bispectrum. Section 3.4 introduces the bias expansion and the points above threshold model for the galactic halo overdensity. The results from Section 3.3 are used to compute the halo power spectrum and bispectrum. We also present the scaling of the n-point function of the halo overdensity in quasi-single field inflation. Concluding remarks are given in section V.

3.2 The model and the mode functions

We consider a quasi-single field inflation theory in which inflation is driven by a single scalar inflaton field ϕ and the inflaton is coupled to a single massive scalar isocurvaton field s. The classical background field of the inflaton, $\phi_0(t)$, is time-dependent but we will impose conditions so that to leading order in slow-roll parameters, the background value of s is zero. We also impose a shift symmetry $\phi \to \phi + c$ and a Z_2 symmetry $\phi \to -\phi$ on the inflaton that is only broken by its potential. This implies that the isocurvaton field s couples to derivatives of the inflaton. The lowest dimension operator coupling the inflaton to the isocurvaton is the dimension five operator,

$$\mathcal{L}_{\mathrm{dim}\ 5} = \frac{1}{\Lambda} g^{\mu\nu}\partial_\mu\phi\partial_\nu\phi s. \tag{3.1}$$

We choose the gauge in which the inflaton is only a function of time, $\phi(x) = \phi_0(t)$. We expand the potential for s in a power series about $s = 0$, $V(s) = V's + V''s^2/2 +$

[3] π and ζ are linearly related.

$V'''s^3/3!+\ldots$ and assume the tadpole in s cancels, $(\dot{\phi}_0)^2/\Lambda - V' = 0$. Since we work to leading order in slow-roll parameters, we can neglect $\ddot{\phi}_0$, making this cancellation possible. To obtain long wavelength enhancements to the correlations of biased objects, we need m, the mass of s ($m^2 = V''$), to be less than the Hubble constant during inflation, H. We assume there is some inflaton potential (likely non-analytic in ϕ) that gives values of the power spectrum tilt n_S and the tensor to scalar ratio r consistent with observations.

The Goldstone field $\pi(x)$, associated with time translational invariance breaking by the time dependence of ϕ_0, gives rise to the curvature fluctuations. In a de-Sitter background, the Lagrangian describing $\pi(x)$ and $s(x)$ is

$$\mathcal{L} = \mathcal{L}_0 + \mathcal{L}_{int} \tag{3.2}$$

where

$$\mathcal{L}_0 = \frac{1}{2(H\tau)^2}\left((\partial_\tau\pi)^2 - \nabla\pi\cdot\nabla\pi + (\partial_\tau s)^2 - \frac{m^2}{(H\tau)^2}s^2 - \nabla s\cdot\nabla s - \frac{2\mu}{H\tau}s\partial_\tau\pi\right) \tag{3.3}$$

and

$$\mathcal{L}_{int} = \frac{1}{(H\tau)^4}\left(\frac{(H\tau)^2}{\Lambda}\left((\partial_\tau\pi)^2 - \nabla\pi\cdot\nabla\pi\right)s - \frac{V'''}{3!}s^3 - \frac{V^{(4)}}{4!}s^4\ldots\right). \tag{3.4}$$

In eq. (3.3) we have introduced

$$\mu = 2\dot{\phi}_0/\Lambda \tag{3.5}$$

and conformal time $\tau = -e^{-Ht}/H$. We have rescaled π by $\dot{\phi}_0$ (we take $\dot{\phi}_0 > 0$) to obtain a more standard normalization for the π kinetic term. We have also included the measure factor $\sqrt{-g}$ in the Lagrangian so that the action is equal to $\int d^3x d\tau \mathcal{L}$. Note the unusual kinetic mixing term in (3.3) which is a result of the background inflaton field breaking Lorentz invariance.

To compute correlation functions involving π and s, we expand the quantum fields in terms of creation and annihilation operators. Since the fields π and s have kinetic mixing, they share a pair of creation and annihilation operators. Introducing $\eta = k\tau$ we write,

$$\pi(\mathbf{x},\tau) = \int \frac{d^3k}{(2\pi)^3}\left(a^{(1)}(\mathbf{k})\pi_k^{(1)}(\eta)e^{i\mathbf{k}\cdot\mathbf{x}} + a^{(2)}(\mathbf{k})\pi_k^{(2)}(\eta)e^{i\mathbf{k}\cdot\mathbf{x}} + \text{h.}c.\right) \tag{3.6}$$

and

$$s(\mathbf{x},\tau) = \int \frac{d^3k}{(2\pi)^3}\left(a^{(1)}(\mathbf{k})s_k^{(1)}(\eta)e^{i\mathbf{k}\cdot\mathbf{x}} + a^{(2)}(\mathbf{k})s_k^{(2)}(\eta)e^{i\mathbf{k}\cdot\mathbf{x}} + \text{h.}c.\right) \tag{3.7}$$

By varying (3.3) we can obtain the equations of motion for the mode functions $\pi_k^{(i)}(\eta)$ and $s_k^{(i)}(\eta)$. These are

$$\pi_k^{(i)\prime\prime} - \frac{2\pi_k^{(i)\prime}}{\eta} + \pi_k^{(i)} - \frac{\mu}{H}\left(\frac{s_k^{(i)\prime}}{\eta} - \frac{3s_k^{(i)}}{\eta^2}\right) = 0 \tag{3.8}$$

and

$$s_k^{(i)\prime\prime} - \frac{2s_k^{(i)\prime}}{\eta} + \left(1 + \frac{m^2}{H^2\eta^2}\right) s_k^{(i)} + \frac{\mu}{H}\frac{\pi_k^{(i)\prime}}{\eta} = 0\,, \tag{3.9}$$

where a " $'$ " indicates an η derivative.

Power Series Solution

As mentioned in the introduction it is difficult to solve equations (3.8) and (3.9) analytically for general m and μ. Fortunately, in the small m/H and μ/H regime we do not need the mode functions' full time-dependence to determine the leading behavior of the correlation functions of π. Rather, we only need their small $-\eta$ behavior.[4] To determine this, we obtain a power series solution to (3.8) and (3.9). To begin, we rescale the mode functions

$$\pi_k^{(i)}(\eta) = (H/k^{3/2})\pi^{(i)}(\eta) \qquad s_k^{(i)}(\eta) = (H/k^{3/2})s^{(i)}(\eta) \tag{3.10}$$

and then expand $\pi^{(i)}(\eta)$ and $s^{(i)}(\eta)$ as a power series in $-\eta$

$$\pi^i(\eta) = \sum_{n=0}^{\infty} a_{r,n}^{(i)}(-\eta)^{n+r} \qquad s^{(i)}(\eta) = \sum_{n=0}^{\infty} b_{r,n}^{(i)}(-\eta)^{n+r}. \tag{3.11}$$

By plugging (3.11) into (3.8) and (3.9), we derive relations among the coefficients $a_{r,n}^{(i)}$ and $b_{r,n}^{(i)}$

$$\begin{aligned}
&\left[a_{r,0}^{(i)} r - \frac{\mu}{H} b_{r,0}^{(i)}\right](r-3)(-\eta)^{r-2} + \left[a_{r,1}^{(i)}(r+1) - \frac{\mu}{H} b_{r,1}^{(i)}\right](r-2)(-\eta)^{r-1} \\
&\quad + \sum_{n=0}^{\infty}\left[\left[a_{r,n+2}^{(i)}(n+r+2) - \frac{\mu}{H} b_{r,n+2}^{(i)}\right](n+r-1) + a_{r,n}^{(i)}\right](-\eta)^{n+r} = 0 \\
&\left[\left[b_{r,0}^{(i)}(r-3) + \frac{\mu}{H} a_{r,0}^{(i)}\right] r + b_{r,0}^{(i)}\frac{m^2}{H^2}\right](-\eta)^{r-2} \\
&+ \left[\left[b_{r,1}^{(i)}(r-2) + \frac{\mu}{H} a_{r,1}^{(i)}\right](r+1) + b_{r,1}^{(i)}\frac{m^2}{H^2}\right](-\eta)^{r-1} \\
&\quad + \sum_{n=0}^{\infty}\left[\left[b_{r,n+2}^{(i)}(n+r-1) + \frac{\mu}{H} a_{r,n+2}^{(i)}\right](n+r+2) + b_{r,n+2}^{(i)}\frac{m^2}{H^2} + b_{r,n}^{(i)}\right](-\eta)^{n+r} = 0.
\end{aligned} \tag{3.12}$$

[4] Conformal time η satisfies $-\infty < \eta < 0$ with inflation ending at $\eta = 0$.

Since (3.12) is true for all $\eta < 0$, the coefficient multiplying each power of $-\eta$ vanishes. The constraints due to the coefficients multiplying $(-\eta)^{n+r}$ provide recursion relations relating the $n+2$ coefficients to the n ones. The constraints due to the coefficients multiplying $(-\eta)^{r-2}$ are

$$(a^{(i)}_{r,0} r - \frac{\mu}{H} b^{(i)}_{r,0})(r-3) = 0, \qquad \left[b^{(i)}_{r,0}(r-3) + \frac{\mu}{H} a^{(i)}_{r,0}\right] r + b^{(i)}_{r,0} \frac{m^2}{H^2} = 0. \tag{3.13}$$

Equation (3.13) implies the only possible values of r are

$$r = 0, 3, \ \alpha_-, \ \alpha_+ \tag{3.14}$$

where

$$\alpha_\pm = 3/2 \pm \sqrt{9/4 - (\mu/H)^2 - (m/H)^2}. \tag{3.15}$$

Note α_- and α_+ approach 0 and 3 when m and μ approach zero. Then small μ/H and m/H imply small α_-. Considering odd n instead of even n results in the same exact solution, so we take $a^{(i)}_{r,1} = b^{(i)}_{r,1} = 0$ to eliminate this redundant solution.

There are then four branches of the series solution (3.11). The leading power of each branch is $(-\eta)^r$ and the successive terms go like $(-\eta)^{r+2k}$ where k is a positive integer. The series solutions (3.11) are a linear combination of each branch. The small $-\eta$ behavior of $\pi^{(i)}$ and $s^{(i)}$ is then

$$\begin{aligned}
\pi^{(i)}(\eta) &= a^{(i)}_0 + a^{(i)}_-(-\eta)^{\alpha_-} + a^{(i)}_{0,2}(-\eta)^2 + a^{(i)}_{-,2}(-\eta)^{\alpha_-+2} + a^{(i)}_+(-\eta)^{\alpha_+} + a^{(i)}_3(-\eta)^3 + \ldots \\
s^{(i)}(\eta) &= b^{(i)}_-(-\eta)^{\alpha_-} + b^{(i)}_{0,2}(-\eta)^2 + b^{(i)}_-(-\eta)^{\alpha_-+2} + b^{(i)}_+(-\eta)^{\alpha_+} + b^{(i)}_3(-\eta)^3 + \ldots
\end{aligned} \tag{3.16}$$

Note that we have used the notation $a^{(i)}_{\pm,n} \equiv a^{(i)}_{\alpha_\pm,n}$ and $b^{(i)}_{\pm,n} \equiv b^{(i)}_{\alpha_\pm,n}$, and we have also written the $n = 0$ coefficients as $a^{(i)}_r$. Moreover, $b^{(i)}_0 = 0$ due to (3.13).

As $-\eta \to 0$, $s^{(i)}(\eta) \to 0$ while $\pi^{(i)}(\eta) \to a^{(i)}_0$. However, for $\alpha_- << 1$ the $(-\eta)^{\alpha_-}$ term will remain significant even for $-\eta << 1$ which means π can undergo superhorizon evolution. We can estimate the value of η at which π stops evolving using $\alpha_- \simeq \left(\mu^2 + m^2\right)/(3H^2)$ which is valid for small μ and m. The π modes then stop evolving at $-\eta \sim e^{-3H^2/\left(\mu^2+m^2\right)}$. In this chapter we only consider values of m and μ such that the modes of interest stop evolving before the end of inflation. Then one does not need to consider the details of reheating to make predictions for the curvature perturbations.

Equation (3.13) can also be used to relate the $a^{(i)}$ and $b^{(i)}$ coefficients multiplying the leading $(-\eta)^r$ term of each branch

$$b_0^{(i)} = 0,\ b_-^{(i)} = \frac{Ha_-^{(i)}\alpha_-}{\mu},\ b_+^{(i)} = \frac{Ha_+^{(i)}\alpha_+}{\mu}, b_3^{(i)} = \frac{-3H\mu}{m^2}a_3^{(i)}. \tag{3.17}$$

A full solution to the mode equations is unnecessary. We only need certain combinations of the power series coefficients to derive the leading (for small m and μ) behavior of the correlation functions of π and s. For example, the combinations $\sum_i |a_0^{(i)}|^2$, $\sum_i a_0^{(i)} b_-^{(i)*}$ and $\sum_i |b_-^{(i)}|^2$ determine the two point functions $\langle \pi\pi \rangle$, $\langle \pi s \rangle$ and $\langle ss \rangle$ at late times.

Power Series Coefficients

In this section, we outline the derivation of the combinations of power series coefficients that are needed to compute the correlation functions of π when m/H and μ/H are small. We begin with the combination $\sum_i |b_-^{(i)}|^2$, which can be obtained by matching to an effective field theory that reproduces the correct two point function of s in the small η limit. It turns out that once we know $\sum_i |b_-^{(i)}|^2$ we can determine $\sum_i |a_0^{(i)}|^2$ and $\sum_i a_0^{(i)} b_-^{(i)*}$ from the full theory.

In the small $-\eta$ limit we can neglect the second term appearing in (3.3). Then:

$$\mathcal{L}_0^{EFT} = \frac{1}{2(H\tau)^2}\left((\partial_\tau \pi)^2 + (\partial_\tau s)^2 - \frac{m^2}{(H\tau)^2}s^2 - \nabla s \cdot \nabla s - \frac{2\mu}{H\tau}s\partial_\tau \pi\right) \tag{3.18}$$

The π equation of motion gives

$$\partial_\tau \pi = \frac{\mu}{H}\frac{s(\tau)}{\tau} \tag{3.19}$$

where we have dropped a term proportional to τ^2 in (3.19). The solution of eq. (3.19) is

$$\pi(\tau) = c_1 + \int_{-\infty}^{\tau} \frac{\mu}{H}\frac{s(\tau')}{\tau'}d\tau' \tag{3.20}$$

where c_1 is a constant operator. As mentioned earlier, since (for small η) $s_k^{(i)}(\eta) \simeq b_-^{(i)}(-\eta)^{\alpha_-}$ and α_- is small, the mode functions $s_k^{(i)}$ remain nonzero even after the mode wave-vector has exited the horizon (i.e., when $|\eta| < 1$). Due to the factor of $1/\tau$ in the integral in (3.20), the π mode functions will undergo superhorizon growth and can become quite large if m/H and μ/H are small.

We use eq. (3.20) to express the field π in terms of s. Integrating out π using its equation of motion yields an effective Lagrangian for s:

$$\mathcal{L}_0^{EFT} = \frac{1}{2(H\tau)^2}\left((\partial_\tau s)^2 - \frac{m^2+\mu^2}{(H\tau)^2}s^2 - \nabla s\cdot\nabla s\right). \tag{3.21}$$

Since in this effective theory there is only one field s, it can be written in terms of a single mode function s_k that satisfies the differential equation,

$$s_k''(\eta) - \frac{2}{\eta}s_k'(\eta) + s_k(\eta) + \left(\frac{\mu^2}{H^2}+\frac{m^2}{H^2}\right)\frac{s_k(\eta)}{\eta^2} = 0. \tag{3.22}$$

The solution to (3.22) that satisfies the asymptotic Bunch-Davies vacuum condition and is consistent with the canonical commutation relations is

$$s_k(\eta) = H\sqrt{\frac{\pi}{4k^3}}(-\eta)^{3/2}H_\nu^{(1)}(\eta) \tag{3.23}$$

where $\nu = \sqrt{9/4-(\mu/H)^2-(m/H)^2}$ and $H_\nu^{(1)}$ is a Hankel function of the first kind. The small $-\eta$ limit of (3.23) is

$$s_k(\eta) = H(-\eta)^{\alpha_-}\frac{i}{k^{3/2}}\frac{1}{\sqrt{2}}. \tag{3.24}$$

Using (3.24), we can determine the small $-\eta$ limit of the two-point function of the Fourier transform of s. Denoting this Fourier transform by $s_{\mathbf{k}}$, we obtain

$$\langle s_{\mathbf{k}}s_{\mathbf{k}'}\rangle(\tau') = (2\pi)^3\delta^3(\mathbf{k}+\mathbf{k}')\frac{H^2}{2k^3}(-\eta)^{2\alpha_-}. \tag{3.25}$$

By matching the full theory prediction for $\langle ss\rangle$ to (3.25) we find

$$\sum_i\left|b_-^{(i)}\right|^2 = \frac{1}{2}. \tag{3.26}$$

Equation (3.20) can be used to determine the leading small $-\eta$ behavior of the π mode functions in the full theory. It gives

$$\pi^{(i)}(0) = c_1^{(i)} + \int_{-\infty}^{0}\frac{\mu}{H}\frac{s^{(i)}(\eta')}{\eta'}d\eta'. \tag{3.27}$$

From equation (3.16) we see that the integrand in (3.27) goes like $(-\eta)^{-1+\alpha_-}$ in the IR region of the integral, i.e. $-\eta < 1$. For small m/H and μ/H, α_- is very small and the integral will receive a large contribution from the IR. On the other hand, the contribution from the UV is small because the mode functions become

oscillatory with smaller amplitude when $-\eta > 1$. This means the integral is fixed by the integrand's IR behavior so that[5]

$$\pi^{(i)}(0) \simeq c_1^{(i)} - \frac{\mu b_-^{(i)}}{H}\int_{-1}^{0}(-\eta)^{-1+\alpha_-}d\eta = c_1^{(i)} - \frac{\mu b_-^{(i)}}{H}\frac{1}{\alpha_-} = c_1^{(i)} - \frac{3\mu H b_-^{(i)}}{\mu^2+m^2}. \quad (3.28)$$

In (3.28) we have used $\alpha_-^{-1} \simeq 3H^2/\left(\mu^2+m^2\right)$. The corrections to (3.28) are suppressed by powers of α_- and are unimportant when m/H and μ/H are small. The integral is insensitive to the exact value of the UV cutoff because α_- is small.

We can now compute the two-point function of the Fourier transform of π, which can be written as

$$\langle \pi_{\mathbf{k}}(0)\pi_{\mathbf{k}'}(0)\rangle \simeq (2\pi)^3\delta\left(\mathbf{k}+\mathbf{k}'\right)\frac{H^2}{k^3}C_2(\mu,m). \quad (3.29)$$

We determine $C_2(\mu,m)$ by taking the magnitude squared of (3.28):

$$C_2(\mu,m) \simeq \sum_i\left[\left|c_1^{(i)}\right|^2 + \frac{9\mu^2H^2}{\left(\mu^2+m^2\right)}\left|b_-^{(i)}\right|^2 - \frac{6\mu H}{\mu^2+m^2}\mathrm{Re}\left(c_1^{(i)}b_-^{(i)*}\right)\right]. \quad (3.30)$$

In writing (3.30), we have only kept the terms that are most important for m/H and μ/H small. Now $\langle\pi\pi\rangle$ is invariant under $s \to -s$.[6] This implies the last term in the brackets of (3.30) has to vanish. We can determine the first term by noting that the constant $c_1^{(i)}$ is μ independent. This can be seen from the fact that it is a boundary condition fixed by the UV, thereby independent of the mixing factor μ. We can then fix the first term in (3.30) by demanding that $C_2(0,m) = 1/2$. Finally, using (3.26) we find that

$$C_2(\mu,m) \simeq \frac{1}{2} + \frac{9\mu^2H^2}{2\left(\mu^2+m^2\right)^2}. \quad (3.31)$$

Equation (3.31) gives the leading behavior of $C_2(\mu,m)$ in the limit of small m/H and μ/H. We can determine the accuracy of (3.31) by extending the numerical techniques developed in [42] and chapter two to the region of small m/H and μ/H and computing the power spectrum numerically. This is done in appendix 3.A.

We now compute the leading m and μ dependence of the curvature perturbation two-point function. The curvature perturbation is related to the Goldstone field by

$$\zeta_{\mathbf{k}} = -\frac{H}{\dot\phi_0}\pi_{\mathbf{k}}. \quad (3.32)$$

[5] We will use these same arguments when we evaluate the time integrals involved in the calculation of higher point correlators.

[6] If we treat μ as a perturbation then all of the corrections to $\langle\pi\pi\rangle$ involve even powers of the s field.

The curvature perturbation two-point is then

$$\left\langle \zeta_{\mathbf{k}_1}\zeta_{\mathbf{k}_2}\right\rangle = \left(\frac{H}{\dot\phi_0}\right)^2 \left\langle \pi_{\mathbf{k}_1}\pi_{\mathbf{k}_2}\right\rangle = (2\pi)^3\delta(\mathbf{k}_1+\mathbf{k}_2)\mathcal{P}_\zeta(k)$$
$$= (2\pi)^3\delta(\mathbf{k}_1+\mathbf{k}_2)\left(\frac{H^2}{\dot\phi_0}\right)^2 \frac{1}{k^3}C_2(\mu,m). \quad (3.33)$$

Using (3.33) we can express $\dot\phi_0$ in terms of μ, m, and the measured value of the dimensionless power spectrum Δ_ζ [44]:

$$\Delta_\zeta^2 = 2.12\times 10^{-9} = \frac{k^3}{2\pi^2}\mathcal{P}_\zeta(k) = \left(\frac{H^2}{\dot\phi_0}\right)^2 \frac{1}{2\pi^2}C_2(\mu,m). \quad (3.34)$$

This implies

$$\frac{\dot\phi_0}{H^2} = \sqrt{\frac{C_2(\mu,m)}{2\pi^2\Delta_\zeta^2}}. \quad (3.35)$$

We can determine the combination $\sum_i a_0^{(i)}b_-^{(i)*}$ by multiplying both sides of (3.28) by $b_-^{(i)*}$ and summing over i. This gives

$$\sum_i a_0^{(i)}b_-^{(i)*} = \sum_i c_1^{(i)}b_-^{(i)*} - \frac{3\mu H}{2\left(\mu^2+m^2\right)}. \quad (3.36)$$

We have already shown that $\sum_i \mathrm{Re}\left(c_1^{(i)}b_-^{(i)*}\right) = 0$, which implies

$$\sum_i \mathrm{Re}\left(a_0^{(i)}b_-^{(i)*}\right) = -\frac{3\mu H}{2\left(\mu^2+m^2\right)}. \quad (3.37)$$

The remaining combinations of power series coefficients needed to compute the higher order correlation functions of π are fixed using the canonical commutation relations of s and π. Consider the equal time relation $[s(\mathbf{x},\tau),\pi(\mathbf{y},\tau)] = 0$. By inserting (3.6) and (3.7) into this relation, we find

$$[\pi(\mathbf{x},\tau),s(\mathbf{y},\tau)] = \int \frac{d^3\mathbf{k}}{(2\pi)^3}e^{i\mathbf{k}\cdot(\mathbf{x}-\mathbf{y})}\sum_i\left[\pi_k^{(i)}(\eta)s_k^{(i)*}(\eta) - \mathrm{c.c.}\right] = 0. \quad (3.38)$$

The mode functions must then satisfy

$$\sum_i \mathrm{Im}\left[\pi_k^{(i)}(\eta)s_k^{(i)*}(\eta)\right] = 0 \quad (3.39)$$

for all η. Plugging the leading IR behavior of the mode functions (3.16) into (3.39) and demanding it holds at orders $(-\eta)^{\alpha_-}$, $(-\eta)^{\alpha_+}$, $(-\eta)^2$, and $(-\eta)^3$ respectively yields the following constraints

$$\begin{aligned}\sum_i \mathrm{Im}\left[a_0^{(i)} b_-^{(i)*}\right] &= \sum_i \mathrm{Im}\left[a_0^{(i)} b_+^{(i)*}\right] = \sum_i \mathrm{Im}\left[a_0^{(i)} b_{0,2}^{(i)*}\right] \\ &= \sum_i \mathrm{Im}\left[a_0^{(i)} b_3^{(i)*} + a_+^{(i)} b_-^{(i)*} + a_-^{(i)} b_+^{(i)*}\right] = 0. \end{aligned} \tag{3.40}$$

Given the fact that the recursion relations (3.12) and eq. (3.17) are real, eqs. (3.40) and (3.17) further imply that:

$$\sum_i \mathrm{Im}\left[a_0^{(i)} b_{-,2}^{(i)*}\right] = \sum_i \mathrm{Im}\left[b_-^{(i)} b_{0,2}^{(i)*}\right] = 0 \tag{3.41}$$

Moreover, the recursion relations (3.12) being real along with the fact that $\sum_i \mathrm{Im}\left[|b_-^{(i)}|^2\right] = 0$ imply that

$$\sum_i \mathrm{Im}\left[b_-^{(i)} b_{-,2}^{(i)*}\right] = 0 \tag{3.42}$$

Furthermore, using the commutation relation $[\pi(\mathbf{x},\tau), \Pi_\pi(\mathbf{y},\tau)] = i\delta^3(\mathbf{x}-\mathbf{y})$ gives:

$$\begin{aligned}\sum_i \mathrm{Im}\left[3a_0^{(i)} a_3^{(i)*} + \alpha_+ a_-^{(i)} a_+^{(i)*} + \alpha_- a_+^{(i)} a_-^{(i)*}\right] &= -\frac{1}{2} \\ \sum_i \mathrm{Im}\left[a_-^{(i)} a_3^{(i)*}\right] &= 0 \end{aligned} \tag{3.43}$$

Again using the fact that relations (3.17) are real, we can convert the second equation in (3.43) to:

$$\sum_i \mathrm{Im}\left[b_-^{(i)} b_3^{(i)*}\right] = 0 \tag{3.44}$$

Using (3.17), we can combine the final equation of (3.40) with the first equation of (3.43) to find

$$\begin{aligned}\sum_i \mathrm{Im}\left[a_0^{(i)} b_3^{(i)*}\right] &= \frac{\mu H}{2\left(\mu^2 + m^2\right)} \\ \sum_i \mathrm{Im}\left[b_-^{(i)} b_+^{(i)*}\right] &= \frac{-1}{2\left(\alpha_+ - \alpha_-\right)} \simeq -\frac{1}{6}. \end{aligned} \tag{3.45}$$

The equalities in eq. (3.45) hold for all m and μ such that $m^2 + \mu^2 \leq 9H^2/4$, i.e. for α_- and α_+ real.

Equations (3.26), (3.31), (3.37), (3.41), (3.42), (3.44), and (3.45) comprise the full set of relations among power series coefficients we need to compute the leading m and μ dependence of the correlation functions of π. We will also need the fact that $n > 0$ coefficients $a^{(i)}_{r,n}$ and $b^{(i)}_{r,n}$ are not enhanced by powers of α_-^{-1} compared to $a^{(i)}_r$ and $b^{(i)}_r$ coefficients for small α_-, a fact which is simple to see from the recursion relations (3.12).

3.3 Primordial Non-Gaussianities

In this section we compute the leading m and μ behavior of the connected three- and four-point functions of the curvature perturbation ζ for arbitrary external wave-vectors. We also compute the connected five-and six-point functions in certain kinematic limits. We will use these results to calculate the two- and three-point functions of biased objects.

We perform the computation of these correlation functions using the in-in formalism [47]. We will mostly use the commutator form of the in-in correlator of an operator $O(0)$:

$$\begin{aligned}\langle O(0)\rangle = \sum_{N=0}^{\infty} i^N \int_{-\infty}^{0} d\tau_N \int_{-\infty}^{\tau_N} d\tau_{N-1} \cdots \int_{-\infty}^{\tau_2} d\tau_1 \\ \times \langle [H^I_{int}(\tau_1), [H^I_{int}(\tau_2), \ldots [H^I_{int}(\tau_N), O^I(0)] \ldots]\rangle_I \end{aligned} \tag{3.46}$$

where I denotes a state or operator evolving in the interaction picture and H_{int} denotes the interaction Hamiltonian[7]

$$H_{int}(\tau) = \frac{1}{(H\tau)^4} \int d^3\mathbf{x} \left[\frac{1}{\Lambda} s(x) g^{\mu\nu} \partial_\mu \pi(x) \partial_\nu \pi(x) + \frac{V'''}{3!} s(x)^3 + \frac{V^{(4)}}{4!} s(x)^4 \right]. \tag{3.47}$$

For simplicity, we assume $V^{(4)}$ is much smaller than $(V'''/H)^2$ and can be neglected. We have also explored the importance of the $s\partial\pi\partial\pi$ interaction in comparison with the s^3 interaction for the primordial curvature bispectrum. For the range of parameters that we are using in this chapter, we find numerically that the ratio of these contributions is $O(10^{-3})/f_{NL}$. We suspect that this interaction is subdominant for the other primordial correlation functions as well, and neglect this interaction henceforth. All relevant interactions are then mediated by the V''' term. We assume $|V'''|/H < 1$ so that perturbation theory is valid.

[7] We restrict our attention to renormalizable terms in the potential for s.

Three-Point Function

The three-point function of ζ can be written

$$\left\langle \zeta_{\mathbf{k}_1}\zeta_{\mathbf{k}_2}\zeta_{\mathbf{k}_3}\right\rangle \equiv B_\zeta(\mathbf{k}_1,\mathbf{k}_2,\mathbf{k}_3)(2\pi)^3\delta^3\left(\mathbf{k}_1+\mathbf{k}_2+\mathbf{k}_3\right). \tag{3.48}$$

The leading contribution to the bispectrum $B_\zeta(\mathbf{k}_1,\mathbf{k}_2,\mathbf{k}_3)$ is obtained by inserting a single factor of the V''' interaction into (3.46). This yields

$$B_\zeta(\mathbf{k}_1,\mathbf{k}_2,\mathbf{k}_3) = -2V'''\left(\frac{H}{\dot\phi_0}\right)^3 \mathrm{I}m\int_{-\infty}^{0}\frac{d\tau}{(H\tau)^4}\prod_{l=1}^{3}\left[\pi^{(1)}_{k_l}(0)s^{(1)*}_{k_l}(k_l\tau)+\pi^{(2)}_{k_l}(0)s^{(2)*}_{k_l}(k_l\tau)\right]. \tag{3.49}$$

Equation (3.49), written in terms of the rescaled mode functions (3.10), becomes

$$B_\zeta(\mathbf{k}_1,\mathbf{k}_2,\mathbf{k}_3) = -2\left(\frac{H^2}{\dot\phi_0}\right)^3\left(\frac{V'''}{H}\right)\left(\prod_i^3\frac{1}{k_i^3}\right)\mathrm{I}m\int_{-\infty}^{0}\frac{d\tau}{\tau^4}\prod_{l=1}^{3}\sum_i\pi^{(i)}(0)s^{(i)*}(k_l\tau). \tag{3.50}$$

Let us now focus on the evaluation of the integral in (3.50), which can be written:

$$k_{UV}^3\mathrm{I}m\int_{-\infty}^{0}\frac{d\eta}{\eta^4}\prod_{l=1}^{3}\sum_i\pi^{(i)}(0)s^{(i)*}\left(\frac{k_l}{k_{UV}}\eta\right) \tag{3.51}$$

where we define $k_{UV} = \mathrm{m}ax(k_l)$ and $\eta = k_{UV}\tau$. In the small μ and m regime, (3.51) receives most of its support from the IR region of the integral (when the arguments of the mode functions are less than 1 in magnitude) due to the superhorizon growth mentioned in the discussion following (3.20). The contribution from the UV region is subdominant. Our choice of k_{UV} implies the leading m and μ contribution to the integral comes from the region $-1 \le \eta \le 0$, and (3.51) becomes:

$$\begin{aligned}k_{UV}^3\mathrm{I}m\int_{-1}^{0}\frac{d\eta}{\eta^4}\prod_{l=1}^{3}\sum_i\Bigg[&\left(a_0^{(i)}b_-^{(i)*}\right)\left(-\frac{k_l}{k_{UV}}\eta\right)^{\alpha_-}+\left(a_0^{(i)}b_{0,2}^{(i)*}\right)\left(-\frac{k_l}{k_{UV}}\eta\right)^{2}\\&+\left(a_0^{(i)}b_{-,2}^{(i)*}\right)\left(-\frac{k_l}{k_{UV}}\eta\right)^{\alpha_-+2}+\left(a_0^{(i)}b_+^{(i)*}\right)\left(-\frac{k_l}{k_{UV}}\eta\right)^{\alpha_+}+\left(a_0^{(i)}b_3^{(i)*}\right)\left(-\frac{k_l}{k_{UV}}\eta\right)^{3}+O(\eta^4)\Bigg].\end{aligned} \tag{3.52}$$

Note the integral is potentially IR divergent because of the factor of $1/\eta^4$. However, eqs. (3.40) and (3.41) imply the coefficients multiplying the IR divergent terms are

zero, and that the leading μ and m behavior of (3.52) is

$$\left(\sum_i \mathrm{Re}\left[a_0^{(i)} b_-^{(i)*}\right]\right)^2 \left(\sum_i \mathrm{Im}\left[a_0^{(i)} b_3^{(i)*}\right]\right)\left[k_1^3\left(\frac{k_2 k_3}{k_{UV}^2}\right)^{\alpha_-} + cyc.\ perm\right]$$
$$\times \int_{-1}^{0} d\eta (-\eta)^{-1+2\alpha_-}$$
$$= \frac{27}{16}\frac{\mu^3 H^5}{\left(\mu^2+m^2\right)^4}\left[k_1^3\left(\frac{k_2 k_3}{k_{UV}^2}\right)^{\alpha_-} + cyc.\ perm\right]. \qquad (3.53)$$

As long as α_- is small, the answer does not depend on the precise choice of k_{UV}, we only have to choose it to be of the same order as the hardest wave-vector entering the vertex.[8] Equivalently, the answer is insensitive to the precise choice of the lower bound of the η integral. Plugging (3.53) into (3.50), we find that the leading m and μ behavior of the $O(V''')$ contribution to the bispectrum is

$$B_\zeta(\mathbf{k}_1,\mathbf{k}_2,\mathbf{k}_3) = -\left(\frac{H^2}{\dot\phi_0}\right)^3\left(\frac{V'''}{H}\right)\frac{1}{k_1^3 k_2^3 k_3^3}\frac{(3\mu/2)^3 H^5}{\left(\mu^2+m^2\right)^4}$$
$$\times\left[k_1^3\left(\frac{k_2 k_3}{k_{UV}^2}\right)^{\alpha_-} + k_2^3\left(\frac{k_1 k_3}{k_{UV}^2}\right)^{\alpha_-} + k_3^3\left(\frac{k_1 k_2}{k_{UV}^2}\right)^{\alpha_-}\right] \qquad (3.54)$$

where $k_{UV} = max(k_i)$. Equation (3.54) was computed numerically in [15] and is valid for any external wave-vector configuration. Note that when the wave-vectors k_1, k_2 and k_3 are the same order of magnitude, the terms raised to the power α_- can be set to unity. Then the bispectrum has the same form as local non-Gaussianity, *i*.e., $B_\zeta(\mathbf{k}_1,\mathbf{k}_2,\mathbf{k}_3) \propto \left[P_\zeta(k_1)P_\zeta(k_2) + P_\zeta(k_1)P_\zeta(k_3) + P_\zeta(k_2)P_\zeta(k_3)\right]$.

We now study (3.54) in a couple interesting kinematic limits. First, consider (3.54) in the equilateral limit $k_i \equiv k$

$$B_\zeta^{equil}(k) = -\left(\frac{H^2}{\dot\phi_0}\right)^3\left(\frac{V'''}{H}\right)\frac{1}{k^6}\frac{3\,(3\mu/2)^3 H^5}{\left(\mu^2+m^2\right)^4}. \qquad (3.55)$$

We can use (3.55) to relate V''' to the model's prediction for f_{NL}. We estimate f_{NL} using

$$f_{NL} = \frac{5}{18}\times\frac{B_\zeta^{equil}(k)}{\mathcal{P}_\zeta(k)^2}. \qquad (3.56)$$

[8] The ratios of external wave-vectors to k_{UV} raised to the power α_- in equation (3.53) can be interpreted as the re-summation of leading logs in the α_- expansion.

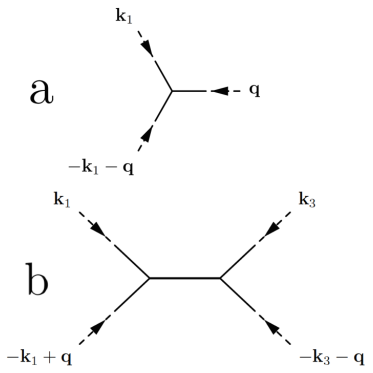

Figure 3.1: Diagrams that contribute to three- and four-point correlations of ζ in the squeezed and collapsed limits respectively. These diagrams contribute to the galactic halo power spectrum. Dashed lines represent π, while solid lines represent s.

Substituting (3.33), (3.35) and (3.55) into (3.56) gives

$$\frac{V'''}{H} = -\frac{6}{5} f_{NL} \sqrt{2\pi^2 \Delta_\zeta^2} C_2(\mu, m)^{\frac{3}{2}} \frac{(\mu^2 + m^2)^4}{(3\mu/2)^3 H^5}. \tag{3.57}$$

The current Planck 95% C.L. constraint for local non-Gaussianity is $f_{NL} = 2.7 \pm 11.6$. For $f_{NL} = 10$ and $\mu/H = m/H = 0.3$, we find that $|V'''|/H \simeq 10^{-3}$.

The two kinematic configurations we will be most interested in when we compute galactic halo correlators are when all three external wave-vectors are soft (Fig. 3.2c), and when one leg is soft while the other two are hard - the so-called squeezed limit (Fig. 3.1a). In what follows, we will denote hard wave-vectors by k and soft wave-vectors by q. First we consider the squeezed limit. We choose $\mathbf{k}_2 = -\mathbf{k}_1 - \mathbf{q}$ and $k_1 = k_2 \equiv k >> k_3 \equiv q$. The full $O(V''')$ contribution (3.50) to the bispectrum in this limit can be written

$$B_\zeta^{sq}(k, q) = -\left(\frac{H^2}{\dot{\phi}_0}\right)^3 \left(\frac{V'''}{H}\right) \frac{2\,(3\mu/2)^3\, H^5}{\left(\mu^2 + m^2\right)^4} \frac{1}{k^{3+\alpha_-} q^{3-\alpha_-}}. \tag{3.58}$$

The wave-vector dependence of equation (3.58) was first determined in [15, 56]. Finally, the bispectrum in the limit where all three external wave-vectors are soft can be obtained simply by making the replacement $k_i \to q_i$ in (3.54).

Four-Point Function

The four-point function of ζ can be written

$$\left\langle \zeta_{\mathbf{k}_1} \zeta_{\mathbf{k}_2} \zeta_{\mathbf{k}_3} \zeta_{\mathbf{k}_4} \right\rangle \equiv N_\zeta^{(4)}(\mathbf{k}_1, \mathbf{k}_2, \mathbf{k}_3, \mathbf{k}_4)(2\pi)^3 \delta^3 \left(\sum_i^4 \mathbf{k}_i \right). \tag{3.59}$$

We can derive the leading contribution to $N_\zeta^{(4)}$ by inserting two factors of the V''' interaction into (3.46). It is convenient to define

$$A(x) \equiv \sum_i \pi^{(i)}(0) s^{(i)*}(x) \qquad B(x) \equiv \sum_i b_-^{(i)} s^{(i)*}(x). \tag{3.60}$$

By expanding the commutators and performing all possible contractions, we find:

$$\begin{aligned} N_\zeta^{(4)}(\mathbf{k}_1, \mathbf{k}_2, \mathbf{k}_3, \mathbf{k}_4) = 4 \left(\frac{H^2}{\dot\phi_0}\right)^4 \left(\frac{V'''}{H}\right)^2 \left(\prod_i^4 \frac{1}{k_i^3}\right) \frac{1}{k_{12}^3} \int_{-\infty}^{0} \frac{d\tau}{\tau^4} \int_{-\infty}^{\tau} \frac{d\tau'}{\tau'^4} \\ \times \mathrm{Im}\left[A(k_1\tau)A(k_2\tau)\right] \mathrm{Im}\left[A(k_3\tau')A(k_4\tau') \sum_i s^{(i)}(k_{12}\tau) s^{(i)*}(k_{12}\tau')\right] \\ + (k_1 \leftrightarrow k_3, k_2 \leftrightarrow k_4) + \mathrm{c}yc.\ perms(\mathbf{k}_2, \mathbf{k}_3, \mathbf{k}_4) \end{aligned} \tag{3.61}$$

where $k_{12} = |\mathbf{k}_1 + \mathbf{k}_2|$.

Unlike the calculation of the three-point function, the four-point one involves nested time integrals. Again, the four-point integral is dominated by the IR for $\alpha_- << 1$ and the integrand reduces to polynomials in τ and τ'. Like before, we make the change of variable $\eta \equiv k_{UV_{12}}\tau$ and $\eta' \equiv k_{UV_{34}}\tau'$, where $k_{UV_{ij}} \equiv \max\{k_i, k_j, |\mathbf{k}_i + \mathbf{k}_j|\}$ and cut off the integrals at $\eta_{UV} = -1$ and $\eta'_{UV} = -1$ (recall that the result is not sensitive to this cutoff value as long as α_- is small). The relationships among the power series coefficients deduced in section 3.2 imply the integral converges in the IR.

Without loss of generality, assume that k_1 is the largest external wave-vector (this implies that $k_{UV_{12}} \geq k_{UV_{34}}$). Using the identities relating the power series coefficients

derived in section 3.2, the time integral in (3.61) becomes:

$$\int_{-\infty}^{0}\frac{d\tau}{\tau^4}\int_{-\infty}^{\tau}\frac{d\tau'}{\tau'^4}\mathrm{Im}\left[A(k_1\tau)A(k_2\tau)\right]\mathrm{Im}\left[A(k_3\tau')A(k_4\tau')\sum_i s^{(i)}(k_{12}\tau)s^{(i)*}(k_{12}\tau')\right]+(k_1\leftrightarrow k_3,k_2\leftrightarrow k_4)$$

$$=\frac{9}{32}\frac{\mu^4H^4}{\left(\mu^2+m^2\right)^4}\left[\left(\frac{k_I^2}{k_{UV_{12}}^2k_{UV_{34}}^2}\right)^{\alpha_-}\left[k_1^3k_2^{\alpha_-}+k_2^3k_1^{\alpha_-}\right]\left[k_3^3k_4^{\alpha_-}+k_4^3k_3^{\alpha_-}\right]\right.$$

$$\times\left[\int_{-1}^{0}d\eta(-\eta)^{-1+2\alpha_-}\int_{-1}^{\frac{k_{UV_{34}}}{k_{UV_{12}}}\eta}d\eta'(-\eta')^{-1+2\alpha_-}+\int_{-\frac{k_{UV_{34}}}{k_{UV_{12}}}}^{0}d\eta(-\eta)^{-1+2\alpha_-}\int_{-1}^{\frac{k_{UV_{12}}}{k_{UV_{34}}}\eta}d\eta'(-\eta')^{-1+2\alpha_-}\right]$$

$$+\left(\frac{k_I^3}{{k_{UV_{12}}}^{2\alpha_-}{k_{UV_{34}}}^{\alpha_-}}\right)\left[k_1^3k_2^{\alpha_-}+k_2^3k_1^{\alpha_-}\right]\left[k_3^{\alpha_-}k_4^{\alpha_-}\right]\int_{-1}^{0}d\eta(-\eta)^{-1+2\alpha_-}\int_{-1}^{\frac{k_{UV_{34}}}{k_{UV_{12}}}\eta}d\eta'(-\eta')^{-1+\alpha_-}$$

$$\left.+\left(\frac{k_I^3}{{k_{UV_{12}}}^{\alpha_-}{k_{UV_{34}}}^{2\alpha_-}}\right)\left[k_1^{\alpha_-}k_2^{\alpha_-}\right]\left[k_3^3k_4^{\alpha_-}+k_3^{\alpha_-}k_4^3\right]\int_{-\frac{k_{UV_{34}}}{k_{UV_{12}}}}^{0}d\eta(-\eta)^{-1+2\alpha_-}\int_{-1}^{\frac{k_{UV_{12}}}{k_{UV_{34}}}\eta}d\eta'(-\eta')^{-1+\alpha_-}\right]. \tag{3.62}$$

Notice not all of the lower bounds of the η integrals equal -1, some are cutoff by $-\frac{k_{UV_{34}}}{k_{UV_{12}}}$. This is to ensure that the upper bound of the η' integral is greater than -1. Evaluating the time integrals, we find the four-point function for general external wave-vectors is

$$N_\zeta^{(4)}(\mathbf{k}_1,\mathbf{k}_2,\mathbf{k}_3,\mathbf{k}_4)=\left(\frac{H^2}{\dot\phi_0}\right)^4\left(\frac{V'''}{H}\right)^2\left(\prod_{i=1}^4\frac{1}{k_i^3}\right)\frac{1}{k_{12}^3}\frac{(3\mu/2)^4H^8}{2(\mu^2+m^2)^6}$$

$$\times\left[\left(k_1^3k_2^{\alpha_-}+k_1^{\alpha_-}k_2^3\right)\left(k_3^3k_4^{\alpha_-}+k_3^{\alpha_-}k_4^3\right)\left(\frac{k_{12}}{k_{UV_{12}}k_{UV_{34}}}\right)^{2\alpha_-}\right.$$

$$+2\left(1-\frac{2}{3}\left(\frac{k_{UV_{34}}}{k_{UV_{12}}}\right)^{\alpha_-}\right)(k_1^3k_2^{\alpha_-}+k_1^{\alpha_-}k_2^3)(k_3k_4)^{\alpha_-}\frac{k_{12}^3}{k_{UV_{12}}^{2\alpha_-}k_{UV_{34}}^{\alpha_-}}$$

$$\left.+\frac{2}{3}(k_1k_2)^{\alpha_-}\left(k_3^3k_4^{\alpha_-}+k_3^{\alpha_-}k_4^3\right)\frac{k_{12}^3}{k_{UV_{12}}^{3\alpha_-}}\right]+\text{cyc. perm}(\mathbf{k}_2,\mathbf{k}_3,\mathbf{k}_4) \tag{3.63}$$

We now focus on kinematic limits of (3.63) that are most important in the calculation of the two- and three-point functions of galactic dark matter halos. The enhance-

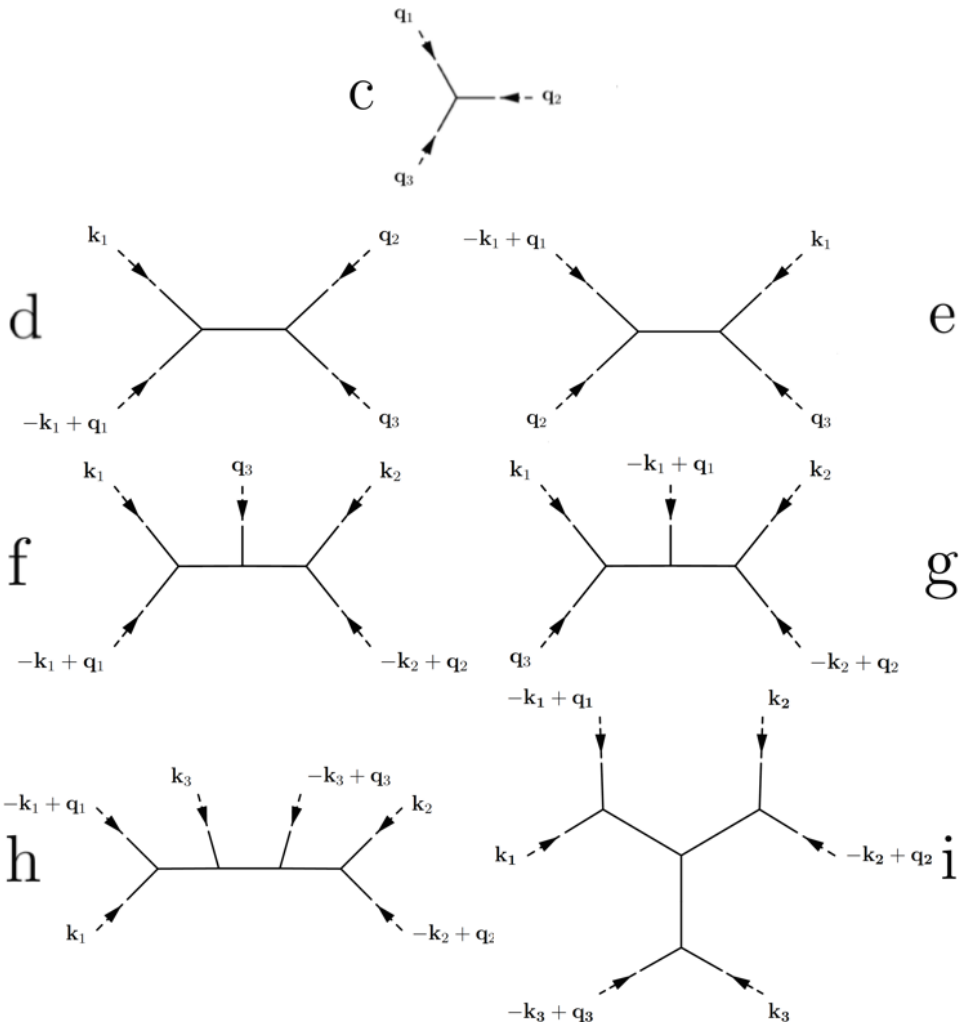

Figure 3.2: Diagrams that contribute to the three-, four-, five-, and six-point correlations of ζ in the kinematic regimes that contribute to the enhanced part of the galactic halo bispectrum. Dashed lines represent π, while solid lines represent s.

ments discovered in [30] and [49] respectively occur when the magnitude of a sum of wave-vectors in the correlation function of ζ is small or when the magnitude of an external wave-vector is small. For the four-point correlation, the first of these is referred to as the collapsed limit. Suppose that q denotes small wave-vectors, and k denotes large wave-vectors. In these computations (as well as in later computations of the five- and six-point functions of ζ), we assume that $(k_i/k_j)^{\alpha_-} \simeq 1$ and $(q_i/q_j)^{\alpha_-} \simeq 1$. This approximation is justified in our application to galactic halos since we will want to consider k's roughly on the order of the inverse of the galactic halo radius, and since the q's will be taken to be within an order of magnitude from each other (i.e. between about $(50\ \mathrm{M}pc/h)^{-1}$ and $(1000\ \mathrm{M}pc/h)^{-1}$). However, we

do not take $(q/k)^{\alpha_-}$ to be approximately 1 since q and k may differ by several orders of magnitude. We first specialize to the collapsed limit of (3.63) which occurs when two pairs of legs have nearly equal and opposite wave-vectors. Let $\mathbf{k}_2 = -\mathbf{k}_1 + \mathbf{q}$ and $\mathbf{k}_4 = -\mathbf{k}_3 - \mathbf{q}$ where $q << k_1,\ k_3$. Then the most important permutation of (3.63) in this collapsed limit is when $\mathbf{k}_1$ and $\mathbf{k}_2$ are attached to one vertex, and $\mathbf{k}_3$ and $\mathbf{k}_4$ are attached to the other. The wave-vector of the internal line becomes very small (Fig. 3.1*b*) and eq. (3.63) becomes

$$N_\zeta^{(4),\,\mathrm{coll}}(\mathbf{k}_1, -\mathbf{k}_1 + \mathbf{q}, \mathbf{k}_3, -\mathbf{k}_3 - \mathbf{q}) = \left(\frac{H^2}{\dot\phi_0}\right)^4 \left(\frac{V'''}{H}\right)^2 \frac{1}{q^{3-2\alpha_-}} \frac{1}{(k_1 k_3)^{3+\alpha_-}} \frac{2(3\mu/2)^4 H^8}{(\mu^2+m^2)^6}. \tag{3.64}$$

The four-point in the collapsed limit was previously computed in [33].

The other interesting kinematic limit of (3.63) is when one pair of legs have nearly equal and opposite wave-vectors and the wave-vectors of the other two legs are soft. We find for the sum of Figs. 3.2*d* and 3.2*e*:

$$N_\zeta^{(4)}(\mathbf{k}_1, -\mathbf{k}_1 + \mathbf{q}_1, \mathbf{q}_2, \mathbf{q}_3) = \left(\frac{H^2}{\dot\phi_0}\right)^4 \left(\frac{V'''}{H}\right)^2 \frac{(3\mu/2)^4 H^8}{\left(\mu^2+m^2\right)^6} \frac{1}{k_1^3} \left(\frac{q}{k_1}\right)^{\alpha_-} \times \left[\frac{1}{q_1^3 q_2^3} + \frac{1}{q_1^3 q_3^3} + 2\left(1 + \frac{1}{2}\left(\frac{q}{k_1}\right)^{\alpha_-}\right) \frac{1}{q_2^3 q_3^3}\right]. \tag{3.65}$$

Five- and Six-Point Functions

Given the techniques we have developed so far, it is possible to compute the five- and six-point functions of ζ for general external wave-vectors. However, our primary purpose in studying these objects is to compute their most important contributions to the three-point function of galactic dark matter halos in the limit of large halo separation. We then only focus on the kinematic limits of the five- and six-points giving rise to the largest long wavelength enhanced terms. Even in these limits, the calculation is too long to present here. In this section we just quote results and relegate an outline of the derivation to Appendix 3.B.

The strongest long wavelength enhanced behavior of the five-point function is achieved when one leg is soft and the other four come in pairs of nearly equal and opposite wave-vectors. Panels *f* and *g* of Fig. 3.2 illustrate this kinematic

setup. The contribution of these graphs to the five-point function is:

$$N_\zeta^{(5)}(\mathbf{k}_1, \mathbf{q}_1 - \mathbf{k}_1, \mathbf{k}_2, \mathbf{q}_2 - \mathbf{k}_2, \mathbf{q}_3) = -\left(\frac{H^2}{\dot\phi_0}\right)^5 \left(\frac{V'''}{H}\right)^3 \frac{(3\mu/2)^5 H^{11}}{(\mu^2+m^2)^8} \frac{1}{k_1^3 k_2^3} \left(\frac{q^2}{k_1 k_2}\right)^{\alpha_-} \times \left[\frac{1}{q_1^3 q_2^3} + \left(2 - \frac{1}{6}\left(\frac{q}{k_2}\right)^{\alpha_-}\right)\frac{1}{q_2^3 q_3^3} + \left(2 - \frac{1}{6}\left(\frac{q}{k_1}\right)^{\alpha_-}\right)\frac{1}{q_1^3 q_3^3}\right] \tag{3.66}$$

where we have defined $q = \max\{q_i\}$.

The most important long wavelength contributions to the six-point function occur when all six legs come in pairs of nearly equal and opposite wave-vectors. The most important diagrams are displayed in panels *h* and *i* of Fig. 3.2 and the sum of their contributions is

$$N_\zeta^{(6)}(\mathbf{k}_1, \mathbf{q}_1 - \mathbf{k}_1, \mathbf{k}_2, \mathbf{q}_2 - \mathbf{k}_2, \mathbf{k}_3, \mathbf{q}_3 - \mathbf{k}_3) = \left(\frac{H^2}{\dot\phi_0}\right)^6 \left(\frac{V'''}{H}\right)^4 \frac{1}{k_1^3 k_2^3 k_3^3} \frac{2(3\mu/2)^6 H^{14}}{(\mu^2+m^2)^{10}} \times \left(1 + \frac{1}{2}\left(\frac{q^3}{k_1 k_2 k_3}\right)^{\alpha_-/3}\right)\left(\frac{q_1 q_2 q_3}{k_1 k_2 k_3}\right)^{\alpha_-}\left[\frac{1}{q_2^3 q_3^3} + \frac{1}{q_1^3 q_3^3} + \frac{1}{q_1^3 q_2^3}\right] \tag{3.67}$$

3.4 Correlation Functions of Biased Objects

In this section we review the computation of the galactic halo power spectrum, and compute the bispectrum in the limit of large halo separation. At large enough separation, the primordial non-Gaussian contributions to the power spectrum and bispectrum are larger than the Gaussian ones. This leads to interesting observable long wavelength effects. The long wavelength scaling of the power spectrum was already discussed in [50]. Here we compute the long wavelength enhanced contributions and present results for the bispectrum as well.

We start by assuming halos form instantaneously, at the same time t_{coll}, and at points where the matter overdensity $\delta(\mathbf{x})$ averaged over a spherical region with comoving radius R exceeds a threshold δ_c. We choose the smoothing radius R to be of order the characteristic length scale of the region of space that collapses to form a halo.[9] The smoothed matter overdensity is related to the matter overdensity by

$$\delta_R(\mathbf{x}, a) = \int d^3\mathbf{y}\; W_R(|\mathbf{x} - \mathbf{y}|)\delta(\mathbf{y}, a). \tag{3.68}$$

[9] We set $R = 1.9\mathrm{h}^{-1}\mathrm{M}pc$.

Here $W_R(|\mathbf{x}-\mathbf{y}|) = \Theta_H(R-|\mathbf{x}-\mathbf{y}|)$ is the top hat window function.[10] The Fourier transform of the window function is:

$$W_R(k) = \frac{3\,(sinkR - kRcoskR)}{(kR)^3}. \tag{3.69}$$

Assuming $\delta(\mathbf{x}, a)$ undergoes linear growth before the collapse time, we can express the density perturbations at the time of collapse in terms of the linearly evolved density perturbations today, $\delta_R(\mathbf{x}, a_{coll}) = \delta_R(\mathbf{x})D(a_{coll})$ where today $a = 1$ and the growth factor $D(1) = 1$.

We will ignore the evolution of halos after collapse, and so the number density of halos today, up to an irrelevant dimensionful normalization constant, is given by:

$$n_h(\mathbf{x}) = \Theta_H(\delta_R(\mathbf{x}, a_{coll}) - \delta_c(a_{coll})) = \Theta_H(\delta_R(\mathbf{x}) - \delta_c) \tag{3.70}$$

where $\delta_c \equiv \delta_c(a_{coll})/D(a_{coll})$. We use $\delta_c = 4.215$, which assumes that $\delta_c(a_{coll}) = 1.686$ with $z_{coll} = 1.5$ [54]. The halo overdensity $\delta_h(\mathbf{x})$ at a point $\mathbf{x}$ today is defined by

$$\delta_h(\mathbf{x}) = \frac{n_h(\mathbf{x}) - \langle n_h\rangle}{\langle n_h\rangle}. \tag{3.71}$$

where $\langle n_h\rangle$ is the average halo density.

We are interested in the two- and three-point functions of $\delta_h(\mathbf{x})$. These can be computed using (3.70) and the path integral techniques discussed in [57]. A more general approach that we adopt here is to write δ_h as[11,12]

$$\delta_h(\mathbf{x}) = b_1\delta_R(\mathbf{x}) + b_2(\delta_R^2(\mathbf{x}) - \langle\delta_R^2\rangle) + \dots \tag{3.72}$$

The constants b_1 and b_2 are bias coefficients. They can be computed using a specific model of halo formation such as (3.70) that expresses the halo overdensity in terms of δ_R or determined from data. The two-point function of the halo overdensity is then:

$$\begin{aligned}\langle\delta_h(\mathbf{x})\delta_h(\mathbf{y})\rangle \;=\;& b_1^2\,\langle\delta_R(\mathbf{x})\delta_R(\mathbf{y})\rangle \\ &+b_1b_2\left\langle(\delta_R^2(\mathbf{x}) - \left\langle\delta_R^2\right\rangle)\delta_R(\mathbf{y})\right\rangle + \left\langle\delta_R(\mathbf{x})(\delta_R^2(\mathbf{y}) - \left\langle\delta_R^2\right\rangle)\right\rangle \\ &+b_2^2\left\langle(\delta_R^2(\mathbf{x}) - \left\langle\delta_R^2\right\rangle)(\delta_R^2(\mathbf{y}) - \left\langle\delta_R^2\right\rangle)\right\rangle + \dots\ .\end{aligned} \tag{3.73}$$

[10] Θ_H is the Heaviside step function.

[11] The ellipses denote higher order terms in the bias expansion. They are not needed to the order we work in (qR) and (V'''/H). However it is important to remember that they are defined with subtractions. For example, the next order term is $b_3(\delta_R^3(\mathbf{x}) - 3\langle\delta_R^2\rangle\delta_R(\mathbf{x}))$.

[12] A completely general approach is possible; for a review, see [58].

Note

$$\left\langle \delta_R^2(\mathbf{x})\delta_R^2(\mathbf{y})\right\rangle = \left\langle \delta_R^2\right\rangle^2 + \langle \delta_R(\mathbf{x})\delta_R(\mathbf{y})\rangle^2 + \left\langle \delta_R^2(\mathbf{x})\delta_R^2(\mathbf{y})\right\rangle_c . \tag{3.74}$$

We can neglect the second term because it is very small at large halo separations compared to the b_1^2 term in (3.73). All factors of $\left\langle \delta_R^2\right\rangle$ cancel and we find

$$\begin{aligned}\langle \delta_h(\mathbf{x})\delta_h(\mathbf{y})\rangle \simeq\ & b_1^2 \langle \delta_R(\mathbf{x})\delta_R(\mathbf{y})\rangle + b_1 b_2(\left\langle \delta_R^2(\mathbf{x})\delta_R(\mathbf{y})\right\rangle + \left\langle \delta_R(\mathbf{x})\delta_R^2(\mathbf{y})\right\rangle) + b_2^2 \left\langle \delta_R^2(\mathbf{x})\delta_R^2(\mathbf{y})\right\rangle_c \\ & + \dots .\end{aligned} \tag{3.75}$$

The term proportional to b_1^2 comes from the Gaussian two-point function of ζ and the remaining terms arise from the connected three- and four-point functions of ζ that we computed earlier.

Similarly, we can express the three-point function of δ_h as:

$$\begin{aligned}\langle \delta_h(\mathbf{x})\delta_h(\mathbf{y})\delta_h(\mathbf{z})\rangle =\ & b_1^3 \langle \delta_R(\mathbf{x})\delta_R(\mathbf{y})\delta_R(\mathbf{z})\rangle_c + b_2^3 \left\langle \delta(\mathbf{x})^2\delta(\mathbf{y})^2\delta(\mathbf{z})^2\right\rangle_c \\ & + \left[2b_1^2 b_2 \langle \delta_R(\mathbf{x})\delta_R(\mathbf{y})\rangle \langle \delta_R(\mathbf{x})\delta_R(\mathbf{z})\rangle + b_1^2 b_2 \left\langle \delta_R^2(\mathbf{x})\delta_R(\mathbf{y})\delta_R(\mathbf{z})\right\rangle_c \right. \\ & \left. + b_1 b_2^2 \left\langle \delta_R^2(\mathbf{x})\delta_R^2(\mathbf{y})\delta_R(\mathbf{z})\right\rangle_c + cyc.\ perm(\mathbf{x},\mathbf{y},\mathbf{z})\right] + \dots\end{aligned} \tag{3.76}$$

The first term proportional to $b_1^2 b_2$ is the three-point halo correlation when the underlying curvature perturbations are Gaussian, which was first calculated in [57]. The remaining terms arise from the non-Gaussian correlations of the primordial fluctuations. In the next section we present a power counting argument showing that for widely separated points $|\mathbf{x}-\mathbf{y}| >> R$ and $|V'''|/H < 1$, the higher order terms in the bias expansion are negligible in the threshold model. Only b_1 and b_2 are needed to compute the halo overdensity power spectrum and bispectrum evaluated at wave-vectors $q << 1/R$.

Using, for example, path integral methods, it is straightforward to derive expressions for $\langle n_h\rangle$ and the bias coefficients b_1 and b_2 in the threshold model mentioned above. They can be expressed in terms of δ_c and

$$\sigma_R^2 = \langle \delta_R(\mathbf{x})\delta_R(\mathbf{x})\rangle \tag{3.77}$$

as

$$\langle n_h\rangle = \frac{1}{2} erfc\left(\frac{\delta_c}{\sqrt{2}\sigma_R}\right) \tag{3.78}$$

and

$$b_1 = \frac{e^{-\delta_c^2/(2\sigma_R^2)}}{\sqrt{2\pi}\sigma_R \langle n_h\rangle} \quad b_2 = \frac{e^{-\delta_c^2/(2\sigma_R^2)}\delta_c}{2\sqrt{2\pi}\sigma_R^3 \langle n_h\rangle}. \tag{3.79}$$

The Fourier transformed smoothed matter overdensity $\delta_R(\mathbf{k})$ is related to the curvature perturbation through

$$\delta_R(\mathbf{k}) = \frac{2k^2}{5\Omega_m H_0^2} T(k) W_R(k) \zeta_{\mathbf{k}} \tag{3.80}$$

where $T(k)$ is the transfer function, Ω_m is the ratio of the matter density to the critical density today, and H_0 is the Hubble constant evaluated today [1]. When performing integrals against $T(k)$ we use the BBKS approximation to the transfer function [59]:

$$T\left(k = \left(\Omega_m h^2 \mathrm{M}pc^{-1}\right) u\right) = \frac{\ln\left[1 + 2.34u\right]}{(2.34u)} \left[1 + 3.89u + (16.2u)^2 + (5.47u)^3 + (6.71u)^4\right]^{-1/4} \tag{3.81}$$

We can then write σ_R^2 as

$$\sigma_R^2 = \left(\frac{H^2}{\dot{\phi}_0} \frac{2}{5} \frac{1}{\Omega_m H_0^2 R^2}\right)^2 C_2(\mu, m) \mathcal{J} \tag{3.82}$$

where

$$\mathcal{J} = \frac{1}{2\pi^2} \int_0^\infty dx x^3 T(x/R)^2 W(x)^2 \tag{3.83}$$

and $W(x) \equiv W_R(x/R)$ is independent of R.

The Fourier transform of the halo two-point gives the halo power spectrum

$$P_{hh}(q) = \int d^3\mathbf{x} \, \langle \delta_h(\mathbf{x}) \delta_h(\mathbf{0}) \rangle \, e^{-i\mathbf{q}\cdot\mathbf{x}}. \tag{3.84}$$

Fourier transforming (3.75) and plugging in (3.80) to express the correlation functions of $\delta_R(\mathbf{k})$ in terms of those of $\zeta_{\mathbf{k}}$, we find for $q << 1/R$:

$$P_{hh}(\mathbf{q}) = b_1^2 \alpha_R(q)^2 P_\zeta(\mathbf{q}) + 2 b_1 b_2 \alpha_R(\mathbf{q}) \int \frac{d^3k}{(2\pi)^3} \alpha_R(k)^2 B_\zeta(\mathbf{q}, \mathbf{k}, -\mathbf{k} - \mathbf{q}) + b_2^2 \int \frac{d^3k_1}{(2\pi)^3} \frac{d^3k_2}{(2\pi)^3} \alpha_R(k_1)^2 \alpha_R(k_2)^2 N_\zeta^{(4)}(\mathbf{k}_1, \mathbf{q} - \mathbf{k}_1, \mathbf{k}_2, -\mathbf{k}_2 - \mathbf{q}). \tag{3.85}$$

To condense the expression we have defined

$$\alpha_R(k) = \frac{2k^2}{5\Omega_m H_0^2} T(k) W_R(k). \tag{3.86}$$

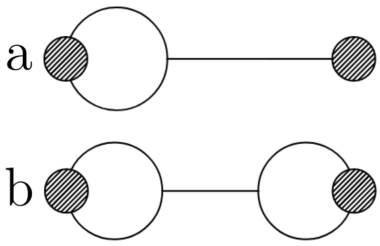

Figure 3.3: A diagrammatic representation of terms contributing to the galactic halo power spectrum. Cf. Fig. 3.1.

The wave-vectors integrated over in the integrals of (3.85) are of order $1/R$. Since we are interested in $q << 1/R$ the curvature bispectrum and trispectrum appearing in (3.85) are in their squeezed and collapsed configurations. Equations (3.58) and (3.64) imply the strongest small q scaling of the primordial squeezed bispectrum and collapsed trispectrum are $1/q^{3-\alpha_-}$ and $1/q^{3-2\alpha_-}$. Note that the bispectrum's contribution to the halo power spectrum is suppressed by a factor of $\alpha_R(q) \propto q^2$, so that term goes like $1/q^{1-\alpha_-}$.

An intuitive picture of the non-Gaussian contributions to (3.85) is given by Fig. 3.3. The shaded circles represent the halo overdensity, while the lines they are attached to are ζ legs. In these graphs, the external ζ legs are each multiplied by α_R. If one ζ leg is attached to a shaded circle it carries a soft wave-vector and a factor of b_1. If two legs are attached to a shaded circle, they carry equal and opposite wave-vectors with magnitude approximately $1/R$. In this case, the shaded circle also contains a factor of b_2 and a wave-vector integral.

The halo power spectrum is then[13]

$$P_{hh}(q) = P^G_{hh}(q)\left[1 + \gamma(\mu, m)\left(2\frac{\beta(\mu, m)}{(qR)^{2-\alpha_-}T(q)} + \frac{\beta(\mu, m)^2}{(qR)^{4-2\alpha_-}T(q)^2}\right)\right] \tag{3.87}$$

[13]In writing (3.87) we have used $\int_0^\infty dx x^{3-n\alpha_-}T(x/R)^2W(x)^2 \simeq \int_0^\infty dx x^3 T(x/R)^2W(x)^2$, where n is an O(1) integer.

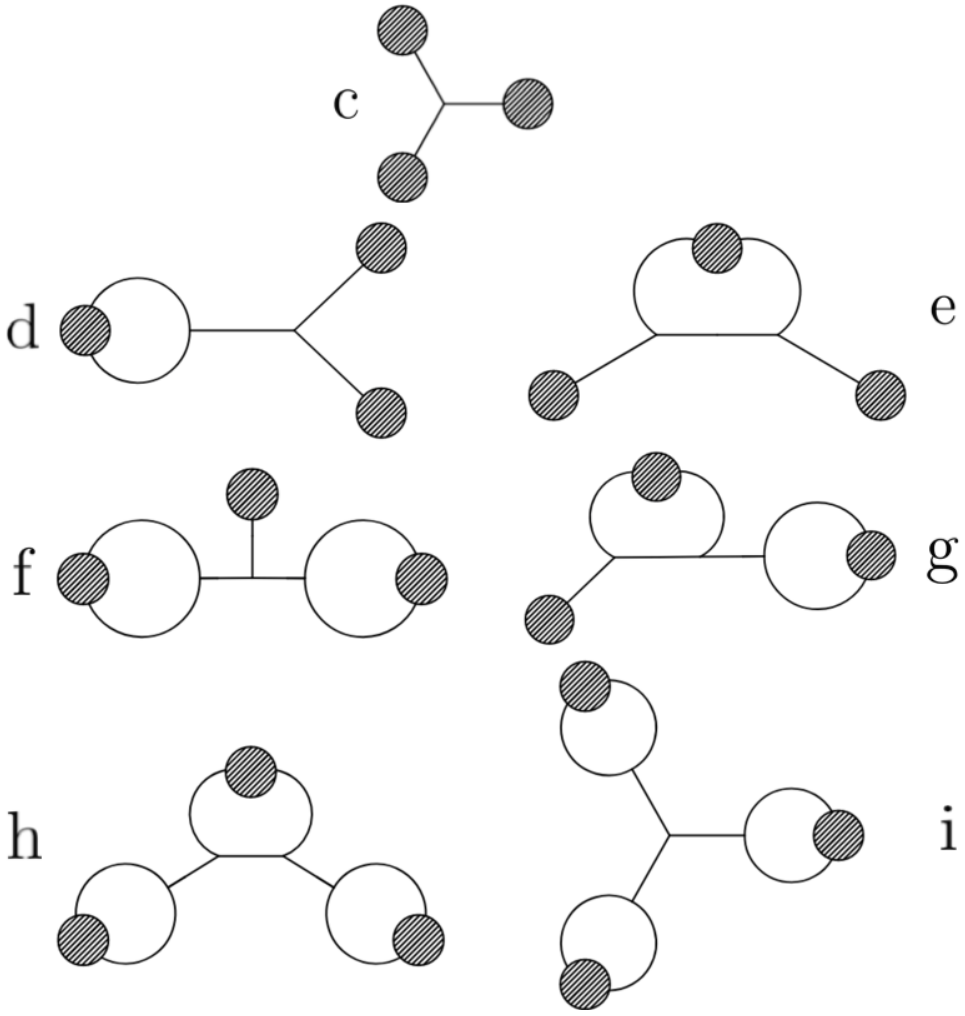

Figure 3.4: A diagrammatic representation of terms contributing to the galactic halo bispectrum. Cf. Fig. 3.2.

where

$$
\begin{aligned}
P^G_{hh}(q) &= b_1^2 P_{mm}(q) \\
P_{mm}(q) &= R^3 C_2(\mu, m) \left(\frac{H^2}{\dot\phi_0}\right)^2 \left(\frac{2}{5\Omega_m H_0^2 R^2}\right)^2 (qR) T(q)^2 \\
\gamma(\mu, m) &= \frac{9\mu^2 H^2}{(\mu^2 + m^2)^2 + 9\mu^2 H^2} \\
\beta(\mu, m) &= \frac{6}{5}\frac{b_2}{b_1}\frac{H^2}{\dot\phi_0}\frac{2}{5\Omega_m H_0^2 R^2} \mathcal{J} f_{NL} \sqrt{2\pi^2 \Delta_\zeta^2} C_2(\mu, m)^{\frac{3}{2}} \frac{(\mu^2 + m^2)^2}{(3\mu/2)^2 H^2}.
\end{aligned} \tag{3.88}
$$

P_{mm} denotes the "matter-matter" power spectrum, *i.e.*, the Fourier transform of $\langle \delta_R(\mathbf{x}) \delta_R(\mathbf{y}) \rangle$.

Since $0 < \gamma(\mu, m) < 1$, it is simple to show that $P_{hh}(q)$ is positive definite, as it must be. Note that for $f_{NL} < 0$, this would not be true at very small wave-vectors without the contribution due to the four-point function of ζ. The scale non-Gaussianities begin to dominate is $(qR)^2 \sim \beta(\mu, m) \propto f_{NL}$ (up to $(qR)^{\alpha_-}$ terms). Current measurements of the galactic power spectrum have not seen significant deviations from Gaussian initial conditions at wave-vectors around $q \sim h/(100\ \mathrm{M}pc)$ [60].

In the threshold model, we find that $\beta \propto R^2$, indicating that the scale at which non-Gaussianities begin to dominate is independent of model parameter R.

On the other hand, we can also compute the matter-halo cross correlation power spectrum $P_{hm}(q)$, which corresponds to the two-point function $\langle \delta_h(\mathbf{x}) \delta_R(\mathbf{y}) \rangle$. The "$h$" in P_{hm} stands for halo, and the "m" for matter. The result is

$$P_{hm}(q) = b(q) P_{mm}(q) \tag{3.89}$$

where

$$b(q) \equiv b_1 + b_1 \gamma(\mu, m) \beta(\mu, m) \frac{1}{(qR)^{2-\alpha_-} T(q)}. \tag{3.90}$$

This implies a scale-dependent bias:[14]

$$\Delta b(q) = b_1 \gamma(\mu, m) \beta(\mu, m) \frac{1}{(qR)^{2-\alpha_-} T(q)}. \tag{3.91}$$

In local non-Gaussianity, $\Delta b(q) \propto q^{-2}$. Then QSFI predicts a different shape for the scale-dependent bias, which is distinguishable from local non-Gaussianity if α_- is large enough.

Note that P_{hh} can be written in this notation as:

$$P_{hh}(q) = \left(b(q)^2 + b_1^2 \beta(\mu, m)^2 \gamma(\mu, m) \left(1 - \gamma(\mu, m)\right) \frac{1}{(qR)^{4-2\alpha_-} T(q)^2} \right) P_{mm}(q). \tag{3.92}$$

In this form, the second term in the brackets is due to stochastic bias. Note that this term is proportional to $1 - \gamma(\mu, m)$, which approaches 0 in the limit that $\mu \gtrsim m$ as μ/H and m/H go to zero. This suppression is evident in Fig. 3.5. If the stochastic bias were zero, then the purple curves' minimum value would be 0. Since they all reach a minimum value less than around 0.1, this indicates that the stochastic bias

[14] Recall that we have neglected the time evolution of the distribution of galaxies after they have formed.

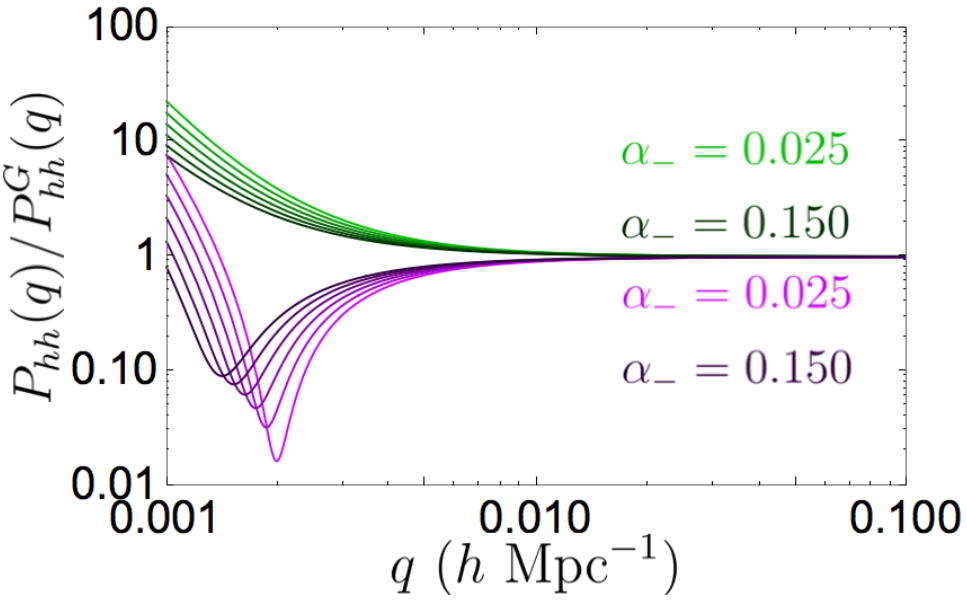

Figure 3.5: We plot the ratio of the galactic halo power spectrum in quasi-single field inflation to the halo power spectrum in which there are no primordial non-Gaussianities for a range of α_-: $\alpha_- = 0.025$ (lightest), 0.050, 0.075, 0.100, 0.125, 0.150 (darkest). We plot for $\mu = m$ and $f_{NL} = 10$ (green) and $f_{NL} = -10$ (purple).

is small in the $\mu \sim m$ regime. However, for $\mu << m$ the stochastic bias can become large, see Fig. 3.6. For local non-Gaussianity, stochastic bias is absent. As we will show toward the end of this section, for μ several orders of magnitude smaller than m, other contributions to the power spectrum that we have neglected become important.

In figures 3.5 and 3.6, we plot the ratio of the galactic halo power spectrum in quasi-single field inflation divided by the Gaussian contribution P^G_{hh}. Notice that for reasonable model parameters, $P_{hh}(q)$ begins to differ from $P^G_{hh}(q)$ at $q \sim 0.005h/\mathrm{M}pc$. The difference becomes very large for values of q significantly less than this. Figures 3.5 and 3.6 use $f_{NL} = \pm 10$, and various values for α_- and μ.

Let us now study the halo three-point function given in equation (3.76). The non-Gaussian contributions are depicted in Figure 3.4. Fourier transforming equation

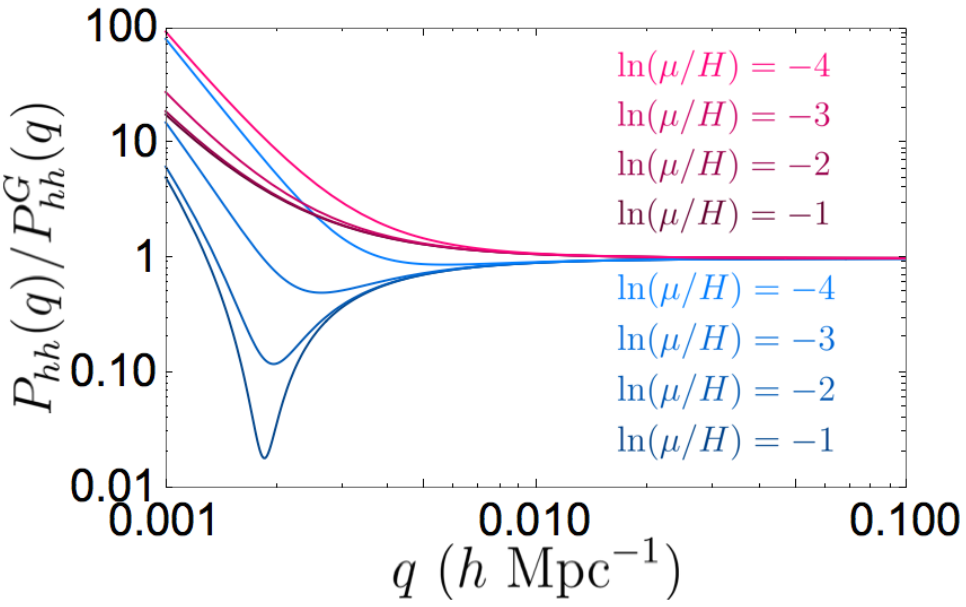

Figure 3.6: We plot the ratio of the galactic halo power spectrum in quasi-single field inflation to the halo power spectrum in which there are no primordial non-Gaussianities for a range of μ. We plot for $\ln(\mu/H) = -1$ (darkest), -2, -3, -4 (lightest), with $\alpha_- = 0.05$ and $f_{NL} = 10$ (pink) and $f_{NL} = -10$ (blue).

(3.76), we find that the bispectrum of the halo overdensity is

$$
\begin{aligned}
&B_{hhh}(\mathbf{q}_1,\mathbf{q}_2,\mathbf{q}_3) = b_1^3\alpha_R(q)^3 B_\zeta(\mathbf{q}_1,\mathbf{q}_2,\mathbf{q}_3)\\
&+\big[2b_1^2 b_2\alpha_R(q_2)^2\alpha_R(q_3)^2 P_\zeta(q_2)P_\zeta(q_3)\\
&+b_1^2 b_2\alpha_R(q_2)\alpha_R(q_3)\int\frac{d^3k}{(2\pi)^3}\alpha_R(k)^2 N_\zeta^{(4)}(\mathbf{k},\mathbf{q}_1-\mathbf{k},\mathbf{q}_2,\mathbf{q}_3)\\
&+b_1 b_2^2\alpha_R(q_3)\int\frac{d^3k_1}{(2\pi)^3}\frac{d^3k_2}{(2\pi)^3}\alpha_R(k_1)^2\alpha_R(k_2)^2 N_\zeta^{(5)}(\mathbf{k}_1,\mathbf{q}_1-\mathbf{k}_1,\mathbf{k}_2,\mathbf{q}_2-\mathbf{k}_2,\mathbf{q}_3)\\
&+\text{cyc. perm}(\mathbf{q}_1,\mathbf{q}_2,\mathbf{q}_3)\big]\\
&+b_2^3\int\frac{d^3k_1}{(2\pi)^3}\frac{d^3k_2}{(2\pi)^3}\frac{d^3k_3}{(2\pi)^3}\alpha_R(k_1)^2\alpha_R(k_2)^2\alpha_R(k_3)^2\\
&\times N_\zeta^{(6)}(\mathbf{k}_1,\mathbf{q}_1-\mathbf{k}_1,\mathbf{k}_2,\mathbf{q}_2-\mathbf{k}_2,\mathbf{k}_3,\mathbf{q}_3-\mathbf{k}_3).
\end{aligned}
\tag{3.93}
$$

Similar to the calculation of the two-point, we can simplify the wave-vector integrals

to express the bispectrum as

$$
\begin{aligned}
B_{hhh}(\mathbf{q}_1,\mathbf{q}_2,\mathbf{q}_3) = 2b_1^2 b_2 R^6 \left(\frac{H^2}{\dot\phi_0}\right)^4 \left(\frac{2}{5\Omega_m H_0^2 R^2}\right)^4 C_2^2 \Bigg[& T(q_1)^2 T(q_2)^2 q_1 q_2 R^2 . \\
+\ \omega(\mu,m) \Bigg(& \beta(\mu,m) \frac{q_1^2}{q_2 q_3} T(q_1)T(q_2)T(q_3) \\
& + \beta(\mu,m)^2 T(q_2)T(q_3)(qR)^{\alpha_-} \left[\frac{q_2^2}{R^2 q_1^3 q_3} + \frac{q_3^2}{R^2 q_1^3 q_2} + 2\Big(1+\frac{1}{2}(qR)^{\alpha_-}\Big)\frac{1}{R^2 q_2 q_3} \right] \\
& + \beta(\mu,m)^3 T(q_3)(qR)^{2\alpha_-} \left[\frac{q_3^2}{q_1^3 q_2^3 R^4} + 2\Big(1-\frac{1}{12}\left(qR\right)^{\alpha_-}\Big)\frac{1}{R^4 q_2^3 q_3} \right. \\
& \left. +2\Big(1-\frac{1}{12}\left(qR\right)^{\alpha_-}\Big)\frac{1}{R^4 q_1^3 q_3} \right] \\
& + \beta(\mu,m)^4 (qR)^{3\alpha_-}\left(2+(qR)^{\alpha_-}\right)\frac{1}{R^6 q_1^3 q_2^3} \Bigg) \Bigg] + \text{ cyc. perm}(q_1,q_2,q_3).
\end{aligned}
\tag{3.94}
$$

where $q \equiv max(q_i)$, and

$$
\omega(\mu,m) = \frac{b_1^2}{4b_2^2}\frac{1}{\mathcal{J}C_2}\left(\frac{\dot\phi_0}{H^2}\right)^2\left(\frac{5\Omega_m H_0^2 R^2}{2}\right)^2 \gamma(\mu,m). \tag{3.95}
$$

Again, the scale at which the non-Gaussian contributions begin to dominate is $(qR)^2 \sim \beta(\mu,m)$, which means the galactic power spectrum and bispectrum both begin to deviate from their Gaussian contributions at roughly the same scale. Since it is easier to measure the halo two-point function than the halo three-point function, it is more likely that we will see these non-Gaussian effects in the halo two-point before we see them in the three-point.

The equilateral configuration of the galactic halo bispectrum is plotted in Figs. 3.7 and 3.8 for various values of α_- and μ. Note that we have scaled the bispectrum by its value when $V''' = 0$,

$$
\begin{aligned}
B^G_{hhh}(\mathbf{q}_1,\mathbf{q}_2,\mathbf{q}_3) = 2b_1^2 b_2 R^6 \left(\frac{H^2}{\dot\phi_0}\right)^4 \left(\frac{2}{5\Omega_m H_0^2 R^2}\right)^4 & C_2^2 T(q_1)^2 T(q_2)^2 q_1 q_2 R^2 \\
+\ cyc.\ perm(q_1,q_2,q_3). &
\end{aligned}
\tag{3.96}
$$

In the equilateral configuration with $f_{NL} < 0$, this scaled bispectrum never falls significantly below unity. Note also that it rises more rapidly than the scaled power spectrum shown in Figs. 3.5 and 3.6 as q becomes small.

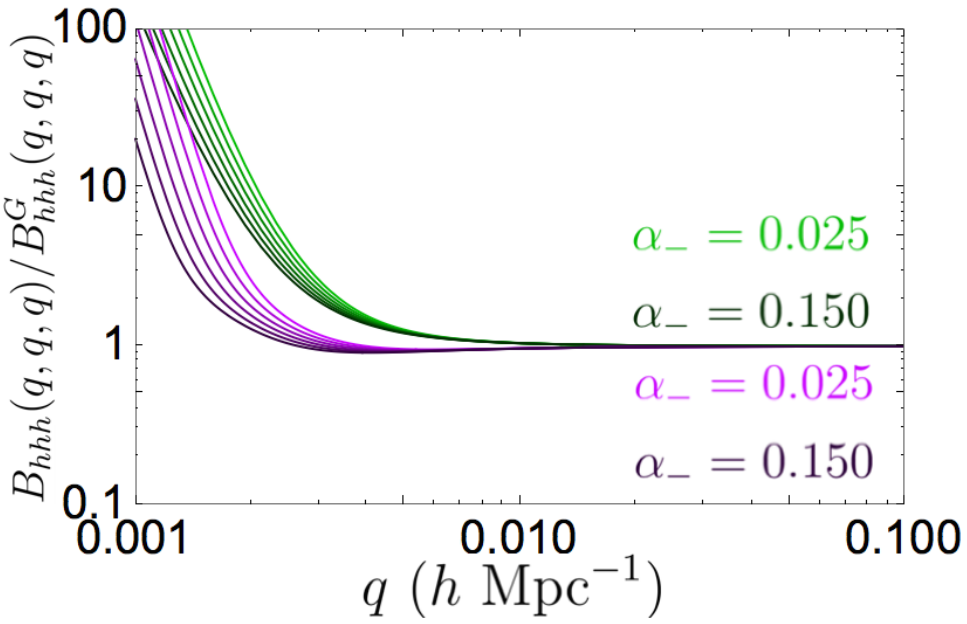

Figure 3.7: We plot the ratio of the galactic halo bispectrum in quasi-single field inflation to the galactic halo bispectrum with no primordial non-Gaussianities (B^G_{hhh}) in the equilateral configuration for a range of α_-: $\alpha_- = 0.025$ (lightest), 0.050, 0.075, 0.100, 0.125, 0.150 (darkest). We plot for $\mu = m$ and $f_{NL} = 10$ (green) and $f_{NL} = -10$ (purple).

Equation (3.94) expresses the bispectrum in terms of the magnitude of the wave-vectors $\mathbf{q}_1, \mathbf{q}_2$ and $\mathbf{q}_3$. It could also be expressed in terms of q_1 and q_2 and the angle between them. This angular dependence is usually displayed as a multipole expansion.

Currently, there are measurements of the galaxy bispectrum at wave-vectors as small as about $h/(20\ \mathrm{M}pc)$ [61]. There is no evidence in this data for the type of effects we have found.

We have ignored the evolution of the galactic halo distribution after their collapse. These effects are $O(1)$. However, we do not expect that including them greatly shifts at what scale non-Gaussianities or their rapid growth become important. One can include these effects either by numerical simulation or analytic methods [62–64]. Evolution during this period is expected to decrease the influence of bias, drawing the galactic distribution closer to the dark matter distribution. Some of these effects cancel out in the ratios we have plotted.

We have chosen to plot the power spectrum and bispectrum scaled by P^G_{hh} and B^G_{hhh} since these ratios are less sensitive to the value of R than the power spectrum and

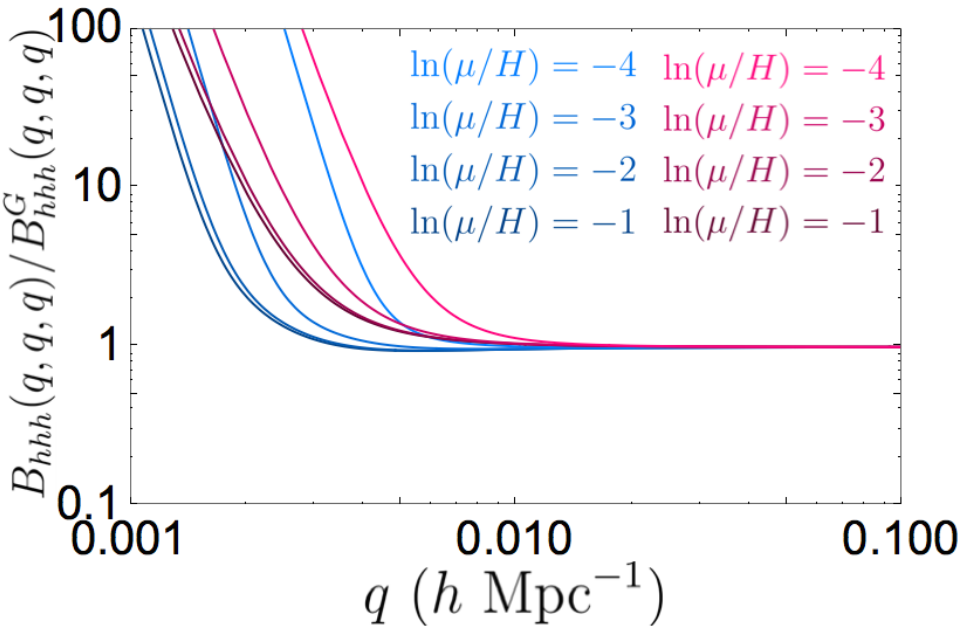

Figure 3.8: We plot the ratio of the galactic halo bispectrum in quasi-single field inflation to the galactic halo bispectrum with no primordial non-Gaussianities (B^G_{hhh}) in the equilateral configuration for a range of μ: $\ln(\mu/H) = -1$ (darkest), -2, -3, -4 (lightest). We plot for $\alpha_- = 0.05$ and $f_{NL} = 10$ (pink) and $f_{NL} = -10$ (blue).

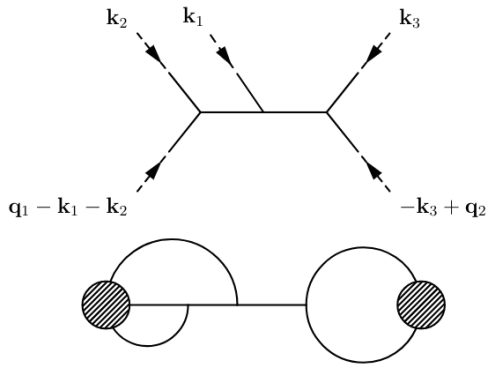

Figure 3.9: The above diagram can contribute significantly to the galactic halo power-spectrum if $|V'''|/H$ is not very small. However, it can be ignored as long as $|V'''|/H << 1$. In the context of eq. (3.97), this is a $p = 1$, $j = 0$ term.

bispectrum alone.

It is possible to use the methods developed here to consider even higher correlations of the halo overdensity. The dependence of galactic halo n-point correlations on the parameters V''', q, and R in quasi-single field inflation with the halo number density

modeled by eq. (3.70) is given by

$$\langle \delta_h^n \rangle \sim R^{3(n-1)} (qR)^{n-1} \left[1 + \sum_{i=n-2}^{2n-2} \left(\frac{V'''}{H(qR)^2} \right)^i \sum_{j=0}^{n-1} \sum_{p=0}^{\infty} (qR)^{3j} \left(\frac{V'''}{H} \right)^p \right] \tag{3.97}$$

where for simplicity, factors of $(qR)^{\alpha_-}$ have been set to unity. In our analysis of the power spectrum ($n = 2$) and the bispectrum ($n = 3$), we have included only the $j = p = 0$ terms in the sums.

Recall, the validity of our calculations relies on the several assumptions. First of all we have assumed that $\alpha_- = (\mu^2 + m^2)/3H^2 << 1$. However, we must also have $\alpha_- \gtrsim 1/60$ or else superhorizon evolution would have persisted to the end of inflation. Finally, we assumed $qR << 1$ and $|V'''|/H << 1$. Note that for fixed $|f_{NL}| = 10$ and $\alpha_- = 0.05$, then $|V'''|/H > 1$ for $\mu < 0.005$. Therefore, our results do not apply at very small μ/m. For $|V'''|/H$ not small, we would need to include additional contributions, *e.g.*, the diagram shown in Fig. 3.9.

3.5 Conclusions

The $1/q^3$ dependence of the de-Sitter propagator for massless scalar fields implies that if the primordial curvature fluctuations are non-Gaussian, they have the potential to give rise to enhancements in the correlations of biased objects at small wave-vectors [30, 49]. This effect cannot be produced by nonlinear gravitational evolution without primordial non-Gaussianities. The main goal of this chapter was to explore these enhancements within quasi-single field inflation.

We developed a method to analytically compute the correlation functions of the curvature perturbation ζ in quasi-single field inflation in the limit of small m/H and μ/H. We computed the three- and four-point functions of ζ for arbitrary external wave-vectors and computed the five- and six-point functions in the kinematic limits that give the strongest long wavelength enhanced contributions to the three-point function of the galactic halo overdensity δ_h.

We applied these results to the computation of the two- and three-point correlations of δ_h (*i*.e., the power spectrum and bispectrum). For model parameters consistent with the constraints on f_{NL}, we found that non-Gaussian contributions to these correlation functions are larger than the Gaussian ones at scales around $h/(200\mathrm{M}pc)$. Even larger scales will be probed in upcoming large scale surveys such as SPHEREx. Prospects for future improvements in measurements of the galactic power spectrum and bispectrum are reviewed in [65].

After making a number of approximations, we obtained analytic expressions for the power spectrum and bispectrum[15] of δ_h that are valid at small wave-vectors. We studied the dependence of the stochastic bias on the parameters μ and m, and found that it could be small or significant depending on the values of μ and m.

The departure from the predictions of Gaussian primordial perturbations in both the equilateral configuration of the bispectrum and the power spectrum begin at wave-vectors around $h/(200\mathrm{M}pc)$ (when $|f_{NL}|$ is near its upper bound). However, for the bispectrum the deviation grows much more rapidly as the wave-vectors decrease than in the power spectrum. Unfortunately, it is more difficult to measure the three-point correlation than the two-point correlation of δ_h. If these enhancements exist, it is more likely we will first see them in the power spectrum than in the bispectrum. Finally, we identified the scaling of the n-point function of δ_h.

The calculations (at small wave-vectors) of the galactic power spectrum and bispectrum presented in this chapter can be improved and made more model independent. We hope to address this in future work.

3.A Numerical Checks

In this appendix we check that the analytical results we derived for the two- and three-point functions of ζ agree with the numerical evaluation of these quantities. First, consider the two-point function. In equation (3.29), we absorbed all of the μ and m dependence of the curvature perturbation power spectrum into the constant $C_2(\mu, m)$. We can express this quantity in terms of the exact mode functions of π as

$$C_2(\mu, m) = \sum_i |\pi^{(i)}(0)|^2. \tag{3.98}$$

We found in equation (3.31) that the leading behavior was

$$C_2(\mu, m) \simeq \frac{1}{2} + \frac{9\mu^2 H^2}{2(\mu^2 + m^2)^2}. \tag{3.99}$$

up to terms suppressed by α_-. By extending the numerical techniques developed in [42] and [66] to the region of small μ/H and m/H we can compute (3.98) numerically. In Fig. 3.10 we compare (3.99) to the numerical evaluation of (3.98). The fit is good even for modest values of μ/H as long as m/H is small.

To determine the accuracy of our formula for the bispectrum of ζ (3.54), we compare it with the numerical evaluation of the exact result (3.50) in a couple of kinematic

[15] Since galactic halos are biased objects, even if the primordial fluctuations are Gaussian a halo bispectrum is not zero.

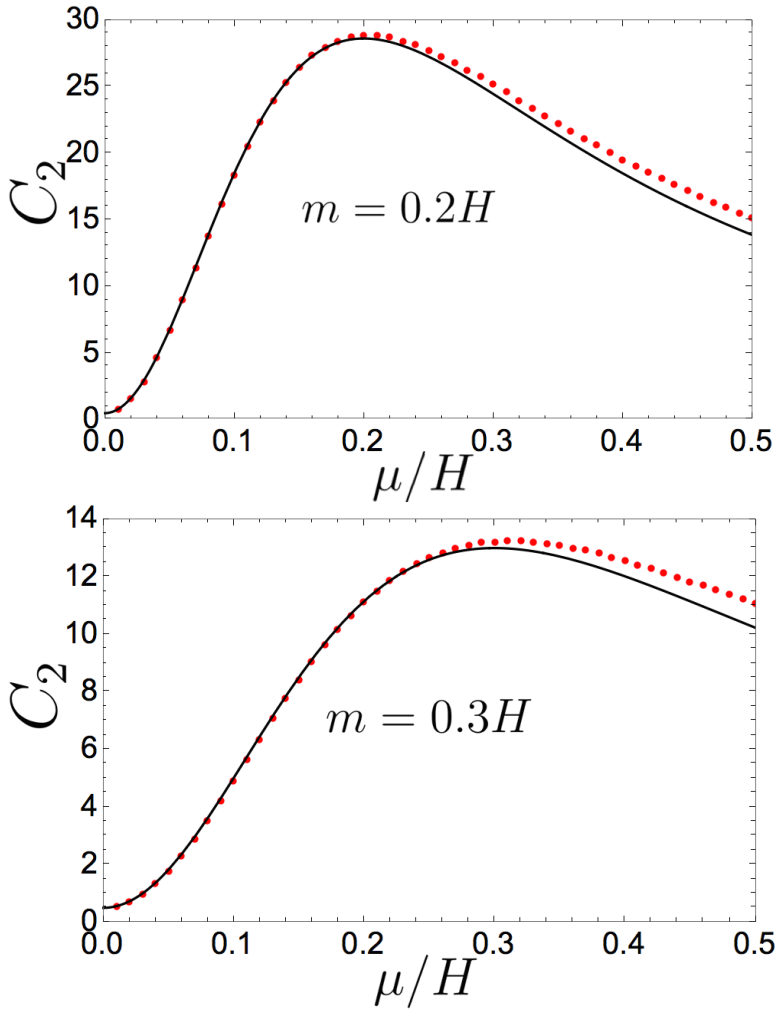

Figure 3.10: We compare the power spectrum (3.33) (red) computed with the numeric mode functions against the leading μ and m expression (3.31) (black) for $m = 0.2H$ (top) and $m = 0.3H$ (bottom).

limits. Let's first consider the equilateral configuration. We define $C_3^{equil}(\mu, m)$ to be the integral in eq. (3.50) in the equilateral configuration:

$$C_3^{equil}(\mu, m) \equiv \int_{-\infty}^{0} \frac{d\eta}{\eta^4} \mathrm{Im}\left[\left(\pi^{(1)}(0)s^{(1)*}(\eta) + \pi^{(2)}(0)s^{(2)*}(\eta)\right)^3\right]. \tag{3.100}$$

Equation (3.55) gives the leading behavior of this integral for small α_-, which we reproduce here for convenience

$$C_3^{equil}(\mu, m) = \frac{3(3\mu/2)^3 H^5}{2\left(\mu^2 + m^2\right)^4}. \tag{3.101}$$

Again, we can use the same numerical techniques to compute (3.100). However, there is a subtlety in its evaluation that needs to be addressed.

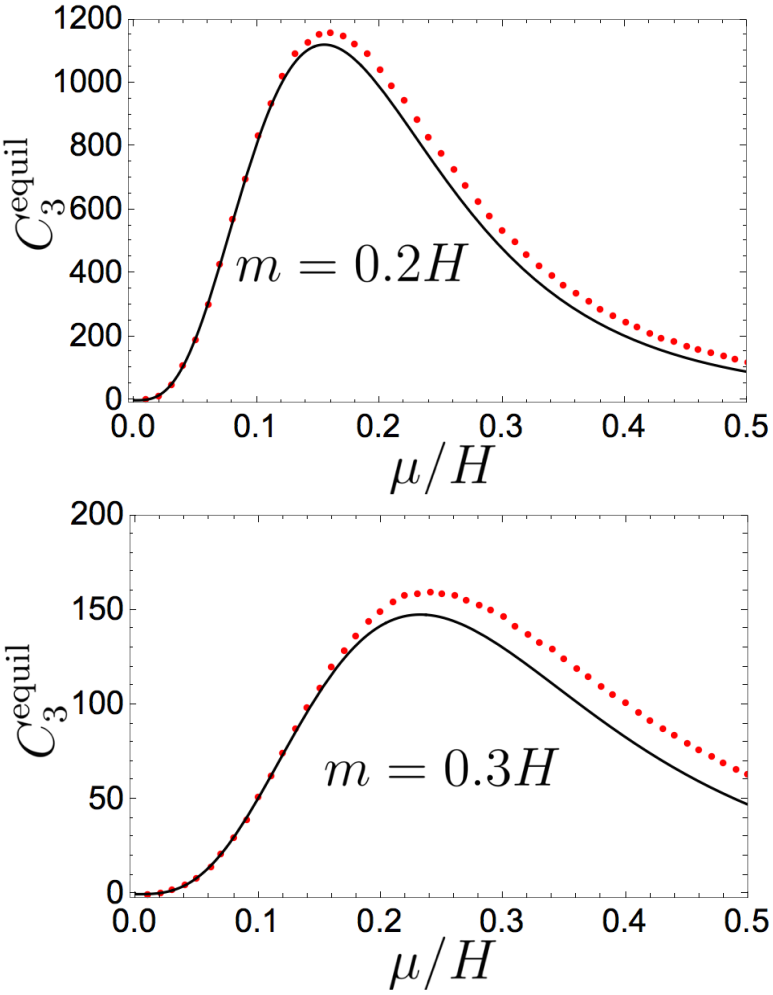

Figure 3.11: We plot the numerical evaluation of (3.100) (red) with the leading μ and m expression (3.101) (black) for $m = 0.2H$ (top) and $m = 0.3H$ (bottom).

As mentioned in section 3.3, the integral is naively IR divergent because of the factor of $1/\eta^4$. However, through the commutation relations, we proved the leading IR behavior is $(-\eta)^{-1+2\alpha_-}$ in the IR, and that the integral is IR finite. However, numerical error prevents the coefficients in front of the potentially IR divergent terms from canceling exactly, giving rise to spurious infinities. The way around this is to define the integrand piecewise about some point η_{IR}. For $\eta < \eta_{IR}$ we use the numerical mode functions in the integrand, and for $\eta > \eta_{IR}$ we set the integrand equal to $a(-\eta)^{-1+2\alpha_-}$, where a is some proportionality constant that can be obtained by fitting the integrand to the correct power law.

In Fig. 3.11 we compare (3.101) to the numerical evaluation of (3.100). As expected the fit is better for smaller values of m, however it is still accurate to around 25 percent

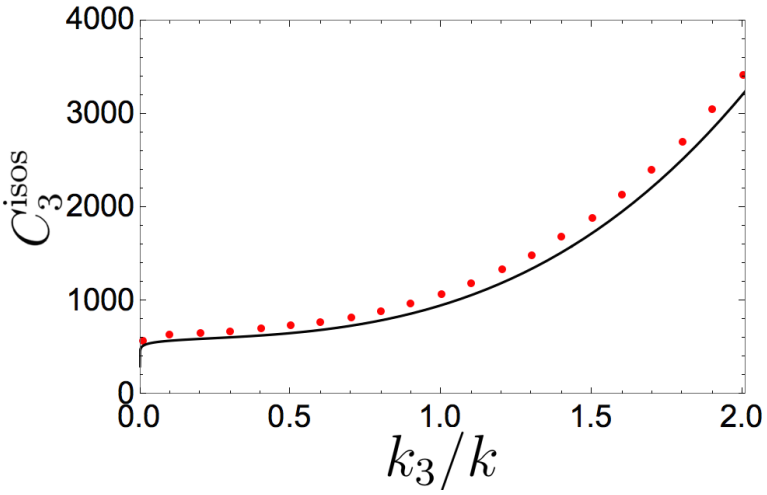

Figure 3.12: We plot the numerical evaluation of (3.51) (red) taking $\mu = 0.3H$, $m = 0.2H$ against (3.104) (black).

even for $\mu = 0.5H$ and $m = 0.3H$.

The previous tests have confirmed the μ and m dependence of our analytic expressions. To test the dependence on the external wave-vectors, we consider the isosceles configuration in which $k_1 = k_2 \equiv k$ and $0 \leq k_3 \leq 2k$. In this limit, equation (3.54) becomes

$$B_\zeta^{isos}(k, k_3) = -\left(\frac{H^2}{\dot\phi_0}\right)^3 \left(\frac{V'''}{H}\right) \frac{1}{k^3 k_3^3} C_3^{isos} \tag{3.102}$$

where we have defined

$$C_3^{isos} \equiv 2\,\mathrm{Im} \int_{-\infty}^{0} \frac{d\eta}{\eta^4} \left(\sum_i \pi^{(i)}(0) s^{(i)*}(\eta)\right)^2 \left(\sum_i \pi^{(i)}(0) s^{(i)*}\left(\frac{k_3}{k}\eta\right)\right). \tag{3.103}$$

Equation (3.53) approximates C_3^{isos} as

$$C_3^{isos}(\mu, m, k, k_3) \simeq \frac{(3\mu/2)^3}{(\mu^2 + m^2)^4} \left[2\left(\frac{k_3}{k}\right)^{\alpha_-} + \frac{k_3^3}{k^3}\right]. \tag{3.104}$$

In Fig. 3.12 we plot (3.104) against the numerical evaluation of (3.103). The errors are around 10 percent for each data point, suggesting the error is not in the wave-vector dependence of the formula, but rather in its μ and m dependent normalization.

3.B Outline of Five- and Six-Point Calculations

In order to compute the three-point correlation of biased objects, it is necessary to compute five- and six-point correlation functions in certain kinematic regimes. The

contribution due to the diagram in panel f of Fig. 3.2, $N^{(5)}_{\zeta,f}$, can be computed using the commutator form of the in-in formalism:

$$
\begin{aligned}
N^{(5)}_{\zeta,f}(\mathbf{k}_1, \mathbf{q}_1 - \mathbf{k}_1, \mathbf{k}_2, \mathbf{q}_2 - \mathbf{k}_2, \mathbf{q}_3) = &- \left(\frac{H^2}{\dot\phi_0}\right)^2 \left(\frac{V'''}{H}\right)^3 \frac{8}{k_1^6 k_2^6 q_1^3 q_2^3 q_3^3} (q_1 q_2)^{\alpha_-} \\
&\int_{-\infty}^{0} \frac{d\tau}{\tau^4} \int_{-\infty}^{\tau} \frac{d\tau'}{\tau'^4} \int_{-\infty}^{\tau'} \frac{d\tau''}{\tau''^4} \\
&\times \Big(\mathrm{Im}\left\{A(k_1\tau)^2\right\} \mathrm{Im}\left\{A(k_2\tau')^2\right\} \mathrm{Im}\left\{A(q_3\tau'')B(q_1\tau'')B(q_2\tau'')\right\} (-\tau)^{\alpha_-}(-\tau')^{\alpha_-} \\
&+ \mathrm{Im}\left\{A(k_1\tau)^2\right\} \mathrm{Im}\left\{A(q_3\tau')B(q_1\tau')\right\} \mathrm{Im}\left\{A(k_2\tau'')^2 B^*(q_2\tau')\right\} (-\tau)^{\alpha_-}(-\tau'')^{\alpha_-} \\
&+ \mathrm{Im}\left\{A(q_3\tau)\right\} \mathrm{Im}\left\{A(k_1\tau')^2 B^*(q_1\tau)\right\} \mathrm{Im}\left\{A(k_2\tau'')^2 B^*(q_2\tau)\right\} (-\tau')^{\alpha_-}(-\tau'')^{\alpha_-} \\
&+ 1 \longleftrightarrow 2 \Big).
\end{aligned}
\tag{3.105}
$$

where $N^{(5)}_{\zeta}$ is defined in an analogous way to $N^{(4)}_{\zeta}$, and

$$
A(x) \equiv \sum_i \pi^{(i)}(0) s^{(i)*}(x) \qquad B(x) \equiv \sum_i b_-^{(i)} s^{(i)*}(x). \tag{3.106}
$$

We also compute the contribution due to the diagram in panel g of Fig. 3.2, $N^{(5)}_{\zeta,g}$:

$$
\begin{aligned}
N^{(5)}_{\zeta,g}(\mathbf{k}_1, \mathbf{q}_1 - \mathbf{k}_1, \mathbf{k}_2, \mathbf{q}_2 - \mathbf{k}_2, \mathbf{q}_3) = &- \left(\frac{H^2}{\dot\phi_0}\right)^2 \left(\frac{V'''}{H}\right)^3 \frac{16 \sum_{i,j} a_0^{(i)} b_-^{(i)*} |b_-^{(j)}|^2}{k_1^9 k_2^6 q_2^3 q_3^3} (q_1 q_2^2)^{\alpha_-} \\
&\int_{-\infty}^{0} \frac{d\tau}{\tau^4} \int_{-\infty}^{0} \frac{d\tau'}{\tau'^4} \int_{-\infty}^{\tau'} \frac{d\tau''}{\tau''^4} (-\tau\tau'\tau'')^{\alpha_-} \\
&\Bigg(\mathrm{Im}\left\{(A(k_1\tau)^2\right\} \mathrm{Im}\left\{(A(k_2\tau')\right\} \mathrm{Im}\left\{ (A(k_1\tau'') \sum_i s^{(i)}(k_1\tau') s^{(i)*}(k_1\tau'') \right\} \\
&\qquad + 1 \longleftrightarrow 2 \Bigg).
\end{aligned}
\tag{3.107}
$$

Two diagrams also contribute to the six-point function. These diagrams are shown in panels h and i of Fig. 3.2. For panel h, we find

$$
\begin{aligned}
N^{(6)}_{\zeta,h}(\mathbf{k}_1, \mathbf{q}_1 - \mathbf{k}_1, \mathbf{k}_2, \mathbf{q}_2 - \mathbf{k}_2, \mathbf{k}_3, \mathbf{q}_3 - \mathbf{k}_3) = &\left(\frac{H^2}{\dot\phi_0}\right)^6 \left(\frac{V'''}{H}\right)^4 \frac{64 (|b_-^{(i)}|^2)^2 q^3 (q_1^2 q_2^2)^{\alpha_-}}{k_1^6 k_2^6 k_3^6 q_1^3 q_2^3 q_3^3} \\
&\int_{-\infty}^{0} \frac{d\tau}{\tau^4} \int_{-\infty}^{0} \frac{d\tau'}{\tau'^4} \int_{-\infty}^{0} \frac{d\tau''}{\tau''^4} \int_{-\infty}^{\tau''} \frac{d\tau'''}{\tau'''^4} (\tau\tau'\tau''\tau''')^{\alpha_-} \\
&\Big(\mathrm{Im}\left\{A(k_1\tau)^2\right\} \mathrm{Im}\left\{A(k_2\tau')^2\right\} \mathrm{Im}\left\{A(k_3\tau'')\right\} \mathrm{Im}\left\{A(k_3\tau''')s^{(i)}(k_3\tau'')s^{(i)*}(k_3\tau''')\right\} \\
&+ \text{ cyc. perm}(1,2,3) \Big).
\end{aligned}
\tag{3.108}
$$

For panel i, on the other hand,

$$N^{(6)}_{\zeta i}(\mathbf{k}_1, \mathbf{q}_1 - \mathbf{k}_1, \mathbf{k}_2, \mathbf{q}_2 - \mathbf{k}_2, \mathbf{k}_3, \mathbf{q}_3 - \mathbf{k}_3) = \left(\frac{H^2}{\dot\phi_0}\right)^6 \left(\frac{V'''}{H}\right)^4 \frac{16 q^3 (q_1 q_2 q_3)^{\alpha_-}}{k_1^6 k_2^6 k_3^6 q_1^3 q_2^3 q_3^3}$$
$$\int_{-\infty}^{0} \frac{d\tau}{\tau^4} \int_{-\infty}^{\tau} \frac{d\tau'}{\tau'^4} \int_{-\infty}^{\tau'} \frac{d\tau''}{\tau''^4} \int_{-\infty}^{\tau''} \frac{d\tau'''}{\tau'''^4}$$
$$\Big(\mathrm{Im}\left\{A(k_1\tau)^2\right\} \mathrm{Im}\left\{A(k_2\tau')^2\right\} \mathrm{Im}\left\{A(k_3\tau'')^2\right\} \mathrm{Im}\left\{B(q_1\tau''')B(q_2\tau''')B(q_3\tau''')\right\} (-\tau\tau'\tau'')^{\alpha_-}$$
$$+ \mathrm{Im}\left\{A(k_1\tau)^2\right\} \mathrm{Im}\left\{A(k_2\tau')^2\right\} \mathrm{Im}\left\{B(q_1\tau'')B(q_2\tau'')\right\} \mathrm{Im}\left\{A(k_3\tau''')^2 B^*(q_3\tau'')\right\} (-\tau\tau'\tau''')^{\alpha_-}$$
$$+ \mathrm{Im}\left\{A(k_1\tau)^2\right\} \mathrm{Im}\left\{B(q_1\tau'')\right\} \mathrm{Im}\left\{A(k_2\tau'')^2 B^*(q_2\tau')\right\} \mathrm{Im}\left\{A(k_3\tau''')^2 B^*(q_3\tau')\right\} (-\tau\tau'\tau''')^{\alpha_-}$$
$$+ \text{all perm}(1,2,3)\Big). \tag{3.109}$$

As with the four-point function of ζ, our task of evaluating these integrals is simplified by the fact that these integrals are IR dominated. We keep terms leading in α_- and q/k. As mentioned in section 3.3, we take $(k_i/k_j)^{\alpha_-} \simeq 1$ and $(q_i/q_j)^{\alpha_-} \simeq 1$, but not $(q_i/k_j)^{\alpha_-}$. With this assumption, we can integrate the above expressions in a way similar to our integration of the four-point function's nested integrals.

Chapter 4

STOCHASTIC BIAS FROM LOOPS OF MASSIVE PARTICLES DURING INFLATION

Primordial non-Gaussianities enhanced at small wavevectors can induce a power spectrum of the galaxy overdensity that differs greatly from that of the matter overdensity at large length scales. In previous work, it was shown that “squeezed" three-point and “collapsed" four-point functions of the curvature perturbation ζ can generate these non-Gaussianities and give rise to so-called scale-dependent and stochastic bias in the galaxy overdensity power spectrum. We explore a third way to generate non-Gaussianities enhanced at small wavevectors: the infrared behavior of quantum loop contributions to the four-point correlations of ζ. We show that these loop effects can give the largest contributions to the four-point function of ζ in the collapsed limit and be observable in the context of quasi-single field inflation.

4.1 Introduction

The inflationary paradigm [2, 4–7] proposes an era in the very early universe during which the energy density is dominated by vacuum energy and the universe undergoes exponential expansion. Such a period elegantly explains why the universe is close to flat and the near isotropy of the cosmic microwave background (CMB). It also provides a simple quantum mechanical mechanism for generating energy density perturbations which have an almost scale-invariant Harrison-Zel’dovich power spectrum.

The simplest inflation models consist of a single scalar field ϕ, called the inflaton, whose time-dependent vacuum expectation value drives the expansion of the universe. The quantum fluctuations in the Goldstone mode π associated with the breaking of time translation invariance by the inflaton [27] source the energy density fluctuations. In the simplest of these single field models, the density perturbations are very nearly Gaussian [28]. One way to generate measurable non-Gaussianities is to introduce a second field s that interacts with the inflaton field during the inflationary era. A simple realization of such a model is quasi-single field inflation (QSFI) [15].

These non-Gaussianities affect the correlation functions of biased tracers of the un-

derlying matter distribution such as galaxies. It was first pointed out in [30] and [49] that the power spectrum of the galaxy overdensity can become greatly enhanced relative to the Harrison-Zel'dovich spectrum on large scales if the primordial mass density perturbations are non-Gaussian.[1] These enhancements are known as scale-dependent bias and stochastic bias and were systematically explored in the context of QSFI in [50] and chapter 3.[2]

The enhancements studied in [30] and [49] result from tree-level contributions to the three- and four-point functions of π that are in their "squeezed" and "collapsed" limits. In this paper, we consider quantum loop contributions to the correlation functions of π which (in the same kinematic limits) can also give rise to these long-distance effects. These loops arise from virtual excitations of massive scalar fields that existed during inflation.[3] We find that the infrared region of loop integrals can induce sizable stochastic bias on large scales without introducing any scale-dependent bias. In section 4.2 we illustrate this loop effect using a higher dimension operator that would appear in a generic effective theory of multi-field inflation. In section 4.3 we show that the loop effect can be observable in the context of QSFI and estimate the distance scale at which the loop contribution to the galaxy power spectrum could exceed the usual Harrison-Zel'dovich one.

4.2 Loop-Induced Stochastic Bias

Consider a theory of inflation that consists of two fields, the inflaton ϕ and a massive scalar s. Working in the gauge where $\phi(x) = \phi_0(t)$, the Lagrangian describing the Goldstone mode π due to the breaking of time translational invariance and s can be written as

$$\mathcal{L} = \frac{1}{2}g^{\mu\nu}\partial_\mu\pi\partial_\nu\pi + \frac{1}{2}g^{\mu\nu}\partial_\mu s\partial_\nu s - \frac{m^2}{2}s^2 + \frac{1}{\Lambda^2}g^{\mu\nu}\partial_\mu\pi\partial_\nu\pi s^2 + \ldots, \tag{4.1}$$

where the action is $S = \int d^4x\sqrt{-g}\mathcal{L}$. The dimension six operator in (4.1) induces the one-loop contribution to the four-point function of π depicted in Fig. 4.1. The complete theory includes additional interactions denoted by the ellipsis above [68, 69][4], which will give rise to other one-loop contributions that are comparable to

[1] We refer to these effects as "enhancements" even though for certain model parameters they can interfere destructively with the usual Gaussian primordial density fluctuations.

[2] By stochastic bias, we mean the difference between the collapsed trispectrum and the squeezed bispectrum squared; see for example Eq. (2.7) of [50]. This stochastic bias can depend on the scale.

[3] These quantum loop contributions are distinct from loop contributions coming from, for example, higher-order terms in a bias expansion (see [67]).

[4] For example, the interaction $2\dot{\phi}_0\partial_\tau\pi s^2/\Lambda^2$ will also appear.

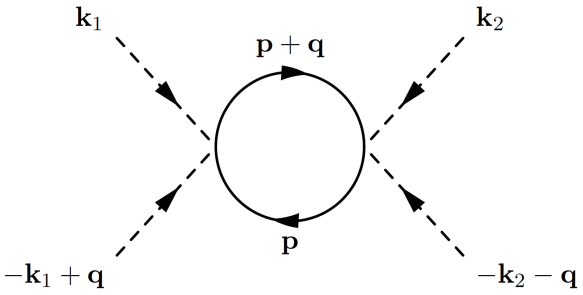

Figure 4.1: One-loop contribution to the collapsed trispectrum of the primordial curvature perturbation. Dashed lines represent π, and solid lines represent s.

or may even dominate this diagram. The goal of this section is to illustrate the infrared behavior of loop contributions to the correlation functions of π, which have interesting implications for the correlation functions of galaxies. For simplicity, we only consider the interaction given in (4.1) and leave a more complete study to future work.

We focus on the "collapsed" limit of the diagram, which occurs when the external wavevectors come in pairs that are nearly equal and opposite, as shown in Fig. 4.1 with $q \ll k_i$. This contribution to the four-point function has previously been computed in [35], where the role of conformal symmetry was emphasized. In this section, we review this calculation and describe its effect on the power spectrum of galaxy overdensities.

To begin, we express the quantum fields π and s in terms of creation and annihilation operators

$$\pi(\mathbf{x},\tau) = \int \frac{d^3k}{(2\pi)^3} a(\mathbf{k})\pi_k(\eta)e^{i\mathbf{k}\cdot\mathbf{x}} + \text{h.}c.\,, \quad s(\mathbf{x},\tau) = \int \frac{d^3k}{(2\pi)^3} b(\mathbf{k})s_k(\eta)e^{i\mathbf{k}\cdot\mathbf{x}} + \text{h.}c.\,, \tag{4.2}$$

where $k = |\mathbf{k}|$, and $\eta = k\tau$ for conformal time $\tau < 0$. The mode functions satisfy the equations of motion of the free theory with appropriate boundary conditions and are

$$\pi_k(\eta) = \frac{H}{k^{3/2}}\pi(\eta), \qquad \pi(\eta) = \frac{1}{\sqrt{2}}(1+i\eta)e^{-i\eta}, \tag{4.3}$$

$$s_k(\eta) = \frac{H}{k^{3/2}}s(\eta), \qquad s(\eta) = -ie^{i(2-\nu)\frac{\pi}{2}}\frac{\sqrt{\pi}}{2}(-\eta)^{3/2}H^{(1)}_{\frac{3}{2}-\nu}(-\eta), \tag{4.4}$$

where $\nu = 3/2 - \sqrt{9/4 - m^2/H^2}$ and $H^{(1)}_z$ is the Hankel function of the first kind. We assume that the mass m of the field s is much less than the Hubble constant

H during inflation, or equivalently $\nu \ll 1$.[5] We are interested in this region of parameter space because it leads to the largest infrared enhanced contributions to the four-point function.

Let us now compute the contribution in Fig. 4.1 to the collapsed trispectrum of the primordial curvature perturbation $\zeta = -(H/\dot{\phi}_0)\pi$. The primordial curvature trispectrum T_ζ is defined by

$$\langle \zeta_{\mathbf{k}_1} \zeta_{\mathbf{k}_2} \zeta_{\mathbf{k}_3} \zeta_{\mathbf{k}_4} \rangle_c = T_\zeta(\mathbf{k}_1, \mathbf{k}_2, \mathbf{k}_3, \mathbf{k}_4)(2\pi)^3 \delta^3(\mathbf{k}_1 + \mathbf{k}_2 + \mathbf{k}_3 + \mathbf{k}_4) \tag{4.5}$$

where the subscript c denotes the connected part of the four-point function. In Fig. 4.1 $\mathbf{k}_3 = -\mathbf{k}_1 + \mathbf{q}$ and $\mathbf{k}_4 = -\mathbf{k}_2 - \mathbf{q}$. The collapsed configuration T_ζ^{coll} occurs when $q \ll k_i$.

Using the in-in formalism [47] and introducing the variables $\eta = k_1\tau$ and $\eta' = k_2\tau'$ we find

$$\begin{aligned} T_\zeta^{coll} &= 32 \left(\frac{H}{\Lambda}\right)^4 \left(\frac{H^2}{\dot{\phi}_0}\right)^4 \frac{1}{k_1^3 k_2^3} \int \frac{d^3p}{(2\pi)^3} \frac{1}{|\mathbf{p}+\mathbf{q}|^3 p^3} \int_{-\infty}^{0} \frac{d\eta}{\eta^2} \int_{-\infty}^{\frac{k_1}{k_2}\eta} \frac{d\eta'}{\eta'^2} e^{\epsilon(\eta+\eta')} \mathrm{Im}\left[F(\eta)\right] \\ &\times \mathrm{Im}\left[F(\eta') s\left(\frac{|\mathbf{p}+\mathbf{q}|}{k_1}\eta\right) s^*\left(\frac{|\mathbf{p}+\mathbf{q}|}{k_2}\eta'\right) s\left(\frac{p}{k_1}\eta\right) s^*\left(\frac{p}{k_2}\eta'\right)\right] + \left(k_1 \leftrightarrow k_2\right) \end{aligned} \tag{4.6}$$

where

$$F(\eta) = \pi(0)^2 \left([\partial_\eta \pi^*(\eta)]^2 - [\pi^*(\eta)]^2 \right) . \tag{4.7}$$

In Eq. (4.6), ϵ is an infinitesimal positive quantity that regulates the time integrations in the distant past and we have expanded in $q \ll k_i$.

The dominant contribution of the loop integral in (4.6) comes from $p \sim q$. Moreover, the time integrals are dominated at late times $\eta, \eta' \sim -1$. We can thus use the small η expansion of the s mode function

$$s(\eta) \overset{\eta\to 0}{\simeq} b_1(-\eta)^\nu, \qquad |b_1|^2 = 2^{1-2\nu}\Gamma(3/2-\nu)^2/\pi \overset{\nu\to 0}{\simeq} 1/2 \tag{4.8}$$

to find

$$T_\zeta^{coll} \simeq 8 \left(\frac{H}{\Lambda}\right)^4 \left(\frac{H^2}{\dot{\phi}_0}\right)^4 \frac{1}{(k_1 k_2)^{3+2\nu}} I_{2\nu}(q) J^2 \tag{4.9}$$

[5] In (4.1), the mass m includes contributions from terms such as $(\dot{\phi}_0^2/\Lambda^2)s^2$. Tuning is required for $m \ll H$.

where

$$I_{2\nu}(q) = \int \frac{d^3p}{(2\pi)^3} \frac{1}{|\mathbf{p}+\mathbf{q}|^{3-2\nu} p^{3-2\nu}} \overset{\nu\to 0}{\simeq} \frac{1}{2\pi^2}\frac{1}{\nu} q^{-3+4\nu}, \tag{4.10}$$

$$J = \int_{-\infty}^{0} \frac{d\eta}{\eta^2} e^{\epsilon\eta}(-\eta)^{2\nu} \mathrm{Im}\left[F(\eta)\right] = 2^{-2-2\nu}\frac{\Gamma(2+2\nu)}{1-2\nu} \overset{\nu\to 0}{\simeq} \frac{1}{4}. \tag{4.11}$$

In (4.10) we have kept only the term singular in ν as it goes to zero. Note that our result is finite because we focused on the relevant region $p \sim q \ll k_i$ and neglected the region of large loop momenta which is not as important in the limit $q \to 0$. The UV divergence due to the region of large loop momentum would be rendered finite by a counterterm.

Our final result for the four-point function of the curvature perturbation for $m \ll H$ and $q \ll k_i$ is

$$T_\zeta^{coll} \simeq \frac{1}{4\pi^2}\frac{1}{\nu}\left(\frac{H}{\Lambda}\right)^4 \left(\frac{H^2}{\dot\phi_0}\right)^4 \frac{1}{k_1^3 k_2^3 q^3}\left(\frac{q^2}{k_1 k_2}\right)^{2\nu}. \tag{4.12}$$

The factors of wavevector magnitudes in (4.12) essentially follow from the form of $s(\eta)$ expanded for small η in the limit $m \ll H$, and from dimensional analysis. For $m \ll H$ the four-point function is enhanced by $1/\nu \simeq 3H^2/m^2$. This arises because for small m/H the the mode function $s(\eta)$ falls off slowly as the mode k redshifts outside the de-Sitter horizon. Note also that there is no IR divergence in the loop integration since the s field is massive. Three- and four-point curvature fluctuations generated by loop effects have been considered in Refs. [70–73] using the δN formalism. It would be interesting to see if this method can reproduce (4.12).

For small q the dependence of T_ζ on q in eq. (4.12) is almost the same as would result from a tree graph that contributes to it, say from iterating twice the interaction vertex that arises from $\mathcal{L}_{int} = g^{\mu\nu}\partial_\mu\pi\partial_\nu\pi s/\Lambda'$ in the Lagrange density. That is because for small m, the s propagator in de-Sitter space goes roughly as $1/q^3$. This is very different from flat space. To illustrate this, consider the flat space equal time expectation value $\langle \pi_{\mathbf{k}_1}\pi_{\mathbf{k}_2}\pi_{\mathbf{k}_3}\pi_{\mathbf{k}_4}\rangle$ in the kinematic limit,[6] $k_j \gg q \gg m$. At small q, the loop contribution is q-independent while the tree diagram goes as $1/q$.

We now qualitatively discuss the effects of (4.12) on the galaxy power spectrum. To begin, the matter overdensity δ_R averaged over a spherical volume of radius R is

[6] Because of time translation invariance in flat space this expectation value is independent of the time the fields π are evaluated at.

related to the primordial curvature fluctuation via

$$\delta_R(\mathbf{k}) = \frac{2k^2}{5\Omega_m H_0^2} T(k) W_R(k) \zeta_{\mathbf{k}} \tag{4.13}$$

where $W_R(k)$ is the window function, $T(k)$ is the transfer function, Ω_m is the ratio of the matter density to the critical density today, and H_0 is the Hubble constant evaluated today.

We consider an expansion for the galaxy overdensity δ_h in terms of δ_R of the following form

$$\delta_h(\mathbf{x}) = b_1 \delta_R(\mathbf{x}) + b_2(\delta_R^2(\mathbf{x}) - \sigma_R^2) + b_3(\delta_R^3(\mathbf{x}) - 3\delta_R(\mathbf{x})\sigma_R^2) + \dots, \tag{4.14}$$

where $\sigma_R^2 = \langle \delta_R(\mathbf{x}) \delta_R(\mathbf{x}) \rangle$ and the constants b_1, b_2, and b_3 are bias coefficients (for a more complete treatment, see [58]). The bias coefficients can be determined from data or computed using a specific model of galaxy halo formation that expresses the galaxy overdensity in terms of δ_R. The two-point function of the galaxy overdensity is then:

$$\begin{aligned} \langle \delta_h(\mathbf{x}) \delta_h(\mathbf{y}) \rangle = b_1^2 \langle \delta_R(\mathbf{x}) \delta_R(\mathbf{y}) \rangle + b_1 b_2 \big(\big\langle (\delta_R^2(\mathbf{x}) - \sigma_R^2) \delta_R(\mathbf{y}) \big\rangle + \big\langle \delta_R(\mathbf{x}) (\delta_R^2(\mathbf{y}) - \sigma_R^2) \big\rangle \big) \\ + b_2^2 \big\langle (\delta_R^2(\mathbf{x}) - \sigma_R^2)(\delta_R^2(\mathbf{y}) - \sigma_R^2) \big\rangle + \dots \end{aligned} \tag{4.15}$$

A similar expression could be derived for the galaxy-matter cross-correlation $\langle \delta_h(\mathbf{x}) \delta_R(\mathbf{y}) \rangle$.

Ignoring other contributions to the non-Gaussianities of ζ besides the one given in (4.12), the term proportional to b_2^2 in (4.15) yields a contribution to the galaxy power spectrum of the form $P_{hh}(q) \sim 1/q^{3-4\nu}$, but not to the galaxy-matter cross-correlation $P_{hm}(q)$. Hence this loop contributes to stochastic bias, but not to scale-dependent bias. Note that in the absence of primordial non-Gaussianity, $P_{hh}(q) \sim q$, so the trispectrum contribution is enhanced by a relative factor of $q^{-4+4\nu}$ and dominates as $q \to 0$.

It is worth emphasizing that we have only considered one particular interaction in this theory, and have ignored other interactions which may give even more important contributions to stochastic and scale-dependent bias. We now turn to a model within QSFI in order to make a full prediction in a consistent theory.

4.3 Loop-Induced Stochastic Bias in Quasi-Single Field Inflation

In this section, we show that loop-induced non-Gaussianities in QSFI [15] can give rise to stochastic bias that is potentially observable given the stringent constraints

from CMB data on non-Gaussianities. The model we consider consists of an inflaton ϕ and a massive scalar s with the symmetries $\phi \to \phi + c$, $\phi \to -\phi$, and $s \to -s$. These symmetries are broken by the potential of ϕ as well as by the lowest dimension operator that couples ϕ and s, $g^{\mu\nu}\partial_\mu\phi\partial_\nu\phi s/\Lambda$. The Lagrangian written in terms of the Goldstone mode π is

$$\mathcal{L} = \frac{1}{2}g^{\mu\nu}\partial_\mu\pi\partial_\nu\pi\left(1+\frac{2}{\Lambda}s\right) + \frac{1}{2}g^{\mu\nu}\partial_\mu s\partial_\nu s - \mu H\tau s\partial_\tau\pi - \frac{m^2}{2}s^2 - \frac{V^{(4)}}{4!}s^4 \quad (4.16)$$

where the kinetic mixing term is parameterized by the coupling $\mu = 2\dot{\phi}_0/\Lambda$ and we have ignored higher order terms in the potential for s. Similar to the previous section, we focus here on the region where $m \ll H$ and $\mu \ll H$, which gives the most significant long wavelength enhancement to the galaxy power spectrum.

Due to the kinetic mixing, π and s share a set of creation and annihilation operators:

$$\pi(\mathbf{x},\tau) = \int \frac{d^3k}{(2\pi)^3}\left(a^{(1)}(\mathbf{k})\pi_k^{(1)}(\eta)e^{i\mathbf{k}\cdot\mathbf{x}} + a^{(2)}(\mathbf{k})\pi_k^{(2)}(\eta)e^{i\mathbf{k}\cdot\mathbf{x}} + \text{h.}c.\right) \quad (4.17)$$

$$s(\mathbf{x},\tau) = \int \frac{d^3k}{(2\pi)^3}\left(a^{(1)}(\mathbf{k})s_k^{(1)}(\eta)e^{i\mathbf{k}\cdot\mathbf{x}} + a^{(2)}(\mathbf{k})s_k^{(2)}(\eta)e^{i\mathbf{k}\cdot\mathbf{x}} + \text{h.}c.\right). \quad (4.18)$$

The mode functions $\pi_k^{(i)} = (H/k^{3/2})\pi^{(i)}$ and $s_k^{(i)} = (H/k^{3/2})s^{(i)}$ are difficult to solve for exactly. However, analytic progress can be made by considering series solutions. It can easily be checked that the most general series solutions to the mode equations derived from (4.16) are

$$\pi^{(i)}(\eta) = \sum_{n=0}^{\infty}\left[a_{0,2n}^{(i)}(-\eta)^{2n} + a_{-,2n}^{(i)}(-\eta)^{2n+\alpha_-} + a_{+,2n}^{(i)}(-\eta)^{2n+\alpha_+} + a_{3,2n}^{(i)}(-\eta)^{2n+3}\right] \quad (4.19)$$

$$s^{(i)}(\eta) = \sum_{n=0}^{\infty}\left[b_{0,2n}^{(i)}(-\eta)^{2n} + b_{-,2n}^{(i)}(-\eta)^{2n+\alpha_-} + b_{+,2n}^{(i)}(-\eta)^{2n+\alpha_+} + b_{3,2n}^{(i)}(-\eta)^{2n+3}\right] \quad (4.20)$$

where $\alpha_\pm = 3/2 \pm \sqrt{9/4 - \mu^2/H^2 - m^2/H^2}$ and $b_{0,0}^{(i)} = 0$. For ease of notation we denote $a_{r,0}^{(i)}$ and $b_{r,0}^{(i)}$ as $a_r^{(i)}$ and $b_r^{(i)}$. In chapter 3, it was shown that the non-Gaussianities can be well approximated by a finite set of combinations of the power series coefficients when $\mu, m \ll H$. The combinations of power series coefficients needed to compute the loop in Fig. 4.2 are

$$\text{Re}\left[a_0^{(i)}b_-^{*(i)}\right] \simeq \frac{-3\mu H}{2(\mu^2+m^2)}, \quad \text{Im}\left[a_0^{(i)}b_3^{*(i)}\right] = \frac{\mu H}{2(\mu^2+m^2)}, \quad \left|b_-^{(i)}\right|^2 \simeq \frac{1}{2}, \quad (4.21)$$

$$\text{Im}\left[a_0^{(i)}b_-^{*(i)}\right] = \text{Im}\left[a_0^{(i)}b_{0,2}^{*(i)}\right] = \text{Im}\left[a_0^{(i)}b_{-,2}^{*(i)}\right] = \text{Im}\left[a_0^{(i)}b_+^{*(i)}\right] = 0, \quad (4.22)$$

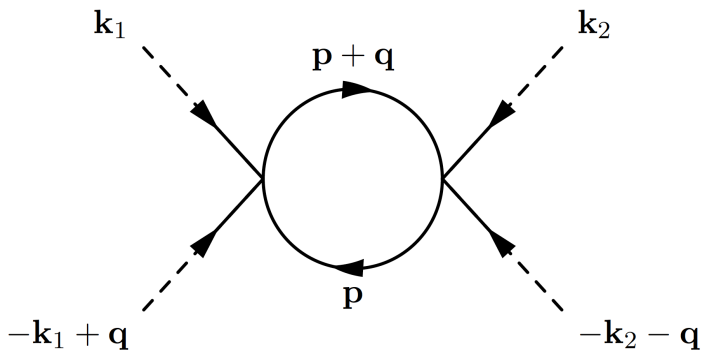

Figure 4.2: One-loop contribution to the collapsed trispectrum of the primordial curvature perturbation in QSFI. Dashed lines represent π, and solid lines represent s.

which were determined in chapter 3. The repeated superscripts (i) are summed over $i = 1, 2$. The above expressions are valid for $\mu/H, m/H \ll 1$.

We can now compute the loop contribution to the collapsed limit of the curvature perturbation trispectrum shown in Fig. 4.2. Again, using the in-in formalism and the variables $\eta = k_1\tau$ and $\eta' = k_2\tau'$, we find

$$T_\zeta^{coll} = 2V^{(4)2}\left(\frac{H^2}{\dot\phi_0}\right)^4 \frac{1}{k_1^3k_2^3}\int\frac{d^3p}{(2\pi)^3}\frac{1}{|\mathbf{p}+\mathbf{q}|^3p^3}\int_{-\infty}^0\frac{d\eta}{\eta^4}\int_{-\infty}^{\frac{k_1}{k_2}\eta}\frac{d\eta'}{\eta'^4}\mathrm{Im}\left[(\pi^{(i)}(0)s^{*(i)}(\eta))^2\right]$$
$$\times\,\mathrm{Im}\left[[\pi^{(j)}(0)s^{*(j)}(\eta')]^2 s^{(k)}\left(\frac{|\mathbf{p}+\mathbf{q}|}{k_1}\eta\right)s^{*(k)}\left(\frac{|\mathbf{p}+\mathbf{q}|}{k_2}\eta'\right)s^{(l)}\left(\frac{p}{k_1}\eta\right)s^{*(l)}\left(\frac{p}{k_2}\eta'\right)\right]$$
$$+\left(k_1\leftrightarrow k_2\right). \tag{4.23}$$

Similar to before, the dominant contribution to the loop integral occurs for loop momenta $p \sim q \ll k_i$ and the time integrals are dominated by late times. We can immediately expand the s mode functions to find

$$T_\zeta^{coll} \simeq \frac{1}{2}V^{(4)2}\left(\frac{H^2}{\dot\phi_0}\right)^4\frac{1}{(k_1k_2)^{3+2\alpha_-}}I_{2\alpha_-}(q)K(\mu,m)^2, \tag{4.24}$$

where $I_\nu(q)$ is given in (4.10) and

$$K(\mu,m) = \int_{-\infty}^0 d\eta(-\eta)^{-4+2\alpha_-}\mathrm{Im}\left[(\pi^{(i_1)}(0)s^{*(i_1)}(\eta))^2\right]. \tag{4.25}$$

It was shown in chapter 3 that the most important contribution to (4.25) is obtained by cutting off the lower bound of the integral at η_0 which is around horizon crossing.

Inserting the power series expansions of the mode functions in (4.19) and (4.20), we find

$$K(\mu, m) \simeq 2\,\mathrm{Im}\left[a_0^{(i)} b_3^{*(i)}\right] \mathrm{Re}\left[a_0^{(j)} b_-^{*(j)}\right] \int_{\eta_0}^{0} d\eta (-\eta)^{-1+3\alpha_-} \simeq -\frac{2}{3}\frac{(3\mu/2)^2 H^4}{(\mu^2+m^2)^3}, \tag{4.26}$$

where we have neglected contributions from higher powers of η which are suppressed in the limit $\alpha_- \ll 1$. Note that this piece most singular in α_- is insensitive to the choice of η_0. Our final result for the four-point function of the curvature perturbation for $m, \mu \ll H$ and $q \ll k_i$ is then

$$T_\zeta^{coll} \simeq \frac{1}{3\pi^2} V^{(4)2} \left(\frac{H^2}{\dot\phi_0}\right)^4 \frac{1}{k_1^3 k_2^3 q^3} \left(\frac{q^2}{k_1 k_2}\right)^{2\alpha_-} \frac{(3\mu/2)^4 H^{10}}{(\mu^2+m^2)^7}\,. \tag{4.27}$$

In (4.27), the factors of wavevector magnitudes and α_-^{-1} from the integral $I_{2\alpha_-}$ are the same as those in (4.12) from the integral $I_{2\nu}$. These features are characteristic of quantum mechanical effects from the exchange of a massive particle [35, 74]. In principle higher loop contributions have q scaling similar to (4.27), but are suppressed because they also have additional factors of the small coupling constant $V^{(4)}$.

We now consider the long wavelength enhancement to the galaxy power spectrum resulting from this collapsed primordial trispectrum. In our numerical evaluation, we make the simplifying assumption that galaxies form at points in space at which the smoothed matter overdensity is greater than a threshold density at the time of collapse $\delta_c(a_{coll})$, *i.e.* $n_h(\mathbf{x}) \propto \Theta_H\left(\delta_R(\mathbf{x}, a_{coll}) - \delta_c(a_{coll})\right) = \Theta_H\left(\delta_R(\mathbf{x}) - \delta_c\right)$, where $\delta_c \equiv \delta_c(a_{coll})/D(a_{coll})$.[7] We further assume that $\delta_c(a_{coll}) = 1.686$ [75], all halos collapse instantaneously at redshift $z = 1.5$, and their number density does not evolve in time after collapse. This corresponds to a value of $\delta_c = 4.215$. The galaxy overdensity is defined by $\delta_h(\mathbf{x}) = (n_h(\mathbf{x}) - \langle n_h\rangle)/\langle n_h\rangle$. With this threshold collapse model, the bias coefficients are given by (see e.g. [76])

$$b_1 = \frac{e^{-\frac{\delta_c^2}{2\sigma_R^2}}}{\sqrt{2\pi}\sigma_R\langle n_h\rangle}, \quad b_2 = \frac{\delta_c}{\sigma_R}\frac{e^{-\frac{\delta_c^2}{2\sigma_R^2}}}{2!\sqrt{2\pi}\sigma_R^2\langle n_h\rangle}, \quad b_3 = \left(\frac{\delta_c^2}{\sigma_R^2} - 1\right)\frac{e^{-\frac{\delta_c^2}{2\sigma_R^2}}}{3!\sqrt{2\pi}\sigma_R^3\langle n_h\rangle} \tag{4.28}$$

where $\langle n_h\rangle = erfc\left(\delta_c/(\sqrt{2}\sigma_R)\right)/2$. We use the BBKS approximation to the transfer function [59] and the top-hat window function $W_R(k) = 3(\sin(kR) -$

[7] $\delta_R(\mathbf{x})$ is the linearly evolved matter overdensity today.

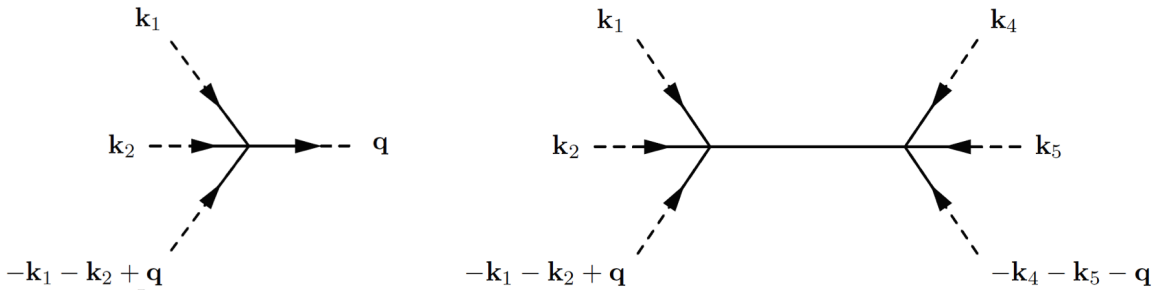

Figure 4.3: These two tree-level diagrams involving the $V^{(4)}$ interaction can also contribute to scale-dependent and stochastic bias. However, these contributions are small compared to the loop contribution in Fig. (4.2) due a suppression arising from the integration over additional hard external wavevectors.

$kR\cos(kR))/(kR)^3$. Moreover, we take $R = 1.9\ \mathrm{M}pc/h$ as the smoothing scale, and numerically we find $\sigma_R = 3.62$.

The Fourier transform of $\langle\delta_R(\mathbf{x})\delta_R(\mathbf{y})\rangle$ gives the matter power spectrum $P_{mm}(q)$:

$$P_{mm}(q) = \left(\frac{2}{5\Omega_m H_0^2}\right)^2 \left(\frac{H^2}{\dot\phi_0}\right)^2 C_2(\mu, m) T(q)^2 q\,, \tag{4.29}$$

where $C_2(\mu, m) = 1/2 + 2(3\mu/2)^2 H^2/(\mu^2 + m^2)^2$. It then follows from (4.15) that the ratio of the galaxy power spectrum to the matter power spectrum normalized by b_1^2 is

$$\frac{P_{hh}(q)}{b_1^2 P_{mm}(q)} = 1 + \frac{b_2^2}{b_1^2}\left(\frac{2}{5\Omega_m H_0^2 R^2}\right)^2 \left(\frac{H^2}{\dot\phi_0}\right)^2 \frac{V^{(4)2}\mathcal{J}^2}{3\pi^2} \frac{(qR)^{-4+4\alpha_-}}{T(q)^2} \frac{(3\mu/2)^4 H^{10}}{(\mu^2 + m^2)^7 C_2(\mu, m)} \tag{4.30}$$

where

$$\mathcal{J} = \frac{1}{2\pi^2}\int_0^\infty du\, T\,(u/R)^2\, W_R\,(u/R)^2\, u^3. \tag{4.31}$$

The $V^{(4)}$ interaction in (4.16) also gives rise to the tree-level diagrams shown in Fig. 4.3 which contribute to the long wavelength enhancement of the galaxy power spectrum. However, these terms contain integrals with three transfer functions rather than two like in (4.31). This integral then gives $\sim \mathcal{J}^{3/2}$ rather than $\mathcal{J}$. Numerically we find $\mathcal{J} \approx 3.1 \times 10^{-5}$ so the contributions from these tree-level diagrams are suppressed, as can be seen in Fig. 4.4.

One could also consider the contribution of the $(\partial\pi)^2 s/\Lambda$ interaction in (4.16) to $P_{hh}(q)$. However, estimating $f_{NL} = 5B_\zeta(k,k,k)/18P_\zeta(k)^2$ from this interaction

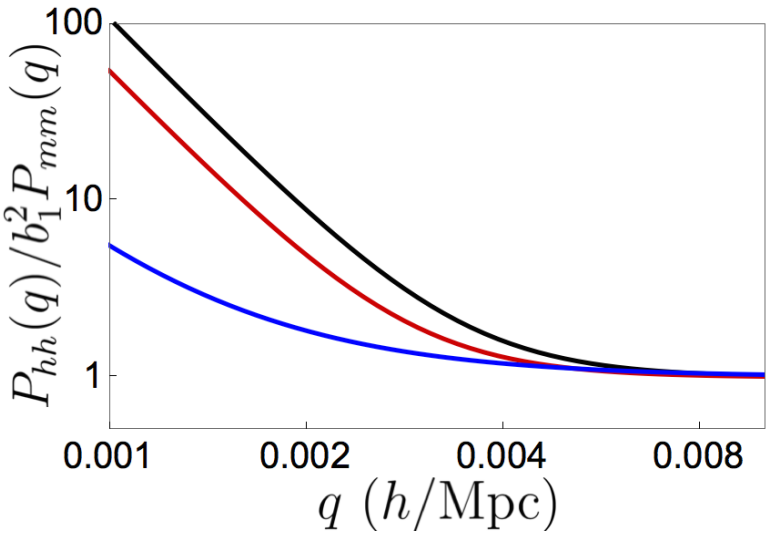

Figure 4.4: The ratio $P_{hh}(q)/b_1^2 P_{mm}(q)$ is plotted for $\tau_{NL}^{2\sigma} = 2800$ (Planck 2013) in black, and $\tau_{NL}^{2\sigma}/2 = 1400$ in red. In blue, we plot the power spectrum ignoring the loop contribution and considering only the tree diagrams in Fig. 4.3, using the $\tau_{NL}^{2\sigma}$ bound. Note that the enhanced behavior begins around $(200\ \mathrm{M}pc/h)^{-1}$ for the black curve, and around $(300\ \mathrm{M}pc/h)^{-1}$ for the red curve. Moreover, note that the tree contributions in blue are very small compared to the loop contribution in black. We plot for $\mu/H = m/H = 0.274$, corresponding to $\alpha_- = 0.05$. Moreover we take $R = 1.9\ \mathrm{M}pc/h$ and $\delta_c = 4.215$.

numerically, we find that $f_{NL} \lesssim 10^{-2}$ for μ/H, $m/H \lesssim 0.4$. This small f_{NL} has a negligible contribution to $P_{hh}(q)$ compared to the loop contribution we have considered.

We can constrain $V^{(4)}$ using the bounds on τ_{NL} and g_{NL} from Planck 2013 and 2015 [44, 77]. The bound due to τ_{NL} is estimated using (4.27), with factors of $(q/k)^{\alpha_-}$ set to 1 in order to match the τ_{NL} shape. The bound due to g_{NL} is estimated using the tree-level four-point diagram with a single $V^{(4)}$ vertex, with factors of $(k_i/k_j)^{\alpha_-}$ set to 1 to match the g_{NL} shape. We take $\tau_{NL}^{2\sigma} = 2.8 \times 10^3$ and $g_{NL}^{2\sigma} = -2.44 \times 10^5$ as the maximum allowed values of τ_{NL} and g_{NL} at a 2σ confidence level. We find that for most of the (μ, m) parameter space $\tau_{NL}^{2\sigma}$ gives the stronger constraints on $V^{(4)}$. For $\mu/H = m/H = 0.274$ (so that $\alpha_- = 0.05$), we find that the $\tau_{NL}^{2\sigma}$ constraint yields $V^{(4)} \leq 0.014$.

In Fig. 4.4, we plot the ratio $P_{hh}(q)/b_1^2 P_{mm}(q)$. The enhanced behavior begins at around $q \sim (200\ \mathrm{M}pc/h)^{-1}$ and $q \sim (300\ \mathrm{M}pc/h)^{-1}$ for the values of $V^{(4)}$ that saturate the $\tau_{NL}^{2\sigma}$ (black curve) and $\tau_{NL}^{2\sigma}/2$ (red curve) bounds. Moreover, the blue curve is the contribution due solely to the tree-level diagrams in Fig. (4.3) using the

$\tau_{NL}^{2\sigma}$ bound, and is significantly smaller than the loop contribution shown in black.

Finally we briefly comment on how our results depend on the parameters R and δ_c. The loop contribution to $P_{hh}(q)/b_1^2 P_{mm}(q)$ is insensitive to the choice of smoothing radius R. The tree-level contributions in Fig. 4.3 increase as R increases, yet even for $R = 2.7\,\mathrm{M}pc/h$, we find that the loop contribution remains an order of magnitude larger than the tree-level contributions. Furthermore, since $b_2/b_1 \sim \delta_c$, the second term in (4.30) goes like $\delta_c^2/q^{4-4\alpha_-}$. This implies that the characteristic scale q_0 at which the long-wavelength enhancements become significant depends on δ_c like $q_0 \sim \delta_c^{1/2}$.

4.4 Concluding Remarks

Using a particular QSFI model, we have shown that one loop contributions to the four-point function of the curvature perturbation ζ in the collapsed limit can be even larger than the tree-level ones. In such cases the dominant contribution to stochastic bias at long wavelengths comes from primordial quantum loops. In this model, the one-loop contribution to the four-point function of primordial curvature perturbations induces a non-Gaussian contribution to the galaxy power spectrum $P_{hh}(q)$ that is five times larger than the Gaussian one at $q \sim h/(500\,\mathrm{M}pc)$ for values of τ_{NL} and g_{NL} at only half their current 2σ bounds. These non-Gaussianities could be observed in upcoming large-scale surveys [78–80].

It would be interesting to study the effects of these loop contributions to the bias within the framework of the effective field theory of inflation. At a minimum, this would require the computation of the one-loop diagram presented in section II and the ones due to the interaction $\mathcal{L}_I \sim \dot{\pi} s^2$.

Chapter 5

NEW SHAPES OF PRIMORDIAL NON-GAUSSIANITY FROM QUASI-SINGLE FIELD INFLATION WITH MULTIPLE ISOCURVATONS

We study a simple extension of quasi-single field inflation in which the inflaton interacts with multiple extra massive scalars known as isocurvatons. Due to the breaking of time translational invariance by the inflaton background, the theory includes kinetic mixings among the inflaton and isocurvatons. These mixings give rise to novel new features in the primordial non-Gaussianities of the scalar curvature perturbation. A noteworthy feature is the amplitude of the squeezed bispectrum can grow nearly as $(k_s/k_l)^{-3}$ while oscillating as $\cos\gamma\log(k_s/k_l)$, where k_s/k_l is the ratio of the lengths of the short and long wavevectors. Observation of such a shape would provide evidence for the existence of multiple isocurvatons during inflation. In addition, we consider the effects of these non-Gaussianities on large-scale structure.

5.1 Introduction

The inflationary paradigm [2, 4–7] posits a period of time shortly after the big bang during which the universe's energy density was dominated by vacuum energy and the size of the universe grew exponentially. Such an era would explain the near isotropy of the CMB and the near flatness of the universe. At the same time, inflation provides a quantum mechanical origin for the energy density perturbations which have an almost scale-invariant Harrison-Zel'dovich power spectrum [9–13] (see [8] for a review).

The simplest inflationary theories are known as single-field inflation models and involve a single scalar field called the "inflaton." In slow-roll models, the inflaton vacuum expectation value ϕ_0 is initially displaced from the minima of the inflaton potential $V_{sr}(\phi)$. The potential is chosen such that there is a period of time (the inflationary era) during which ϕ_0's potential energy dominates over its kinetic energy and drives the exponential expansion of the universe. After more than $50-60$ e-folds of expansion, ϕ_0's kinetic energy becomes large and inflation ends.

Since $\dot{\phi}_0 \neq 0$, time-translational invariance is spontaneously broken. This gives rise to a Goldstone boson π that sources scalar curvature perturbations [27]. In the

simplest single-field models, the curvature perturbations are approximately Gaussian [28]. To produce large primordial non-Gaussianities (PNG), one can add extra fields to the inflationary field content and include interactions between π and the new fields[1]. This leads to interesting new shapes and features of primordial non-Gaussianity that could be observed in the CMB and large-scale structure (LSS) and used to constrain the inflationary theory.

Quasi-single field inflation (QSFI) is a well-studied extension of single-field inflation models [15] that could potentially give rise to significant PNG. In QSFI, one adds a single extra scalar field σ of mass m, known as the isocurvaton, and includes a kinetic mixing between σ and π of the form[2] $\mu\dot{\pi}\sigma$ and a potential for the isocurvaton $V(\sigma)$. In QSFI the isocurvaton never fulfills the roll of the inflaton, rather, its purpose is to generate PNG through its interactions with π.

The connected three- (bispectrum) and four- (trispectrum) point functions of π in QSFI have been studied extensively in chapters 2 and 3 and [15, 31–34, 37]. The squeezed limit of the bispectrum, which occurs when the lengths of two of the three wavevectors are roughly equal and much larger than the length of the third wavevector, has been shown to exhibit particularly interesting behavior. Let k_l denote the length of the larger wavevectors and k_s the length of the shorter one. It has been shown that if m and μ are both much smaller than the Hubble constant during inflation H, then the magnitude of the squeezed bispectrum in QSFI grows approximately as $(k_s/k_l)^{-3}$. In the opposite limit, $m, \mu \gg H$, the magnitude of the squeezed bispectrum was found to oscillate logarithmically in k_s/k_l but grow only as $(k_s/k_l)^{-3/2}$ as seen in chapter 2 and [15].

Since single-isocurvaton QSFI gives rise to distinct PNG, it is worthwhile to study theories that include multiple isocurvatons σ_I (we will call these theories multi-isocurvaton QSFI). It turns out that interactions such as $\rho(\dot{\sigma}_1\sigma_2 - \dot{\sigma}_2\sigma_1)$ and $\mu_1\dot{\pi}\sigma_1$ give rise to novel features in the PNG. Specifically, for certain choices of ρ and μ_1, the squeezed bispectrum undergoes logarithmic oscillations in k_s/k_l and grows approximately as $(k_s/k_l)^{-3}$. This is very different from the behavior of the squeezed bispectrum in single-isocurvaton QSFI, which can only exhibit oscillations or nearly cubic power law growth in different limits of μ and m.

[1] Large non-Gaussianities can also be achieved in more complicated single field models, see for example [29, 81].

[2] Kinetic mixing terms such as $\mu\dot{\pi}\sigma$ can appear in the Lagrangian because the inflaton vev spontaneously breaks Lorentz invariance

Several previously studied inflationary models predict log-oscillating or oscillating shapes for the bispectrum [31, 35, 81–93]. Using shape templates, the Planck collaboration has begun constraining these oscillating/log-oscillating bispectra [14]. However, none of these shapes simultaneously exhibit log-oscillations and nearly cubic power law growth in the squeezed limit. In this chapter, we provide a bispectrum shape template for multi-isocurvaton QSFI that could be searched for experimentally.

Previous work has demonstrated that non-Gaussianities that grow like $(k_s/k_l)^{-3}$ in the squeezed limit can have significant effects on large-scale structure [30, 48–50]. For example, in single-isocurvaton QSFI models with $m, \mu \ll H$, non-Gaussian contributions to the dark matter halo-halo power spectrum $P_{hh}(k_s)$ become much larger than the Gaussian contribution as $k_s \to 0$. The halo-halo power spectrum $P_{hh}(q)$ will also be sensitive to the extra fields and interactions present in multi-isocurvaton QSFI. We will show that for certain choices of the parameters ρ and μ_1, the bispectrum and trispectrum contributions to $P_{hh}(k_s)$ will dominate over the Gaussian contribution while oscillating logarithmically as $k_s \to 0$.

The purpose of this work is to determine the shapes of the bispectrum and trispectrum in multi-isocurvaton QSFI and explore their effects on LSS. In section 5.2 we write down a general quadratic Lagrangian for multi-isocurvaton QSFI and determine the mode functions of the π and σ_I fields. In section 5.3 we compute the primordial bispectrum and trispectrum due to a cubic interaction of the form σ_1^3, and provide a template for the bispectrum shape. Finally, in section 5.4 we calculate the contribution of the PNG to the halo-halo power spectrum $P_{hh}(k_s)$ and halo-matter power spectrum $P_{hm}(k_s)$.

5.2 The Model and Mode Functions

We consider multi-isocurvaton QSFI, which include an inflaton field and N extra scalar fields known as “isocurvatons." The inflaton develops a time-dependent vacuum expectation value ϕ_0 that sources a background de-Sitter metric

$$ds^2 = \frac{1}{(H\tau)^2}\left(d\tau^2 - (dx^i)^2\right) \tag{5.1}$$

where H is the Hubble parameter during inflation and τ is proper time. We assume that ϕ_0 exhibits a slow-roll trajectory, which means $\ddot{\phi}_0 \simeq 0$ and H is approximately constant throughout the inflationary era (see [8] for a review of slow-roll inflation). The quantum fluctuations of the inflaton and isocurvaton fields perturb the metric about (5.1) and source scalar and tensor curvature fluctuations, $\zeta(\tau, \vec{x})$ and $\gamma_{ij}(\tau, \vec{x})$.

To describe the field fluctuations, we use the effective field theory of inflation formalism [27]. Following [27], we choose uniform inflaton gauge in which the inflaton fluctuations are set to zero. We then observe that the time-dependent inflaton vev spontaneously breaks time diffeomorphism invariance, giving rise to a Goldstone boson π that transforms as $\pi(x) \to \pi(x) - \xi(x)$ under time-diffeomorphisms $t \to t+\xi(x)$. The degrees of freedom in the effective theory are π, the metric fluctuations, and the fluctuations of the N isocurvaton fields σ_I. To construct the effective theory, one writes all possible terms invariant under the full set of space-time diffeomorphisms involving these fields (see [34] for a complete derivation in the context of single-isocurvaton QSFI).

We will be interested in computing the momentum space correlation functions of π at the time when the modes exit the horizon. This implies we can work in the "decoupling limit" of the effective theory [27] and set the metric perturbations to zero. Correlation functions of ζ in the gauge where π is zero can be related to correlation functions of π in the decoupling limit by [27]

$$\zeta = -(H/\dot{\phi})\pi. \tag{5.2}$$

The leading quadratic Lagrangian simplifies to any term quadratic in π and σ_I that is consistent with a shift symmetry in π and a background de-Sitter space-time:

$$\begin{aligned}\mathcal{L}_2 = \frac{1}{2(H\tau)^2}\Big((\partial_\tau\pi)^2 - \tilde{c}_\pi^2\,(\partial_i\pi)^2 + \tilde{Z}_{IJ}\partial_\tau\sigma_I\partial_\tau\sigma_J - \tilde{c}^2_{\sigma IJ}\partial_i\sigma_I\partial_i\sigma_J + 2\tilde{\beta}_I\partial_\tau\pi\partial_\tau\sigma_I + \tilde{\delta}_I\partial_i\pi\partial_i\sigma_I \\ - (H\tau)^{-2}\,\tilde{m}^2_{IJ}\sigma_I\sigma_J - 2\,(H\tau)^{-1}\,\tilde{\rho}_{IJ}\sigma_I\partial_\tau\sigma_J - 2\,(H\tau)^{-1}\,\tilde{\mu}_I\sigma_I\partial_\tau\pi\Big)\,.\end{aligned} \tag{5.3}$$

Note, repeated indices are summed over and we have included the $\sqrt{-g}$ factor from the action in the Lagrangian. We have dropped terms quadratic in the fields that have more than two derivatives because they are suppressed by powers of the cutoff Λ of the effective theory.

Several terms in (5.3) can be eliminated by field redefinitions. For example, the $\tilde{\delta}_I\partial_i\pi\partial_i\sigma_I$ interaction can be absorbed into other couplings by performing the time diffeomorphism that induces the shift $\pi \to \pi + \tilde{\delta}_I\sigma_I/(2c_\pi^2)$. Moreover, we can rotate and re-scale σ_I to diagonalize $\tilde{c}^2_{\sigma IJ}$ and set $\tilde{Z}_{IJ} = 1$. Equation (5.3) then simplifies

to

$$\mathcal{L}_2 = \frac{1}{2(H\tau)^2}\big((\partial_\tau\pi)^2 - c_\pi^2\,(\partial_i\pi)^2 + (\partial_\tau\sigma_I)^2 - c_{\sigma I}^2\,(\partial_i\sigma_I)^2 + 2\beta_I\partial_\tau\pi\partial_\tau\sigma_I \\ - (H\tau)^{-2}\,m_{IJ}^2\sigma_I\sigma_J - 2\,(H\tau)^{-1}\,\rho_{IJ}\sigma_I\partial_\tau\sigma_J - 2\,(H\tau)^{-1}\,\mu_I\sigma_I\partial_\tau\pi\big). \tag{5.4}$$

The matrix m_{IJ}^2 is symmetric while ρ_{IJ} is anti-symmetric[3]. The interactions $\mu_I\dot{\pi}\sigma_I$ and $\rho_{IJ}\sigma_I\dot{\sigma}_J$ could result from a UV theory containing terms such as $(\sigma_I/\Lambda)g^{\mu\nu}\partial_\mu\phi\partial_\nu\phi$ and $(\sigma_I/\Lambda)g^{\mu\nu}\partial_\mu\sigma_J\partial_\nu\phi$. The kinetic mixings in (5.4) arise because the inflaton vev spontaneously breaks Lorentz invariance. If $\dot{\phi}_0 = 0$, Lorentz invariance is unbroken and the kinetic mixings must vanish. By dimensional analysis, this means μ_I and ρ_{IJ} are proportional to $\dot{\phi}_0/\Lambda$. Using $(H^2/\dot{\phi}_0)^2 \sim 2\pi^2\Delta_\zeta^2$, where

$$\Delta_\zeta^2 = \frac{k^3}{2\pi^2}P_\zeta(k) \simeq 2.11\times10^{-9} \tag{5.5}$$

is the dimensionless power spectrum [94], the cutoff can be expressed in terms of $|\mu_I|$ as

$$\frac{\Lambda}{H} \sim \frac{H}{|\mu_I|}\times10^4. \tag{5.6}$$

For $\mu_I \sim O(H)$, this implies that $\Lambda \gg H$ and higher derivative terms are suppressed.

We can recover previously studied single-isocurvaton QSFI models by taking limits of (5.4). If we take $N = 1$, $\beta_1 = 0$ and $c_\pi^2 = c_{\sigma 1}^2 = 1$, we recover the quadratic part of the QSFI Lagrangian originally considered by Chen and Wang [15]. The resulting Lagrangian only has two parameters, μ_1 and m_{11}. Single-isocurvaton QSFI with generic speeds of sound and nonzero β_1 was studied in [34]. The presence of a nontrivial ρ_{IJ} matrix is the main new aspect of theories with $N > 1$ isocurvatons.

One way to treat the kinetic mixings parameterized by μ_I, β_I and ρ_{IJ} is to write the Fourier transforms of the π and σ_I fields in terms of a common set of raising and lowering operators

$$\hat{\pi}(\tau,\mathbf{x}) = \int\frac{d^3k}{(2\pi)^3}\frac{H}{k^{3/2}}\sum_{i=1}^{N+1}\left(\hat{a}_{\mathbf{k}}^{(i)}\pi^{(i)}(\eta)e^{-i\mathbf{k}\cdot\mathbf{x}} + c.c\right)$$
$$\hat{\sigma}_I(\tau,\mathbf{x}) = \int\frac{d^3k}{(2\pi)^3}\frac{H}{k^{3/2}}\sum_{i=1}^{N+1}\left(\hat{a}_{\mathbf{k}}^{(i)}\sigma_I^{(i)}(\eta)e^{-i\mathbf{k}\cdot\mathbf{x}} + c.c\right) \tag{5.7}$$

[3]Any symmetric part of ρ_{IJ} can be absorbed into m_{IJ}^2 through an integration by parts.

where $\eta = k\tau$. The mode functions $\pi^{(i)}(\eta)$ and $\sigma^{(i)}(\eta)$ obey the Euler-Lagrange equations obtained from (5.4),

$$\begin{aligned}
&\sigma_I^{(i)\prime\prime} - \frac{2}{\eta}\sigma_I^{(i)\prime} + c_{\sigma I}^2\sigma_I^{(i)} + \frac{m_{IJ}^2}{\eta^2}\sigma_J^{(i)} + \frac{\mu_I}{\eta}\pi^{(i)\prime} + \beta_I\left(\pi^{(i)\prime\prime} - \frac{2}{\eta}\pi^{(i)\prime}\right) + \frac{\rho_{IJ}}{\eta}\left(2\sigma_J^{(i)\prime} - \frac{3}{\eta}\sigma_J^{(i)}\right) = 0 \\
&\pi^{(i)\prime\prime} - \frac{2}{\eta}\pi^{(i)\prime} + c_\pi^2\pi^{(i)} - \frac{\mu_I}{\eta}\left(\sigma_I^{(i)\prime} - \frac{3}{\eta}\sigma_I^{(i)}\right) + \beta_I\left(\sigma_I^{(i)\prime\prime} - \frac{2}{\eta}\sigma_I^{(i)\prime}\right) = 0
\end{aligned} \tag{5.8}$$

where primes denote derivatives with respect to η. The mode functions asymptotically obey the Bunch-Davies vacuum condition. Since equations (5.8) are coupled, they are difficult to solve analytically for general parameters[4]. Instead, we use the numerical solutions of (5.8) to perform most of the calculations in our analysis. However, one can derive the small η behavior of the mode functions analytically, which turns out to fix the wavevector dependence of the squeezed and collapsed limits of the bispectrum and trispectrum.

In the limit[5] $-\eta << 1$, we can neglect the terms in (5.8) proportional to the speeds of sound. The leading late time behavior for the mode functions can be written as

$$\pi^{(i)}(\eta) = a_s^{(i)}(-\eta)^s \quad \sigma_I^{(i)}(\eta) = b_{I,s}^{(i)}(-\eta)^s. \tag{5.9}$$

For example, specializing to $N = 2$ and inserting (5.9) into (5.8) yields the following equation for s,

$$\begin{vmatrix} (s-3)s & (s-3)(s\beta_1 - \mu_1) & (s-3)(s\beta_2 - \mu_2) \\ s((s-3)\beta_1 + \mu_1) & m_{11}^2 + (s-3)s & m_{12}^2 + (3-2s)\rho \\ s((s-3)\beta_2 + \mu_2) & m_{12}^2 + (2s-3)\rho & m_{22}^2 + (s-3)s \end{vmatrix} = 0, \tag{5.10}$$

which can be solved for six different roots:

$$s = 0, s_-, s_-^*, 3 - s_-, 3 - s_-^*, 3. \tag{5.11}$$

In general, s_- is a complex number satisfying[6] $0 < \mathrm{Re}[s_-] \leq 3/2$. The $s = 0$ solution arises from the shift symmetry in π and can only exist in the π mode functions. The leading η behavior of the mode functions is

$$\begin{aligned}
\pi^{(i)}(\eta) &= a_0^{(i)} + a_{s_-}^{(i)}(-\eta)^{s_-} + a_{s_-^*}^{(i)}(-\eta)^{s_-^*} + \ldots \\
\sigma_I^{(i)}(\eta) &= b_{I,s_-}^{(i)}(-\eta)^{s_-} + b_{I,s_-^*}^{(i)}(-\eta)^{s_-^*} + \ldots .
\end{aligned} \tag{5.12}$$

[4] Analytic progress can be made in the context of single-isocurvaton QSFI in the regimes where $\mu_1, m_{11} \ll H$ as explained in chapter 3, or $\mu_1, m_{11} \gg H$ as explained in chapter 2 and [37, 41, 42].

[5] We have chosen the convention in which inflation occurs between $-\infty < \tau \leq 0$

[6] For general model parameters $\mathrm{Re}[s_-]$ can be less than 0, however the modes would then be tachyonic and grow rather than decay as $\eta \to 0$.

Equations (5.12) imply that as $\eta \to 0$, $\pi^{(i)}$ approaches a constant while $\sigma_I^{(i)}$ decays to 0.

The late time behavior of σ_I in multi-isocurvaton QSFI can be very different from its late time behavior in single-isocurvaton QSFI [15]. If we write $s_- \equiv \alpha + i\gamma$, equation (5.12) becomes

$$\sigma_I^{(i)}(\eta) = b_{I,s_-}^{(i)}(-\eta)^{\alpha} e^{i\gamma \log(-\eta)} + b_{I,s_-^*}^{(i)}(-\eta)^{\alpha} e^{-i\gamma \log(-\eta)}. \tag{5.13}$$

Observe that the modes oscillate logarithmically in η with frequency γ. Moreover, α dictates how quickly the modes decay at late times. In the original Chen and Wang theory [15] γ can only be nonzero when $\alpha = 3/2$ (see e.g. chapter 2). This means that while the isocurvaton's mode functions exhibit oscillatory behavior at late times, they decay quickly as $\eta \to 0$. On the other hand, in a multi-isocurvaton QSFI theory with $\rho_{IJ} \neq 0$, one can obtain $\gamma \neq 0$ with $\alpha < 3/2$, which means that $\sigma_I^{(i)}$ can oscillate while decaying slowly.

To illustrate this, we specialize to the case of two isocurvatons and focus on two sets of parameters which will serve as our benchmark models. The first set is

$$\begin{aligned} &\mu_1 = m_{12} = m_{21} = \beta_I = 0,\ c_\pi = c_{\sigma_1} = c_{\sigma_2} = 1, \\ &\mu_2 = 0.6H,\ m_{11}^2 = m_{22}^2 = -\rho_{12}^2 = -(5H)^2 \end{aligned} \tag{5.14}$$

which yields $s_- \simeq 0.06 - 5.00i$, while the second is

$$\begin{aligned} &\mu_1 = m_{12} = m_{21} = \beta_I = 0,\ c_\pi = c_{\sigma_1} = c_{\sigma_2} = 1, \\ &\mu_2 = 0.4H,\ m_{11} = m_{22} = 0.3H,\ \rho_{12} = H \end{aligned} \tag{5.15}$$

which yields $s_- \simeq 0.46 - 1.00i$. Notice, the masses squared in (5.15) are negative, which is usually a signal of tachyonic modes whose mode functions diverge as $\eta \to 0$. However, due to the kinetic mixing, the mass squared parameters that appear in the Lagrangian do not equal the physical masses squared. Indeed, $\alpha > 0$ for this set of parameters, which implies $\sigma_I \to 0$ as $\eta \to 0$.

For $\alpha < 3/2$ and $\gamma \neq 0$, α and γ are typically the same order of magnitude. Some tuning is required in order to produce $\alpha \ll 1$ with $\gamma \sim O(1)$. This means, rapid oscillations that decay slowly cannot be produced without some degree of tuning between model parameters[7].

[7] For example, in eq. (5.15), we tuned $m_{ii}^2 = -\rho^2$.

5.3 Primordial Non-Gaussianity

In the previous section, we showed that theories with multiple-isocurvaton have a kinetic mixing term parameterized by the matrix ρ_{IJ} that cannot exist in single-isocurvaton models. If this term is present, the mode functions of π and σ_I can exhibit oscillatory behavior that decays slowly at late times. We now study the effects of this behavior on the non-Gaussianities of the scalar curvature perturbations of the metric, ζ.

We are interested in computing the "in-in" correlation functions of ζ at $\tau = 0$, which are related to those of π through (5.2). The in-in correlator of an operator O can be expressed in the so-called "commutator form" (see for example [47]) as

$$\langle O(0)\rangle = \sum_{N=0}^{\infty} i^N \int_{-\infty}^{0} d\tau_N \int_{-\infty}^{\tau_N} d\tau_{N-1} \cdots \int_{-\infty}^{\tau_2} d\tau_1 \langle [H_{\rm int}(\tau_1), [H_{\rm int}(\tau_2), \ldots [H_{\rm int}(\tau_N), O(0)] \ldots]]\rangle_I \tag{5.16}$$

where the fields on the right hand side of (5.16) evolve according to (5.7) and (5.8). In general, the interaction Hamiltonian consists of an isocurvaton potential $V(\sigma_I)$ as well as interactions involving combinations of π and σ_I. For simplicity, we assume the potential consists of a cubic interaction involving only the σ_1 field and that the interaction Hamiltonian is dominated by this interaction[8]:

$$H_{\rm int}(\tau) = \frac{1}{(H\tau)^4} \int d^3x \frac{V'''}{3!} \sigma_1(x)^3 + \ldots . \tag{5.17}$$

In the next two subsections, we compute the bispectrum and trispectrum of ζ due to this interaction.

Bispectrum

We first consider the three-point function of ζ. Let $\zeta_{\mathbf{k}}$ denote the Fourier transform of $\zeta(\mathbf{x}, 0)$. The bispectrum B_ζ is defined as

$$\langle \zeta_{\mathbf{k}_1} \zeta_{\mathbf{k}_2} \zeta_{\mathbf{k}_3} \rangle = B_\zeta(\mathbf{k}_1, \mathbf{k}_2, \mathbf{k}_3)(2\pi)^3 \delta^3(\mathbf{k}_1 + \mathbf{k}_2 + \mathbf{k}_3). \tag{5.18}$$

[8] The potential $V(\sigma_I)$ is not related to the other operators in the effective theory by any symmetry and can, in principle, be the largest term in the interaction Hamiltonian.

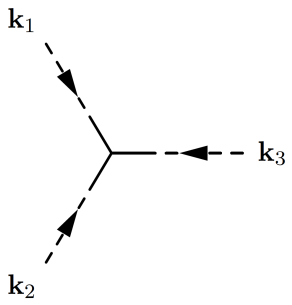

Figure 5.1: A diagramatic representation of the leading contribution to the bispectrum. Dashed lines represent π, while solid lines represent σ_1.

Using equations (5.2), (5.7), (5.16) and (5.17), it is straightforward to show that to leading order in V'''

$$B_\zeta(k_1,k_2,k_3) = -2\left(\frac{H^2}{\dot\phi_0}\right)^3 \frac{V'''}{H}\frac{1}{k_1^3k_2^3k_3^3} \times \int_{-\infty}^{0}\frac{d\tau}{\tau^4}\mathrm{Im}\left(\pi^{(i)}(0)\sigma_1^{(i)*}(k_1\tau)\pi^{(j)}(0)\sigma_1^{(j)*}(k_2\tau)\pi^{(k)}(0)\sigma_1^{(k)*}(k_3\tau)\right) \tag{5.19}$$

where repeated mode labels are summed. Note, the sum $\pi^{(i)}(0)\sigma_1^{(i)*}(k_i\tau)$ is nonzero because of the kinetic mixings.

The τ integral in (5.19) is potentially IR divergent due to the factor of $1/\tau^4$ in the integrand. Even though we do not have explicit expressions for the mode functions, it can be shown using the canonical commutation relations (see Appendix 5.A) that the integral is indeed finite in the IR. One can then evaluate the bispectrum using the numerical solutions of (5.8).

Consider the squeezed limit of (5.19), which occurs when $k_l \equiv k_1 \sim k_2$ and $k_s \equiv k_3 \ll k_l$, *i.e.* there are two long sides and one short side of the triangle traced out by the $\mathbf{k}_i$. We can factor out the momentum dependence from the time integral by changing integration variables to $\eta = k_l\tau$ and expanding to leading order in k_s/k_l using (5.12). We find

$$B_\zeta^{\mathrm{sq}}(k_l,k_s) = -4\left(\frac{H^2}{\dot\phi_0}\right)^3\left(\frac{V'''}{H}\right)\frac{1}{k_l^6}\left(\frac{k_s}{k_l}\right)^{-3+\alpha} \Big(\cos(\gamma\log k_s/k_l)\,\mathrm{Re}\left[a_0^{(i)}b_{1,s_-}^{(i)*}y^*(\alpha,\gamma)\right] + \sin(\gamma\log k_s/k_l)\,\mathrm{Im}\left[a_0^{(i)}b_{1,s_-}^{(i)*}y^*(\alpha,\gamma)\right]\Big) \tag{5.20}$$

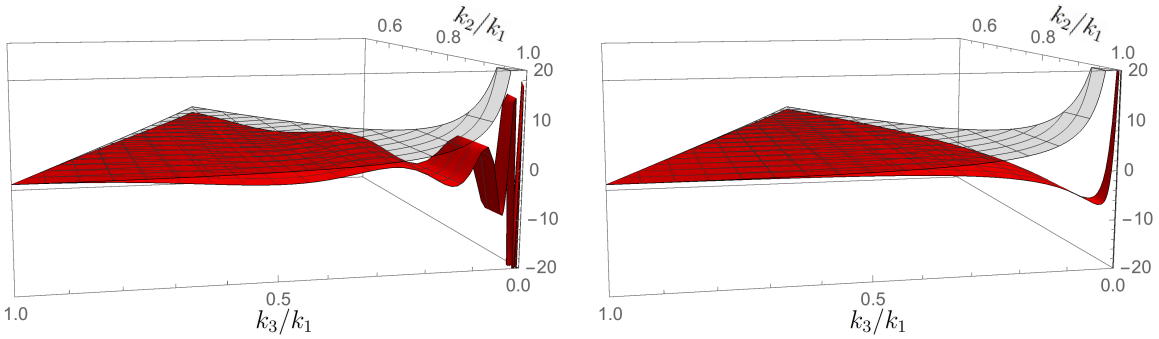

Figure 5.2: Plots of the shape functions $S(k_1, k_2, k_3)$ in the range $k_1 > k_2 > k_3$ for multi-isocurvaton oscillatory shape (red) and local shape (transparent gray). In the left and right panels we plot parameters (5.14) and (5.15) respectively.

where

$$y(\alpha, \gamma) = \int_{-\infty}^{0} \frac{d\eta}{(-\eta)^{4-\alpha-i\gamma}} \mathrm{Im}\left[\left(\pi^{(i)}(0)\sigma_1^{(i)*}(\eta)\right)^2\right]. \tag{5.21}$$

The squeezed bispectrum oscillates logarithmically in k_s/k_l with angular frequency γ and the amplitude grows as $(k_s/k_l)^{-3+\alpha}$. As mentioned earlier, in single-isocurvaton QSFI, γ can only be nonzero when $\alpha = 3/2$, which means the amplitude of an oscillating squeezed bispectrum can only grow as $(k_s/k_l)^{-3/2}$ in these models. This is not the case for the multi-isocurvaton models given by (5.14) or (5.15), whose oscillating bispectrum grow approximately as $(k_s/k_l)^{-2.94}$ and $(k_s/k_l)^{-2.54}$ respectively.

To illustrate the momentum dependence of the full bispectrum, it is useful to define the shape function

$$S(k_1, k_2, k_3) = \kappa(k_1 k_2 k_3)^2 B_\zeta(k_1, k_2, k_3). \tag{5.22}$$

The normalization factor κ is chosen so that $S(k, k, k) = 1$.

In Fig. 5.2, we plot the shape function of multi-isocurvaton QSFI for the model parameters (5.14) and (5.15). For comparison, we also include the shape function of local non-Gaussianity

$$S^{loc}(k_1, k_2, k_3) = \frac{1}{3}(k_1 k_2 k_3)^2 \left[\frac{1}{(k_1 k_2)^3} + \frac{1}{(k_2 k_3)^3} + \frac{1}{(k_3 k_1)^3}\right] \tag{5.23}$$

which is close to the shape function of the single-isocurvaton QSFI originally considered by Chen and Wang in the limit $\mu_1, m_{11} \ll H$, see chapter 3 and [15].

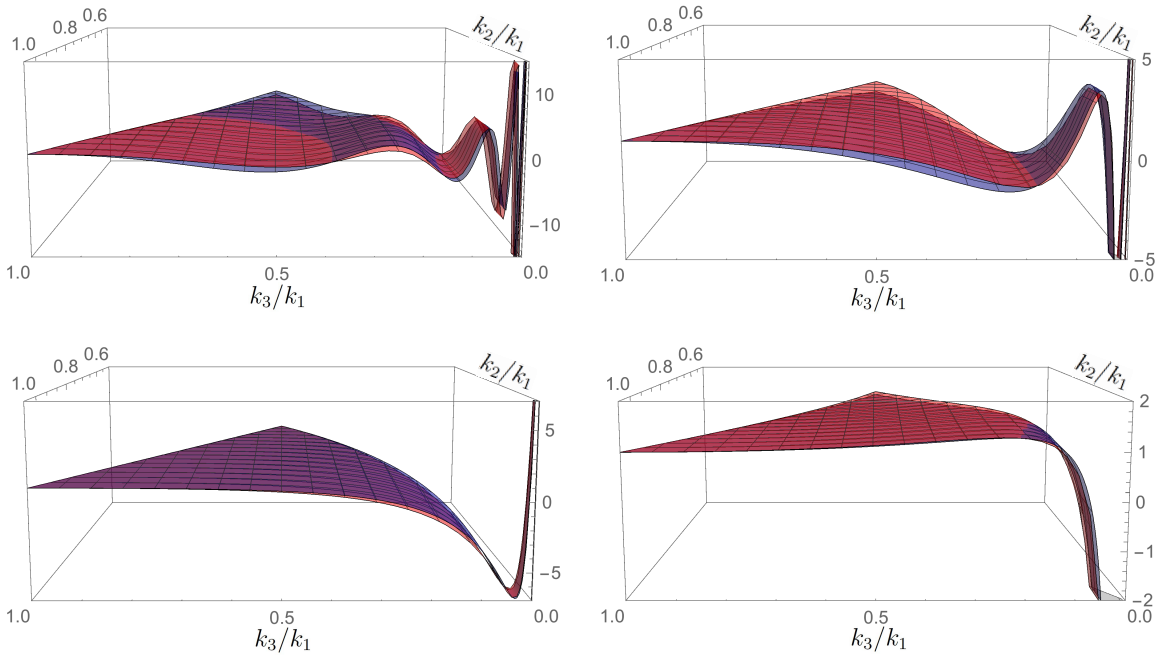

Figure 5.3: We plot shape functions $S(k_1, k_2, k_3)$ of the multi-isocurvaton oscillatory shape in the range $k_1 > k_2 > k_3$. We plot the shape computed numerically in red and plot the approximate shape defined in eq. (5.25) in blue. The top-left plot has parameters $(\alpha, \gamma, \phi) = (0.06, -5.00, -1.55)$, top-right $(0.23, -2.50, -1.58)$, bottom-left $(0.46, -1.00, 3.08)$, and bottom-right $(0.14, -0.50, -2.78)$.

Fig. 5.2 is consistent with the analytic results for the squeezed bispectrum of multi-isocurvaton QSFI. In the limit $k_3/k_1 \to 0$, the shape function oscillates logarithmically in k_3/k_1 and its amplitude has power law growth. On the other hand, in single-isocurvaton QSFI, the shape function for an oscillating bispectrum decays to 0 as $k_3/k_1 \to 0$. Note, to get very rapid oscillations and nearly local power law growth for the multi-isocurvaton shape, one needs to tune parameters as in (5.14). However, even the shape for the untuned parameters (5.15) displays a visible turn due to nonzero γ.

For single-isocurvaton QSFI with $\gamma = 0$, the shape function has been approximated as [15]:

$$S_\alpha^{QSFI}(k_1, k_2, k_3) = 3^{3\alpha-2} \frac{\left(k_1^2 + k_2^2 + k_3^2\right)(k_1 + k_2 + k_3)^{1-3\alpha}}{(k_1 k_2 k_3)^{1-\alpha}} \tag{5.24}$$

A good phenomenological fit to the multi-isocurvaton QSFI shape is

$$S^{\mathrm{OQSFI}}_{\alpha,\gamma,\phi}(k_1,k_2,k_3) = C\left(\cos\left(\gamma\log\left(\frac{k_2k_3}{k_1\,(k_1+k_2+k_3)}\right)+\phi\right)+2\text{ perms.}\right)S^{\mathrm{QSFI}}_{\alpha}(k_1,k_2,k_3) \tag{5.25}$$

where the normalization $C = (3\cos(\gamma\log(1/3)+\phi))^{-1}$ enforces $S^{\mathrm{OQSFI}} = 1$ in the equilateral limit. Note that the shape function is parameterized by three numbers α, γ, and a phase ϕ. In Fig. 5.3, we plot the shape functions evaluated numerically against the shape functions computed with (5.25).

We can also define the parameter $f^{\mathrm{OQSFI}}_{\mathrm{NL}}$, corresponding to the magnitude of this shape. In keeping with convention[9], we define:

$$B_\zeta(k_1,k_2,k_3) = \frac{18}{5}(k^3P_\zeta(k))^2 f^{\mathrm{OQSFI}}_{\mathrm{NL}}\frac{1}{k_1^2k_2^2k_3^2}S^{\mathrm{OQSFI}}_{\alpha,\gamma,\phi}(k_1,k_2,k_3). \tag{5.26}$$

By matching the squeezed limit of (5.26) onto (5.20), we can obtain V'''/H as a function of $f^{\mathrm{OQSFI}}_{\mathrm{NL}}$:

$$\frac{V'''}{H} = -\frac{9}{10}(|a_0^{(i)}|^2)^{3/2}\sqrt{2\pi^2\Delta_\zeta^2}f^{\mathrm{OQSFI}}_{\mathrm{NL}}\frac{C}{\sqrt{\mathrm{Im}\left[a_0^{(i)}b^{(i)*}_{1,s_-}y^*(\alpha,\gamma)\right]^2+\frac{1}{9}\mathrm{Re}\left[a_0^{(i)}b^{(i)*}_{1,s_-}y^*(\alpha,\gamma)\right]^2}}. \tag{5.27}$$

Even for $\gamma \sim O(0.1)$, the oscillating QSFI bispectrum shape still displays qualitatively distinct features. Specifically, the shape can get large and negative in the squeezed limit. This is different from many other bispectrum shapes that grow in the squeezed limit because they typically remain positive rather than become negative (see [14]).

Collapsed Trispectrum

We now consider the four-point function of ζ, which is defined as

$$\langle\zeta_{\mathbf{k}_1}\zeta_{\mathbf{k}_2}\zeta_{\mathbf{k}_3}\zeta_{\mathbf{k}_4}\rangle = T_\zeta(\mathbf{k}_1,\mathbf{k}_2,\mathbf{k}_3,\mathbf{k}_4)(2\pi)^3\delta^3(\mathbf{k}_1+\mathbf{k}_2+\mathbf{k}_3+\mathbf{k}_4). \tag{5.28}$$

We focus on the collapsed limit, which occurs when $k_{l1} \equiv k_1 \sim k_2$, $k_{l2} \equiv k_3 \sim k_4$, and $k_s \equiv |\mathbf{k}_1+\mathbf{k}_2| = |\mathbf{k}_3+\mathbf{k}_4| \ll k_{li}$. The integrand will be symmetric in k_{l1} and k_{l2}, which means we can untangle the limits of the time integrals. The collapsed

[9] Conventionally, f_{NL} is defined via $B_\Phi(k_1,k_2,k_3) = 6A^2 f_{\mathrm{NL}}\frac{1}{k_1^2k_2^2k_3^2}S(k_1,k_2,k_3)$ where A is given by the power spectrum's normalization $P_\Phi(k) = A/k^3$ (see, e.g. [44]).

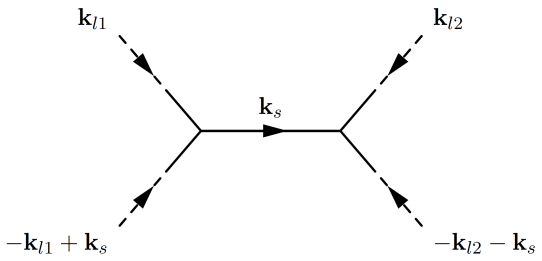

Figure 5.4: A diagramatic representation of the collapsed trispectrum. Dashed lines represent π, while solid lines represent σ_1.

four-point then simplifies to

$$T_\zeta{}^{\rm coll}(k_{l1},k_{l2},k_s) = 4\left(\frac{H^2}{\dot\phi_0}\right)^4\left(\frac{V'''}{H}\right)^2\frac{1}{k_{l1}^{9/2}k_{l2}^{9/2}}\left(\frac{k_s^2}{k_{l1}k_{l2}}\right)^{-3/2+\alpha}$$
$$\left[\cos\left(\gamma\log\frac{k_{l2}}{k_{l1}}\right)\left(|b^{(i)}_{1,s_-}|^2+|b^{(i)}_{1,s_-^*}|^2\right)|y(\alpha,\gamma)|^2\right.$$
$$+2\cos\left(\gamma\log\frac{k_s^2}{k_{l1}k_{l2}}\right)\mathrm{Re}\left[b^{(i)}_{1,s_-}b^{(i)*}_{1,s_-^*}y(\alpha,\gamma)^2\right]$$
$$\left.-2\sin\left(\gamma\log\frac{k_s^2}{k_{l1}k_{l2}}\right)\mathrm{Im}\left[b^{(i)}_{1,s_-}b^{(i)*}_{1,s_-^*}y(\alpha,\gamma)^2\right]\right]. \qquad (5.29)$$

Note, not every term oscillates logarithmically in k_s/k_l. Instead, there are two terms which oscillate with angular frequency 2γ as well as one that does not oscillate at all in k_s/k_l.

It turns out that a loop contribution to the trispectrum can produce terms that oscillate with frequency 4γ. We explore this in Appendix 5.B.

5.4 Large-Scale Structure

In this section, we determine the effects of PNG on large-scale structure, specifically the halo-halo power spectrum P_{hh} and the matter-halo power spectrum P_{hm}. It is well known that in certain inflationary theories, such as single-isocurvaton QSFI, the contributions of PNG to P_{hh} and P_{hm} can become much larger than the Gaussian contributions at wavevectors of order $(10^2\ \mathrm{Mpc}/h)^{-1}$ as illustrated in chapters 3 and 4 and [95]. We now consider this in multi-isocurvaton QSFI.

The primordial curvature perturbations are related to the linearly evolved smoothed matter density perturbations today, $\delta_R(\mathbf{k})$, by [1]

$$\delta_R(\mathbf{k}) = \frac{2k^2}{5\Omega_m H_0^2}T(k)W_R(k)\zeta_{\mathbf{k}} \qquad (5.30)$$

where Ω_m is the ratio of the matter density and the critical density today, H_0 is the Hubble constant today, $T(k)$ is the BBKS transfer function [59] and $W_R(k)$ is a window function smoothing over radius R. We use the top-hat window function

$$W_R(k) = \frac{3\,(sinkR - kRcoskR)}{(kR)^3}. \tag{5.31}$$

.

Since we are interested in scales of order 10^2 Mpc/h, δ_h can be related to δ_R through a bias expansion. For simplicity, we use a local-in-matter-density bias expansion (for a more comprehensive treatment, see [58])

$$\delta_h(\mathbf{x}) = b_1\delta_R(\mathbf{x}) + b_2\left(\delta_R(\mathbf{x})^2 - \langle\delta_R(\mathbf{x})^2\rangle\right) + \dots \tag{5.32}$$

The bias coefficients can be approximated using the threshold model introduced in [55]. We assume that halos form instantaneously at some redshift z_{coll}, and that halos only form at points where the overdensity exceeds some critical threshold $\delta_c(z_{\rm coll})$. We also neglect the evolution of halos after collapse. In this model, the bias coefficients b_1 and b_2 are then

$$b_1 = 2\frac{e^{-\delta_c^2/(2\sigma_R^2)}}{\sqrt{2\pi}\sigma_R\; erfc(\delta_c/(\sqrt{2}\sigma_R))} \qquad b_2 = \frac{e^{-\delta_c^2/(2\sigma_R^2)}\delta_c}{\sqrt{2\pi}\sigma_R^3\; erfc(\delta_c/(\sqrt{2}\sigma_R))} \tag{5.33}$$

where $\sigma_R^2 = \langle\delta_R(\mathbf{x})^2\rangle$. In deriving our numerical results, we use $\delta_c = 4.215$, which corresponds to $\delta_c(z_{coll}) = 1.686$ at $z_{coll} = 1.5$ [54], and $R = 3\ Mpc/h$. While a more sophisticated treatment of halo dynamics will change our precise numerical results, we do not expect them to impact our conclusions qualitatively.

We will be interested in computing the halo-halo power spectrum P_{hh},

$$\langle\delta_h(\mathbf{k}_1)\delta_h(\mathbf{k}_2)\rangle = P_{hh}(k_1)(2\pi)^3\delta^3(\mathbf{k}_1 + \mathbf{k}_2) \tag{5.34}$$

as well as the halo-matter power spectrum P_{hm},

$$\langle\delta_h(\mathbf{k}_1)\delta_R(\mathbf{k}_2)\rangle = P_{hm}(k_1)(2\pi)^3\delta^3(\mathbf{k}_1 + \mathbf{k}_2). \tag{5.35}$$

The Gaussian contributions to P_{hh} and P_{hm} are found to be

$$\begin{aligned} P_{hh}(k_s)\Big|_G &= b_1^2\left(\frac{H^2}{\dot\phi_0}\right)^2\left(\frac{2}{5\Omega_m H_0^2 R^2}\right)^2 k_s R^4|a_0^{(i)}|^2 \\ P_{hm}(k_s)\Big|_G &= b_1\left(\frac{H^2}{\dot\phi_0}\right)^2\left(\frac{2}{5\Omega_m H_0^2 R^2}\right)^2 k_s R^4|a_0^{(i)}|^2. \end{aligned} \tag{5.36}$$

At wavevectors of order $(10^2\ \mathrm{Mpc}/h)^{-1} \ll R^{-1}$, the most significant non-Gaussian contributions to P_{hh} are due to the squeezed and collapsed limits of the bispectrum (5.20) and trispectrum (5.29). Then, plugging (5.30) and (5.32) into (5.34) and using (5.20) and (5.29) gives

$$\begin{aligned}\frac{P_{hh}(k_s)}{P_{hh}(k_s)\big|_G} = 1 &- 8\left(\frac{b_2}{b_1}\right)\left(\frac{H^2}{\dot\phi_0}\right)\left(\frac{2}{5\Omega_m H_0^2 R^2}\right)\left(\frac{V'''}{H}\right)\frac{1}{(k_sR)^{2-\alpha}}\frac{1}{|a_0^{(i)}|^2}\\ &\Bigg(\cos(\gamma\log k_sR)\,\mathrm{Re}\left[J^*(\alpha,\gamma)y^*(\alpha,\gamma)a_0^{(i)}b_{1,s_-}^{(i)*}\right]\\ &\quad+\sin(\gamma\log k_sR)\,\mathrm{Im}\left[J^*(\alpha,\gamma)y^*(\alpha,\gamma)a_0^{(i)}b_{1,s_-}^{(i)*}\right]\Bigg)\\ &+8\left(\frac{b_2}{b_1}\right)^2\left(\frac{H^2}{\dot\phi_0}\right)^2\left(\frac{2}{5\Omega_m H_0^2 R^2}\right)^2\left(\frac{V'''}{H}\right)^2\frac{1}{(k_sR)^{4-2\alpha}}\frac{1}{|a_0^{(i)}|^2}\\ &\Bigg(|J(\alpha,\gamma)|^2\,|y(\alpha,\gamma)|^2\,|b_{1,s_-}^{(i)}|^2\\ &\quad+\cos(2\gamma\log k_sR)\,\mathrm{Re}\left[J(\alpha,\gamma)^2y(\alpha,\gamma)^2b_{1,s_-}^{(i)}b_{1,s_-^*}^{(i)*}\right]\\ &\quad-\sin(2\gamma\log k_sR)\,\mathrm{Im}\left[J(\alpha,\gamma)^2y(\alpha,\gamma)^2b_{1,s_-}^{(i)}b_{1,s_-^*}^{(i)*}\right]\Bigg).\end{aligned}\tag{5.37}$$

where, to compactify notation, we have defined

$$J(\alpha,\gamma)=\frac{1}{2\pi^2}\int_0^\infty dx\ x^{3-\alpha-i\gamma}T(x/R)^2W(x/R)^2\tag{5.38}$$

The most significant non-Gaussian contribution to P_{hm} comes from the squeezed bispectrum:

$$\begin{aligned}\frac{P_{hm}(k_s)}{P_{hm}(k_s)\big|_G} = 1 &- 4\left(\frac{b_2}{b_1}\right)\left(\frac{H^2}{\dot\phi_0}\right)\left(\frac{2}{5\Omega_m H_0^2 R^2}\right)\left(\frac{V'''}{H}\right)\frac{1}{(k_sR)^{2-\alpha}}\frac{1}{|a_0^{(i)}|^2}\\ &\Bigg(\cos(\gamma\log k_sR)\,\mathrm{Re}\left[J^*(\alpha,\gamma)y^*(\alpha,\gamma)a_0^{(i)}b_{1,s_-}^{(i)*}\right]\\ &\quad+\sin(\gamma\log k_sR)\,\mathrm{Im}\left[J^*(\alpha,\gamma)y^*(\alpha,\gamma)a_0^{(i)}b_{1,s_-}^{(i)*}\right]\Bigg).\end{aligned}\tag{5.39}$$

In Figure 5.5 we plot (5.37) for the model parameters (5.14) and (5.15) and $|f_{\mathrm{NL}}^{OQSFI}| = 10$. Note that at around $(10^2\ Mpc/h)^{-1}$, P_{hh} begins to deviate from $P_{hh}|_G$. The oscillations evident in Fig. 5.5 are a consequence of the oscillatory squeezed bispectrum and collapsed trispectrum.

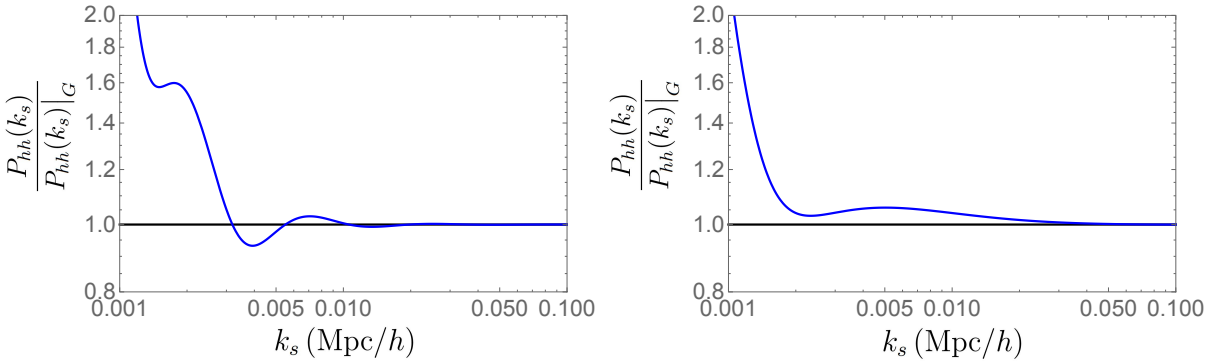

Figure 5.5: We plot the halo-halo power spectrum scaled by the Gaussian halo-halo power spectrum (i.e. the power spectrum for $V''' = 0$). In the left panel, we plot the parameters from eq. (5.14) with $f_{\mathrm{NL}}^{OQSFI} = 10$, and in the right panel, we plot the parameters from eq. (5.15) with $f_{\mathrm{NL}}^{OQSFI} = -10$.

However, for $|f_{\mathrm{NL}}^{OQSFI}| \sim 10$, the amplitude of the oscillations is quite small. Moreover, the non-Gaussian contributions to P_{hh} only begin to dominate over the Gaussian contribution at a scale of order $(10^3\ Mpc/h)^{-1}$, which is unlikely to be detected experimentally in the near future.

This scale is smaller than the scale at which the non-Gaussian contributions to P_{hh} begin to dominate in single-isocurvaton QSFI theories with $f_{NL} \sim 10$ and α small as seen in chapter 3. The reason is the integrals involving the transfer functions, $J(\alpha, \gamma)$, are oscillatory in multi-isocurvaton QSFI when $\gamma \neq 0$, which washes them out. This makes the coefficients of the non-Gaussian contributions smaller in multi-isocurvaton QSFI than in single-isocurvaton QSFI.

5.5 Conclusion

In this chapter, we studied quasi-single field inflation with multiple isocurvatons. Multi-isocurvaton QSFI includes the interaction $\rho_{IJ}\dot{\sigma}_I\sigma_J$ which can give rise to novel inflationary dynamics. In particular, the mode functions of π and σ_I can exhibit late time log oscillations that decay slowly as $\eta \to 0$. Due to these late time oscillations, the primordial non-Gaussianities of ζ exhibit log-oscillatory behavior in ratios of wavevector magnitudes.

For example, the bispectrum is proportional to $(k_s/k_l)^{-3+\alpha}\cos(\gamma \log k_s/k_l)$ in the

squeezed limit, which means for small α it experiences nearly cubic growth while oscillating. This behavior cannot be achieved in single-isocurvaton QSFI. Furthermore, the collapsed trispectrum goes as $(k_s/k_l)^{-3+2\alpha}(a + b\cos(2\gamma \log k_s/k_l))$, *i.e.* there is a term that does not oscillate in k_s/k_l as well as one that does with frequency 2γ.

In models where $\alpha \lesssim 0.5$, the contributions of the squeezed bispectrum and collapsed trispectrum to the halo-halo power spectrum $P_{hh}(k_s)$ and the halo-matter power spectrum $P_{hm}(k_s)$ can dominate over the Gaussian contributions at $k_s \sim (10^3\ Mpc/h)^{-1}$. When $\gamma \neq 0$, P_{hh} and P_{hm} oscillate logarithmically in $k_s R$.

5.A Commutator Constraints

The η integrals of (5.21) are potentially IR divergent because of the factors of $1/\eta^4$ in the integrands. It can be shown that all potentially IR divergent terms are zero. Eq. (5.8) implies that the σ mode functions can be written in series form as

$$\begin{aligned}\sigma_I^{(i)}(\eta) = b^{(i)}_{I,s_-}(-\eta)^{s_-} + b^{(i)}_{I,s_-^*}(-\eta)^{s_-^*} + b^{(i)}_{I,2}(-\eta)^2 + b^{(i)}_{I,2+s_-}(-\eta)^{2+s_-} + b^{(i)}_{I,2+s_-^*}(-\eta)^{2+s_-^*} \\ + b^{(i)}_{I,3-s_-}(-\eta)^{3-s_-} + b^{(i)}_{I,3-s_-^*}(-\eta)^{3-s_-^*} + b^{(i)}_{I,3}(-\eta)^3 + \ldots\end{aligned} \tag{5.40}$$

The equal time commutation relation $[\pi, \sigma_I] = 0$ holds order by order in powers of η and implies the following relations among the power series coefficients

$$\begin{aligned}\pi^{(i)}(0)b^{(i)*}_{I,s_-} = \left(\pi^{(i)}(0)b^{(i)*}_{I,s_-^*}\right)^*, \quad \pi^{(i)}(0)b^{(i)*}_{I,s_-} = \left(\pi^{(i)}(0)b^{(i)*}_{I,s_-^*}\right)^* \\ \pi^{(i)}(0)b^{(i)*}_{I,3-s_-} = \left(\pi^{(i)}(0)b^{(i)*}_{I,3-s_-^*}\right)^*, \quad \mathrm{Im}\left(\pi^{(i)}(0)b^{(i)*}_{I,2}\right) = 0\end{aligned} \tag{5.41}$$

where the sum over mode label i is implicit. Furthermore, the mode equations (5.8) imply

$$b^{(i)}_{I,2+s_-} = c\, b^{(i)}_{I,s_-} \quad b^{(i)}_{I,2+s_-^*} = c^* b^{(i)}_{I,s_-^*}. \tag{5.42}$$

Combining the first relation in (5.41) with (5.42) yields

$$\pi^{(i)}(0)b^{(i)*}_{I,2+s_-} = \left(\pi^{(i)}(0)b^{(i)*}_{I,2+s_-^*}\right)^* \tag{5.43}$$

The leading infrared behavior of (5.21) is then

$$y(\alpha,\gamma) = 2\,\mathrm{Im}\left[\pi^{(i)}(0)b^{(i)*}_{1,3}\right]\int_{-\infty}^{0}\frac{d\eta}{(-\eta)^{1-\alpha-i\gamma}}\mathrm{Re}\left[\pi^{(j)}(0)\sigma_1^{(j)*}(\eta)\right]. \tag{5.44}$$

It is straightforward to fit the $\sigma_1^{(i)}$ mode functions to (5.40) and determine the numerical coefficient in (5.44). The method to evaluate $y(\alpha,\gamma)$ is to choose an $-\eta_{IR} < 1$ and numerically integrate from $-\infty < \eta < \eta_{IR}$ using (5.21) and then integrate from $\eta_{IR} \leq \eta < 0$ using (5.44).

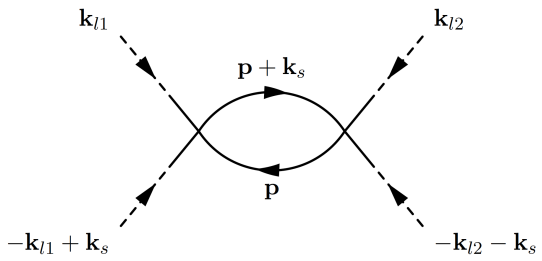

Figure 5.6: A diagramatic representation of the loop contribution to the collapsed trispectrum. Dashed lines represent π, while solid lines represent σ_1.

5.B Loop Contribution to the Collapsed Trispectrum

Recall that the tree-level collapsed trispectrum, which has one internal line, has terms that oscillate with frequency 2γ. We now show that a loop contribution to the collapsed trispectrum, which has two internal lines, can contain terms that oscillate with frequency 4γ. The loop contribution to the collapsed trispectrum then induces terms in the halo-halo power spectrum that oscillate as $cos(4\gamma log k_s R)$.[10]

Consider a theory in which the interaction Hamiltonian is composed of a single σ_1^4 interaction:

$$H_{\rm int}(\tau) = \frac{1}{(H\tau)^4}\int d^3x \frac{V''''}{4!}\sigma_1(x)^4. \tag{5.45}$$

Inserting two factors of (5.45) into (5.16) yields the 1-loop contribution to the trispectrum:

$$\begin{aligned} T_\zeta^{\rm coll}(k_{l1},k_{l2},k_s) = 4\left(\frac{H^2}{\dot\phi_0}\right)^4 V''''^2 \frac{1}{k_{l1}^3 k_{l2}^3}\int_{-\infty}^0 \frac{d\eta}{\eta^4}\int_{-\infty}^{\frac{k_{l2}}{k_{l1}}\eta}\frac{d\eta'}{\eta'^4}\int \frac{d^3p}{(2\pi)^3}\frac{1}{p^3|\mathbf{p}+\mathbf{k}_s|^3} \\ \times {\rm Im}\left[\left(\pi^{(i)}(0)\sigma_1^{(i)*}(\eta)\right)^2\right]{\rm Im}\left[\left(\pi^{(j)}(0)\sigma_1^{(j)*}(\eta')\right)^2\left(\sigma_1^{(l)}\left(\frac{p}{k_{l1}}\eta\right)\sigma_1^{(l)*}\left(\frac{p}{k_{l2}}\eta'\right)\right)\right. \\ \left.\times\left(\sigma_1^{(m)}\left(\frac{|\mathbf{p}+\mathbf{k}_s|}{k_{l1}}\eta\right)\sigma_1^{(m)*}\left(\frac{|\mathbf{p}+\mathbf{k}_s|}{k_{l2}}\eta'\right)\right)\right] \end{aligned} \tag{5.46}$$

As described in chapter 4 and [35, 95], for $k_s \ll k_l$, the loop diagram can give a large contribution to the collapsed trispectrum. In this limit, the loop integral is dominated by the region in which $p \sim k_s$, which means the mode functions on the bottom line of (5.46) can be expanded in p/k_{li}. Defining the integral

$$Z(\epsilon_1,\epsilon_2) \equiv \int \frac{d^3u}{(2\pi)^3}u^{-3+2\epsilon_1}|\mathbf{u}+\hat{\mathbf{x}}|^{-3+2\epsilon_2}, \tag{5.47}$$

[10] Contributions to the halo-halo power spectrum due to primordial non-Gaussianities sourced by quantum loops in the context of single-isocurvaton QSFI were considered in chapter 4 and [95].

where $\hat{\mathbf{x}}$ is an arbitrary unit vector, the loop contribution can be written:

$$
\begin{aligned}
T_\zeta{}^{\rm coll}(k_{l1}, k_{l2}, k_s) = \; & 2\left(\frac{H^2}{\dot\phi_0}\right)^4 V''''^2 \frac{1}{k_{l1}^{9/2} k_{l2}^{9/2}} \left(\frac{k_s^2}{k_{l1}k_{l2}}\right)^{-3/2+2\alpha} \\
& \Bigg[\mathrm{Re}[c_1] + \mathrm{Re}[c_2]\cos\left(2\gamma \log\frac{k_{l2}}{k_{l1}}\right) + \mathrm{Re}[c_3]\cos\left(2\gamma\log\frac{k_s}{k_{l1}}\right) + \mathrm{Re}[c_3]\cos\left(2\gamma\log\frac{k_s}{k_{l2}}\right) \\
& - \mathrm{Im}[c_3]\sin\left(2\gamma\log\frac{k_s}{k_{l1}}\right) - \mathrm{Im}[c_3]\sin\left(2\gamma\log\frac{k_s}{k_{l2}}\right) + \mathrm{Re}[c_4]\cos\left(2\gamma\log\frac{k_s^2}{k_{l1}k_{l2}}\right) \\
& - \mathrm{Im}[c_4]\sin\left(2\gamma\log\frac{k_s^2}{k_{l1}k_{l2}}\right) \Bigg]
\end{aligned}
\tag{5.48}
$$

where

$$
\begin{aligned}
c_1 &= 2y(2\alpha,0)^2 \left(|b^{(i)}_{1,s_-}|^2 |b^{(j)}_{1,s_-^*}|^2 Z(\alpha,\alpha) + |b^{(i)}_{1,s_-} b^{(i)*}_{1,s_-^*}|^2 Z(\alpha+i\gamma, \alpha-i\gamma) \right) \\
c_2 &= |y(2\alpha,2\gamma)|^2 \left(\left(|b^{(i)}_{1,s_-}|^2\right)^2 + \left(|b^{(i)}_{1,s_-^*}|^2\right)^2 \right) Z(\alpha,\alpha) \\
c_3 &= 4y(2\alpha,0)y(2\alpha,2\gamma) b^{(i)}_{1,s_-} b^{(i)*}_{1,s_-^*} \left(|b^{(j)}_{1,s_-}|^2 + |b^{(j)}_{1,s_-^*}|^2 \right) Z(\alpha, \alpha+i\gamma) \\
c_4 &= 2\,|y(2\alpha,2\gamma)|^2 \left(b^{(i)}_{1,s_-} b^{(i)*}_{1,s_-^*} \right)^2 Z(\alpha+i\gamma, \alpha+i\gamma).
\end{aligned}
\tag{5.49}
$$

Note that the loop contribution to the trispectrum has terms that do not oscillate with $\log k_s/k_{li}$, terms that oscillate with frequency 2γ, and terms that oscillate with frequency 4γ.

The loop contribution to P_{hh} due to the quartic σ_1^4 interaction can also be computed:

$$
\begin{aligned}
\frac{P_{hh}(k_s)\big|_{\rm loop}}{P_{hh}(k_s)\big|_G} = \; & 2\left(\frac{b_2}{b_1}\right)^2 \left(\frac{H^2}{\dot\phi_0}\right)^2 \left(\frac{2}{5\Omega_m H_0^2 R^2}\right)^2 V''''^2 \frac{1}{(k_s R)^{4-2\alpha}} \frac{1}{|a_0^{(i)}|^2} \\
& \Big(\mathrm{Re}\left[c_1 J(2\alpha,0)^2 + c_2\,|J(2\alpha,2\gamma)|^2 \right] \\
& + 2\cos(2\gamma\log k_s R)\,\mathrm{Re}\left[c_3 J(2\alpha,0) J(2\alpha,2\gamma)\right] \\
& - 2\sin(2\gamma\log k_s R)\,\mathrm{Im}\left[c_3 J(2\alpha,0) J(2\alpha,2\gamma)\right] \\
& + \cos(4\gamma\log k_s R)\,\mathrm{Re}\left[c_4 J(2\alpha,2\gamma)^2\right] \\
& - \sin(4\gamma\log k_s R)\,\mathrm{Im}\left[c_4 J(2\alpha,2\gamma)^2\right] \Big)
\end{aligned}
\tag{5.50}
$$

While it appears that the terms oscillating with frequency 4γ in (5.50) could induce unique observable features in $P_{hh}(k_s)$, it turns out their coefficients are suppressed

relative to those of the non-oscillating terms since $|J(2\alpha, 2\gamma)| \ll J(2\alpha, 0)$. This can be understood by noting that while the magnitudes of the integrands of $J(2\alpha, 2\gamma)$ and $J(2\alpha, 0)$ are the same, the integrand of $J(2\alpha, 2\gamma)$ is oscillatory and washes $J(2\alpha, 2\gamma)$ out.

BIBLIOGRAPHY

[1] S. Dodelson, *Modern Cosmology* (Academic Press, Amsterdam, 2003).

[2] A. A. Starobinsky, "Spectrum of relict gravitational radiation and the early state of the universe", JETP Lett. **30**, [,767(1979)], 682–685 (1979).

[3] A. A. Starobinsky, "A New Type of Isotropic Cosmological Models Without Singularity", Phys. Lett. **B91**, [,771(1980)], 99–102 (1980).

[4] A. H. Guth, "The Inflationary Universe: A Possible Solution to the Horizon and Flatness Problems", Phys. Rev. **D23**, [Adv. Ser. Astrophys. Cosmol.3,139(1987)], 347–356 (1981).

[5] A. D. Linde, "A New Inflationary Universe Scenario: A Possible Solution of the Horizon, Flatness, Homogeneity, Isotropy and Primordial Monopole Problems", Phys. Lett. **108B**, [Adv. Ser. Astrophys. Cosmol.3,149(1987)], 389–393 (1982).

[6] A. D. Linde, "Coleman-Weinberg Theory and a New Inflationary Universe Scenario", Phys. Lett. **114B**, 431–435 (1982).

[7] A. Albrecht, and P. J. Steinhardt, "Cosmology for Grand Unified Theories with Radiatively Induced Symmetry Breaking", Phys. Rev. Lett. **48**, [Adv. Ser. Astrophys. Cosmol.3,158(1987)], 1220–1223 (1982).

[8] D. Baumann, "Inflation", in Physics of the large and the small, TASI 09, proceedings of the Theoretical Advanced Study Institute in Elementary Particle Physics, Boulder, Colorado, USA, 1-26 June 2009 (2011), pp. 523–686, arXiv:0907.5424 [hep-th].

[9] V. F. Mukhanov, and G. V. Chibisov, "Quantum Fluctuations and a Nonsingular Universe", JETP Lett. **33**, [Pisma Zh. Eksp. Teor. Fiz.33,549(1981)], 532–535 (1981).

[10] S. W. Hawking, "The Development of Irregularities in a Single Bubble Inflationary Universe", Phys. Lett. **115B**, 295 (1982).

[11] A. A. Starobinsky, "Dynamics of Phase Transition in the New Inflationary Universe Scenario and Generation of Perturbations", Phys. Lett. **117B**, 175–178 (1982).

[12] A. H. Guth, and S. Y. Pi, "Fluctuations in the New Inflationary Universe", Phys. Rev. Lett. **49**, 1110–1113 (1982).

[13] J. M. Bardeen, P. J. Steinhardt, and M. S. Turner, "Spontaneous Creation of Almost Scale - Free Density Perturbations in an Inflationary Universe", Phys. Rev. **D28**, 679 (1983).

[14] P. A. R. Ade, et al., "Planck 2015 results. XVII. Constraints on primordial non-Gaussianity", Astron. Astrophys. **594**, A17 (2016), arXiv:1502.01592 [astro-ph.CO].

[15] X. Chen, and Y. Wang, "Quasi-Single Field Inflation and Non-Gaussianities", JCAP **1004**, 027 (2010), arXiv:0911.3380 [hep-th].

[16] R. Penrose, "Difficulties with inflationary cosmology", Annals N. Y. Acad. Sci. **571**, 249–264 (1989).

[17] G. W. Gibbons, and N. Turok, "The Measure Problem in Cosmology", Phys. Rev. **D77**, 063516 (2008), arXiv:hep-th/0609095 [hep-th].

[18] M. Bastero-Gil, A. Berera, R. Brandenberger, I. G. Moss, R. O. Ramos, and J. G. Rosa, "The role of fluctuation-dissipation dynamics in setting initial conditions for inflation", JCAP **1801**, 002 (2018), arXiv:1612.04726 [astro-ph.CO].

[19] P. J. Steinhardt, "Natural inflation", in Very early universe, edited by G. W. Gibbons, S. W. Hawking, and S. T. C. Siklos, (1983), pp. 251–266.

[20] A. Vilenkin, "The Birth of Inflationary Universes", Phys. Rev. **D27**, 2848 (1983).

[21] A. H. Guth, "Inflation and eternal inflation", Phys. Rept. **333**, 555–574 (2000), arXiv:astro-ph/0002156 [astro-ph].

[22] A. Ijjas, P. J. Steinhardt, and A. Loeb, "Inflationary paradigm in trouble after Planck2013", Phys. Lett. **B723**, 261–266 (2013), arXiv:1304.2785 [astro-ph.CO].

[23] L. P. Grishchuk, "Amplification of gravitational waves in an istropic universe", Sov. Phys. JETP **40**, [Zh. Eksp. Teor. Fiz.67,825(1974)], 409–415 (1975).

[24] V. A. Rubakov, M. V. Sazhin, and A. V. Veryaskin, "Graviton Creation in the Inflationary Universe and the Grand Unification Scale", Phys. Lett. **115B**, 189–192 (1982).

[25] R. Fabbri, and M. d. Pollock, "The Effect of Primordially Produced Gravitons upon the Anisotropy of the Cosmological Microwave Background Radiation", Phys. Lett. **125B**, 445–448 (1983).

[26] L. F. Abbott, and M. B. Wise, "Constraints on Generalized Inflationary Cosmologies", Nucl. Phys. **B244**, 541–548 (1984).

[27] C. Cheung, P. Creminelli, A. L. Fitzpatrick, J. Kaplan, and L. Senatore, "The Effective Field Theory of Inflation", JHEP **03**, 014 (2008), arXiv:0709.0293 [hep-th].

[28] J. M. Maldacena, "Non-Gaussian features of primordial fluctuations in single field inflationary models", JHEP **05**, 013 (2003), arXiv:astro-ph/0210603 [astro-ph].

[29] M. Alishahiha, E. Silverstein, and D. Tong, "DBI in the sky", Phys. Rev. **D70**, 123505 (2004), arXiv:hep-th/0404084 [hep-th].

[30] T. J. Allen, B. Grinstein, and M. B. Wise, "Nongaussian Density Perturbations in Inflationary Cosmologies", Phys. Lett. **B197**, 66–70 (1987).

[31] X. Chen, "Primordial Non-Gaussianities from Inflation Models", Adv. Astron. **2010**, 638979 (2010), arXiv:1002.1416 [astro-ph.CO].

[32] D. Baumann, and D. Green, "Signatures of Supersymmetry from the Early Universe", Phys. Rev. **D85**, 103520 (2012), arXiv:1109.0292 [hep-th].

[33] V. Assassi, D. Baumann, and D. Green, "On Soft Limits of Inflationary Correlation Functions", JCAP **1211**, 047 (2012), arXiv:1204.4207 [hep-th].

[34] T. Noumi, M. Yamaguchi, and D. Yokoyama, "Effective field theory approach to quasi-single field inflation and effects of heavy fields", JHEP **06**, 051 (2013), arXiv:1211.1624 [hep-th].

[35] N. Arkani-Hamed, and J. Maldacena, "Cosmological Collider Physics", (2015), arXiv:1503.08043 [hep-th].

[36] A. J. Tolley, and M. Wyman, "The Gelaton Scenario: Equilateral non-Gaussianity from multi-field dynamics", Phys. Rev. **D81**, 043502 (2010), arXiv:0910.1853 [hep-th].

[37] D. Baumann, and D. Green, "Equilateral Non-Gaussianity and New Physics on the Horizon", JCAP **1109**, 014 (2011), arXiv:1102.5343 [hep-th].

[38] A. Achucarro, J.-O. Gong, S. Hardeman, G. A. Palma, and S. P. Patil, "Effective theories of single field inflation when heavy fields matter", JHEP **05**, 066 (2012), arXiv:1201.6342 [hep-th].

[39] A. Achucarro, V. Atal, S. Cespedes, J.-O. Gong, G. A. Palma, and S. P. Patil, "Heavy fields, reduced speeds of sound and decoupling during inflation", Phys. Rev. **D86**, 121301 (2012), arXiv:1205.0710 [hep-th].

[40] H. Jiang, and Y. Wang, "Massive Fields as Systematics for Single Field Inflation", JCAP **1706**, 038 (2017), arXiv:1703.04477 [astro-ph.CO].

[41] R. Gwyn, G. A. Palma, M. Sakellariadou, and S. Sypsas, "Effective field theory of weakly coupled inflationary models", JCAP **1304**, 004 (2013), arXiv:1210.3020 [hep-th].

[42] V. Assassi, D. Baumann, D. Green, and L. McAllister, "Planck-Suppressed Operators", JCAP **1401**, 033 (2014), arXiv:1304.5226 [hep-th].

[43] G. Shiu, and J. Xu, "Effective Field Theory and Decoupling in Multi-field Inflation: An Illustrative Case Study", Phys. Rev. **D84**, 103509 (2011), arXiv:1108.0981 [hep-th].

[44] P. A. R. Ade, et al., "Planck 2015 results. XIII. Cosmological parameters", Astron. Astrophys. **594**, A13 (2016), arXiv:1502.01589 [astro-ph.CO].

[45] P. A. R. Ade, et al., "Improved Constraints on Cosmology and Foregrounds from BICEP2 and Keck Array Cosmic Microwave Background Data with Inclusion of 95 GHz Band", Phys. Rev. Lett. **116**, 031302 (2016), arXiv:1510.09217 [astro-ph.CO].

[46] E. W. Kolb, and S. L. Vadas, "Relating spectral indices to tensor and scalar amplitudes in inflation", Phys. Rev. **D50**, 2479–2487 (1994), arXiv:astro-ph/9403001 [astro-ph].

[47] S. Weinberg, "Quantum contributions to cosmological correlations", Phys. Rev. **D72**, 043514 (2005), arXiv:hep-th/0506236 [hep-th].

[48] J. Gleyzes, R. de Putter, D. Green, and O. Doré, "Biasing and the search for primordial non-Gaussianity beyond the local type", JCAP **1704**, 002 (2017), arXiv:1612.06366 [astro-ph.CO].

[49] N. Dalal, O. Dore, D. Huterer, and A. Shirokov, "The imprints of primordial non-gaussianities on large-scale structure: scale dependent bias and abundance of virialized objects", Phys. Rev. **D77**, 123514 (2008), arXiv:0710.4560 [astro-ph].

[50] D. Baumann, S. Ferraro, D. Green, and K. M. Smith, "Stochastic Bias from Non-Gaussian Initial Conditions", JCAP **1305**, 001 (2013), arXiv:1209.2173 [astro-ph.CO].

[51] A. Moradinezhad Dizgah, and C. Dvorkin, "Scale-Dependent Galaxy Bias from Massive Particles with Spin during Inflation", JCAP **1801**, 010 (2018), arXiv:1708.06473 [astro-ph.CO].

[52] M. Tellarini, A. J. Ross, G. Tasinato, and D. Wands, "Non-local bias in the halo bispectrum with primordial non-Gaussianity", JCAP **1507**, 004 (2015), arXiv:1504.00324 [astro-ph.CO].

[53] S. Mizuno, and S. Yokoyama, "Halo/Galaxy Bispectrum with Equilateral-type Primordial Trispectrum", Phys. Rev. **D91**, 123521 (2015), arXiv:1504.05505 [astro-ph.CO].

[54] W. H. Press, and P. Schechter, "Formation of galaxies and clusters of galaxies by selfsimilar gravitational condensation", Astrophys. J. **187**, 425–438 (1974).

[55] N. Kaiser, "On the Spatial correlations of Abell clusters", Astrophys. J. **284**, L9–L12 (1984).

[56] E. Sefusatti, J. R. Fergusson, X. Chen, and E. P. S. Shellard, "Effects and Detectability of Quasi-Single Field Inflation in the Large-Scale Structure and Cosmic Microwave Background", JCAP **1208**, 033 (2012), arXiv:1204.6318 [astro-ph.CO].

[57] H. D. Politzer, and M. B. Wise, "Relations Between Spatial Correlations of Rich Clusters of Galaxies", Astrophys. J. **285**, L1–L3 (1984).

[58] V. Desjacques, D. Jeong, and F. Schmidt, "Large-Scale Galaxy Bias", Phys. Rept. **733**, 1–193 (2018), arXiv:1611.09787 [astro-ph.CO].

[59] J. M. Bardeen, J. R. Bond, N. Kaiser, and A. S. Szalay, "The Statistics of Peaks of Gaussian Random Fields", Astrophys. J. **304**, 15–61 (1986).

[60] F. Beutler, et al., "The clustering of galaxies in the completed SDSS-III Baryon Oscillation Spectroscopic Survey: Anisotropic galaxy clustering in Fourier-space", Mon. Not. Roy. Astron. Soc. **466**, 2242–2260 (2017), arXiv:1607.03150 [astro-ph.CO].

[61] H. Gil-Marín, J. Noreña, L. Verde, W. J. Percival, C. Wagner, M. Manera, and D. P. Schneider, "The power spectrum and bispectrum of SDSS DR11 BOSS galaxies – I. Bias and gravity", Mon. Not. Roy. Astron. Soc. **451**, 539–580 (2015), arXiv:1407.5668 [astro-ph.CO].

[62] J. N. Fry, "The Galaxy correlation hierarchy in perturbation theory", Astrophys. J. **279**, 499–510 (1984).

[63] M. Mirbabayi, F. Schmidt, and M. Zaldarriaga, "Biased Tracers and Time Evolution", JCAP **1507**, 030 (2015), arXiv:1412.5169 [astro-ph.CO].

[64] R. Angulo, M. Fasiello, L. Senatore, and Z. Vlah, "On the Statistics of Biased Tracers in the Effective Field Theory of Large Scale Structures", JCAP **1509**, 029 (2015), arXiv:1503.08826 [astro-ph.CO].

[65] M. Alvarez, et al., "Testing Inflation with Large Scale Structure: Connecting Hopes with Reality", (2014), arXiv:1412.4671 [astro-ph.CO].

[66] H. An, M. McAneny, A. K. Ridgway, and M. B. Wise, "Quasi Single Field Inflation in the non-perturbative regime", Journal of High Energy Physics **06**, 105 (2018), arXiv:1706.09971 [hep-ph].

[67] S. Yokoyama, and T. Matsubara, "Scale-dependent bias with higher order primordial non-Gaussianity: Use of the Integrated Perturbation Theory", Phys. Rev. **D87**, 023525 (2013), arXiv:1210.2495 [astro-ph.CO].

[68] L. Senatore, and M. Zaldarriaga, "The Effective Field Theory of Multifield Inflation", JHEP **04**, 024 (2012), arXiv:1009.2093 [hep-th].

[69] N. Khosravi, "Effective Field Theory of Multi-Field Inflation a la Weinberg", JCAP **1205**, 018 (2012), arXiv:1203.2266 [hep-th].

[70] H. R. S. Cogollo, Y. Rodriguez, and C. A. Valenzuela-Toledo, "On the Issue of the zeta Series Convergence and Loop Corrections in the Generation of Observable Primordial Non-Gaussianity in Slow-Roll Inflation. Part I: The Bispectrum", JCAP **0808**, 029 (2008), arXiv:0806.1546 [astro-ph].

[71] Y. Rodriguez, and C. A. Valenzuela-Toledo, "On the Issue of the zeta Series Convergence and Loop Corrections in the Generation of Observable Primordial Non-Gaussianity in Slow-Roll Inflation. Part 2. The Trispectrum", Phys. Rev. **D81**, 023531 (2010), arXiv:0811.4092 [astro-ph].

[72] J. Kumar, L. Leblond, and A. Rajaraman, "Scale Dependent Local Non-Gaussianity from Loops", JCAP **1004**, 024 (2010), arXiv:0909.2040 [astro-ph.CO].

[73] J. Bramante, and J. Kumar, "Local Scale-Dependent Non-Gaussian Curvature Perturbations at Cubic Order", JCAP **1109**, 036 (2011), arXiv:1107.5362 [astro-ph.CO].

[74] M. Mirbabayi, and M. Simonović, "Effective Theory of Squeezed Correlation Functions", JCAP **1603**, 056 (2016), arXiv:1507.04755 [hep-th].

[75] J. E. Gunn, and J. R. Gott, III, "On the Infall of Matter into Clusters of Galaxies and Some Effects on Their Evolution", Astrophys. J. **176**, 1–19 (1972).

[76] S. Ferraro, K. M. Smith, D. Green, and D. Baumann, "On the Equivalence of Barrier Crossing, Peak-Background Split, and Local Biasing", Mon. Not. Roy. Astron. Soc. **435**, 934–942 (2013), arXiv:1209.2175 [astro-ph.CO].

[77] P. A. R. Ade, et al., "Planck 2013 Results. XXIV. Constraints on primordial non-Gaussianity", Astron. Astrophys. **571**, A24 (2014), arXiv:1303.5084 [astro-ph.CO].

[78] P. A. Abell, et al., "LSST Science Book, Version 2.0", (2009), arXiv:0912.0201 [astro-ph.IM].

[79] R. Laureijs, et al., "Euclid Definition Study Report", (2011), arXiv:1110.3193 [astro-ph.CO].

[80] O. Doré, et al., "Cosmology with the SPHEREX All-Sky Spectral Survey", (2014), arXiv:1412.4872 [astro-ph.CO].

[81] X. Chen, R. Easther, and E. A. Lim, "Large Non-Gaussianities in Single Field Inflation", JCAP **0706**, 023 (2007), arXiv:astro-ph/0611645 [astro-ph].

[82] X. Chen, M.-x. Huang, S. Kachru, and G. Shiu, "Observational signatures and non-Gaussianities of general single field inflation", JCAP **0701**, 002 (2007), arXiv:hep-th/0605045 [hep-th].

[83] X. Chen, "Folded Resonant Non-Gaussianity in General Single Field Inflation", JCAP **1012**, 003 (2010), arXiv:1008.2485 [hep-th].

[84] I. Agullo, and L. Parker, "Non-gaussianities and the Stimulated creation of quanta in the inflationary universe", Phys. Rev. **D83**, 063526 (2011), arXiv:1010.5766 [astro-ph.CO].

[85] I. Agullo, and L. Parker, "Stimulated creation of quanta during inflation and the observable universe", Gen. Rel. Grav. **43**, [Int. J. Mod. Phys.D20,2861(2011)], 2541–2545 (2011), arXiv:1106.4240 [astro-ph.CO].

[86] P. Adshead, C. Dvorkin, W. Hu, and E. A. Lim, "Non-Gaussianity from Step Features in the Inflationary Potential", Phys. Rev. **D85**, 023531 (2012), arXiv:1110.3050 [astro-ph.CO].

[87] A. Achúcarro, J.-O. Gong, G. A. Palma, and S. P. Patil, "Correlating features in the primordial spectra", Phys. Rev. **D87**, 121301 (2013), arXiv:1211.5619 [astro-ph.CO].

[88] A. Achucarro, V. Atal, B. Hu, P. Ortiz, and J. Torrado, "Inflation with moderately sharp features in the speed of sound: Generalized slow roll and in-in formalism for power spectrum and bispectrum", Phys. Rev. **D90**, 023511 (2014), arXiv:1404.7522 [astro-ph.CO].

[89] S. R. Behbahani, A. Dymarsky, M. Mirbabayi, and L. Senatore, "(Small) Resonant non-Gaussianities: Signatures of a Discrete Shift Symmetry in the Effective Field Theory of Inflation", JCAP **1212**, 036 (2012), arXiv:1111.3373 [hep-th].

[90] R. Flauger, L. McAllister, E. Silverstein, and A. Westphal, "Drifting Oscillations in Axion Monodromy", JCAP **1710**, 055 (2017), arXiv:1412.1814 [hep-th].

[91] R. Flauger, M. Mirbabayi, L. Senatore, and E. Silverstein, "Productive Interactions: heavy particles and non-Gaussianity", JCAP **1710**, 058 (2017), arXiv:1606.00513 [hep-th].

[92] Y. Wang, Y.-P. Wu, J. Yokoyama, and S. Zhou, "Hybrid Quasi-Single Field Inflation", JCAP **1807**, 068 (2018), arXiv:1804.07541 [astro-ph.CO].

[93] N. Bolis, A. Albrecht, and R. Holman, "Non-Gaussianity from Entanglement During Inflation", (2019), arXiv:1902.07567 [hep-th].

[94] N. Aghanim, et al., "Planck 2018 results. VI. Cosmological parameters", (2018), arXiv:1807.06209 [astro-ph.CO].

[95] H. An, M. B. Wise, and Z. Zhang, "De Sitter Quantum Loops as the origin of Primordial Non-Gaussianities", Phys. Rev. **D99**, 056007 (2019), arXiv:1806.05194 [hep-ph].